

DIPLOMA THESIS

**Manual laser deposition welding of high
alloyed hot work steel on age hardened
copper-beryllium-alloy**

accomplished at
Institute for Materials Science and Welding, TU Graz

written by
Leonhard Weingrill

supervised by
Assoc.-Prof. Dipl.-Ing. Dr.techn. Norbert Enzinger
and
Dipl.- Ing. Dragan Djuric, IWE

in association with
Dipl.- Ing. Markus Simschitz
from
MAHLE Filtersysteme Austria GmbH

2012

Abstract

Based on experimental studies this thesis characterizes the weldability of a manual pulsed Nd:YAG laser deposition weld of two high alloyed hot work steel wires on an age hardened copper-beryllium alloy. These claddings are intended for surface enhancement of high-conductivity core inserts for injection molding tools.

The thesis comprises the identification of a weldable laser parameter window with the help of macroscopic examinations of welded samples' bead surfaces and cross sections. A well established interface and a small but notable transition zone at the interface can be found, appropriate dilution given.

The weld quality scatters during the performed experiments. Inside the weld metal defects can be observed. For relatively high dilution the weld metal is inhomogeneous and a typical crack type appears. SEM topography reveal them to be hot cracks.

Process studies are carried out to determine, besides the laser parameters, influencing factors in order to improve welding conditions' constancy. A first phase of this thesis is closed by a definition of an optimum dilution domain within which the amount of weld defects is lowest.

In the second phase of the thesis a bead by bead parameter optimization for a direct steel cladding and a Ni-base buffer layer cladding is done. The amount of defects in the weld metal could be significantly reduced. The direct steel cladding shows better results for hardness and shear strength.

Separately a FEM simulation was performed to estimate the deterioration of the cooling function of a welded core insert against the deposition layer's thickness. The results show minor influence for the intended layer thicknesses.

Contents

1	Introduction	1
1.1	MAHLE Filtersysteme Austria GesmbH	3
1.2	Motivation	5
1.3	Objective	7
1.4	Task	7
2	Theoretical essays	9
2.1	Weldability	11
2.2	Laser deposition welding	13
2.2.1	Mechanisms of heat encapsulation	15
2.3	Dilution	19
2.4	Absorptivity of laser beams	21
2.4.1	Material properties and laser wavelength	22
2.4.2	Polarization	23
2.4.3	Angle of impingement	24
2.4.4	Temperature	25
2.4.5	Surface quality	28
2.5	Welding residual stresses	31
2.6	Welding defects	33
2.6.1	Hot cracking	33
2.6.2	Cold cracking	36
2.6.3	Lack of fusion	37
2.6.4	Pores	38
2.7	Copper-Beryllium-alloys	39
2.7.1	Weldability of copper	40
2.7.2	Weldability of age hardened materials	40
2.8	High alloyed steels	43
2.8.1	Assorted relevant alloying elements	43
2.8.2	Hot work steel	44
2.8.3	Weldability of high alloyed steels	45
2.8.4	Microstructure estimation diagrams	46
2.9	Dissimilar welding of copper and steel	49
2.9.1	Crystallographic similarities	50
2.9.2	Forming of intermetallic phases	51
2.9.3	Buffer layers	55
3	Experimental	57
3.1	Welding experiments	57

Contents

3.2	Used materials	61
3.2.1	Substrate: AMPCOLOY [®] 88	61
3.2.2	0.5mm laser Mold [®] 10 wire	63
3.2.3	0.4mm laser Mold [®] 50 wire	63
3.2.4	0.5mm JOKE [®] Fill 120 wire	63
3.3	Weld bead structures	65
3.4	Laser welding device	67
3.5	Welding experiment setups	71
3.6	Investigations	73
3.6.1	Metallography probe preparation	73
3.6.2	Optical microscopy	75
3.6.3	SEM	75
3.6.4	Weld defects measurement	76
3.6.5	Macro hardness testing	77
3.6.6	Hardness line testing	77
3.6.7	Shear test	78
3.7	Heat transfer simulation	81
3.7.1	Modeling	81
3.7.2	Assumptions	81
3.7.3	Simulation procedure	82
3.7.4	Output	83
4	Results and discussion	85
4.1	VR0: Weldability and process characterization	85
4.1.1	Weld quality	86
4.1.2	Interface	90
4.1.3	Weld metal	95
4.1.4	Weld defects	105
4.2	Process studies	107
4.2.1	Welding velocity	107
4.2.2	Influence of welding speed	108
4.2.3	Wire deposition rate	108
4.2.4	Welding sequence	111
4.2.5	Substrate preparation	113
4.2.6	Substrate initial temperature	113
4.2.7	Welding spot diameter	116
4.3	VR0: Conclusion	119
4.3.1	Changing absorptivity throughout a welding sequence	120
4.3.2	Outlook HI optimization	121

Contents

4.4	VR1: optimized welding	123
4.4.1	Weld quality	123
4.4.2	Hardness lines	128
4.4.3	Shear strength	131
4.4.4	Characterization of failure behavior of direct steel claddings . . .	134
4.5	VR1: Conclusion	143
4.6	Simulation	145
5	Summary	147
5.1	VR0: Initial process characterization	147
5.2	VR0: Additional influencing factors	148
5.3	VR1: Parameter optimization	149
5.4	Heat transfer deterioration	151
5.5	In one sentence	151
6	Outlook	153

1 Introduction

This chapter contains a general introduction to this thesis. It shortly depicts the structure of the report and previews the content of the chapters.

This first chapter contains a short presentation of the industrial partner for this work MAHLE Filtersysteme Austria GesmbH St. Michael (MAHLE). The motivation for the presented work resulting from a challenge MAHLE faces for one of its industrial application, is introduced, followed by initially set tasks and goals.

In the second chapter theoretical essays underlay the presented work. The chapter is divided into three parts with regards to contents.

- Initially the term weldability is discussed.
- After that the second thematic part discusses in three sections laser welding as a welding method, working out also encircling aspects that are assumed to be of importance. A main focus is given to a theoretical characterization of known influencing factors of absorptivity of metals to laser light. The formation of welding residual stresses and welding defects are discussed.
- The third part introduces the used materials and tries to theoretically work out aspects of their weldability. This finally leads to a section that discusses the dissimilar welding of copper and steel.

Chapter three contains descriptions of the experimental realization of the thesis. For what regards weldability investigation this comprises the carried out experiments and the applied examination methods. Additionally the carried out heat transfer simulation is described.

Chapter four contains the results from the experiments and corresponding discussions. The results of the weldability investigations are split up into two sections. The FEM-simulation is separately presented.

Two final chapters summarize the presented work and the findings. A final statement of what was attained and to what extend the set goals are reached is given. A short outlook on the potential of the envisaged application and useful secondary investigation closes this report.

1.1 MAHLE Filtersysteme Austria GesmbH

The experiments of this thesis were entirely realized at the tool making department at MAHLE's plant in St. Michael. With the here presented quotation the author wants to show his appreciation for the will of the responsible and other people involved for professional and financial support.

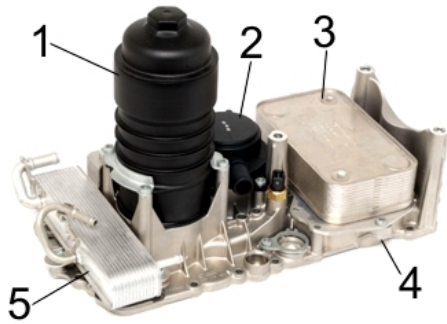
The MAHLE Group and its two divisions Engine Systems & Components, and Filtration & Engine Peripherals is among the top three systems suppliers for piston systems, cylinder components, valve train, air management and fluid management systems worldwide. As one of the 30 largest suppliers and leading global development partner in automotive industries the MAHLE group has unique systems competence in the area of combustion engines and engine peripherals. The MAHLE group international has over 100 production sites on four continents. It employs approximately 43,000 employees worldwide. The turnover in 2009 was nearly 4 billion euros.

For what concerns Austria, at the two locations in Carinthia MAHLE Filtersysteme Austria GesmbH employs more than 2500 people. Both of the sites are to be settled in the engine periphery and filtration business domain. In St. Michael parts and assemblies for combustion engines peripherals, mainly filter systems, are produced. The following listing is an extract from the product portfolio that is produced in St. Michael.

1. oil,fuel and air filters
2. spin on filters
3. air filter elements
4. air duct modules
5. engine design covers
6. aluminum die casted filter parts
7. etc. ...

MAHLE designs and makes tools for their own production as well as special purpose machines and assembly stations in St. Michael. Sheet stamping machines, injection molding and blowing of plastic parts as well various assembly station, including welding stations for both metal and plastic parts, can be found on the production floor. The design of the injection molding tools can be seen as one of their core competences of MAHLE's tool making department.

Fig. 1 shows two exemplary MAHLE products.



(a) Mahle Oil filter module



(b) Mahle Air duct module

Figure 1: Exemplary MAHLE products. **1** plastic oil filter **2** oil mist separator **3** oil/water heat exchanger **4** aluminum base plate **5** diesel/water heat exchanger [1]

1.2 Motivation

The task of the presented work is settled in the field of a surface enhancement of highly loaded injection molding tools. These tools are developed, designed and manufactured at the tool making department of MAHLE. With these tools MAHLE produces among others glass fiber reinforced plastic components for combustion engines' periphery. The very specific demand of an investigation arises due to significant wear that occurs on heat-sucking cores inserts made out of highly thermal conductive AMPCOLOY[®] CuBe-materials during production of oil filter housings. These cores are mounted inside the tool's cavity plate in order to allow for faster cooling of the injected mold at certain areas. With the help of this measure hot spots at the work piece, at e.g. thick walls or contorted geometries that are difficult to be reached via ordinary cooling channels, are countered. More rapid solidification helps to reduce cycle time. As these molded parts are produced in verily large quantities costs are tremendously reduced by some seconds of economized cycle time. Furthermore enhanced wear resistance will decrease down time because of tool replacements.

The wear problems are caused by the solidification mechanism of the glass fibers containing plastic mold. Fibers align because of the dynamics of the liquid mold during injection and subsequent solidification, mainly perpendicular towards the tool surface, forming thousands of very hard and sharp edges. At every opening of the tool and ejection of the solidified parts these fibers act like microscopic blades gnawing off the tool's surface. Additionally it has to be mentioned that the mold is injected at about 280 to 290°C and ejected at about 170°C. Elevated temperatures and temperature changes are known to weaken material's wear resistance.

The mentioned parts and machines and the appearing wear problems are graphically depicted in fig. 2.

Fig. 2(a) shows the form plate of an opened injection molding tool and mounted core inserts. An AMPCOLOY[®] heat conduction core insert after manufacturing is depicted in fig. 2(b).

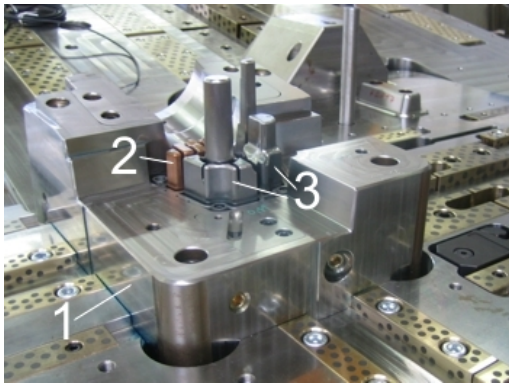
Fig. 2(c) shows a part of the same type after some ten thousand filling cycles. Elutriation and pit mark forming can be observed. Because of this appearances unmounting and disassembling of the entire tool is necessary. This causes down time and therefore loss of production time with accompanying costs.

Fig. 2(d) shows an injection machine at MAHLE's shop floor with the mounted and open tool.

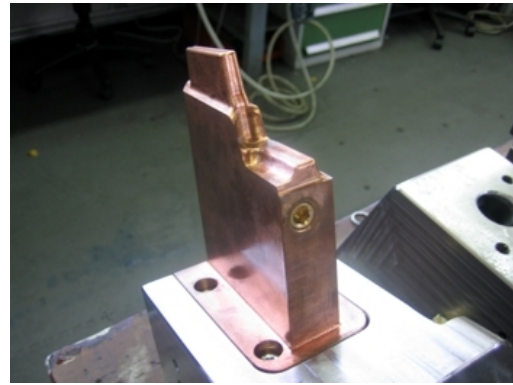
MAHLE is nowadays using TiO protective layers to reduce wear. By this measure the service time of a tool can almost be doubled. Although the improvements from these measures are therefore significant the tool making department is not fully satisfied and searches for alternative wear protection technologies.

1 Introduction

An idea for solving the problem is to produce a protective cladding out of hot work steel at those areas where wear appears more significantly. The protective layer needs to be thick enough to guarantee increased wear protection. However it has to be thin enough to not deteriorate the properties of the manufactured part in terms of thermal conductivity. This contradiction forms the challenge to be solved by this thesis and therefore the initial point of the work. As a manual laser welding device was newly purchased by MAHLE's tool making department for repair-weldments of broken parts it is suggested to manufacture the protective steel layer by manual laser deposition weldments. This method would offer an alternative to the above mentioned TiO coatings and it is believed, if weldable, to provide better protection.



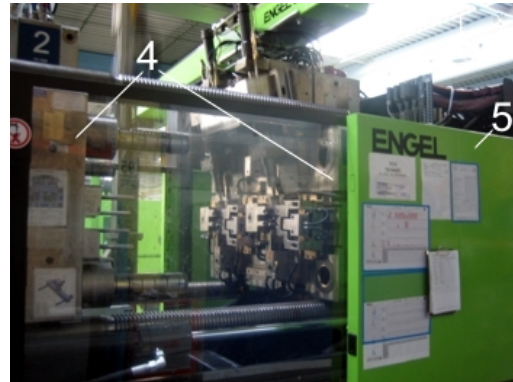
(a) Mounted core inserts.



(b) Newly manufactured heat sucking core insert made out of AMPCOLOY®.



(c) Wear appearance on disassembled TiO protective coated AMPCOLOY® core insert.



(d) Mounted injection molding tool during operation.

Figure 2: Injection molding and wear on core inserts at MAHLE tool making department. **1** cavity plate, **2** AMPCOLOY® core insert, **3** steel core inserts, **4** injection molding tool, **5** injection molding machine.

1.3 Objective

The objective of this diploma thesis is to investigate the weldability of a manual pulsed Nd:YAG-laser deposition weldment (cladding) of a dissimilar material combination. An AMPCOLOY[®] CuBe-alloy is envisaged as substrate material. The material used for the deposited protective layer should be a high alloyed hot work steel which's general properties should resembles to in this domain already used steel qualities, e.g. 1.2311, 1.2343 or 1.2767.

Hence, the goal of this diploma thesis is to give a statement on the potential of this welding process in order to discuss its applicability for the manufacturing of the envisaged protective layer. The cladding should possibly serve as a valuable alternative to the today's applied wear resistance increasing technologies. It is necessary to evaluate the attainable increase of wear resistance to be able to compare alternatives.

In the end this work wants to create know-how, in order to introduce a new technology for a surface enhancement of an AMPCOLOY[®] injection molding core insert by a dissimilar deposition weldment. Welding instructions will be based on the attained insights.

1.4 Task

The tasks of this thesis comprises the following steps:

- Give a principal statement on the weldability of the envisaged material combination.
- Characterize the process and influencing factors, with regards to the manufacturing condition at MAHLE's tool making department.
- Identify problems and counter them.
- Investigate the mechanical properties of the claddings.
 - Primarily the hardness of the protective layer is of interest. MAHLE asks for a hardness greater than HRC 55.
 - Additionally the bonding strength at the interface is to be assessed. A relation to the attained welding quality is to be established.
- Perform a numerical simulation to estimate the deterioration of thermal conductivity of a clad core insert in relation to a pure AMPCOLOY[®] core insert. This deterioration shall be displayed as a function of the deposited steel layer's thickness.

2 Theoretical essays

This chapter of the report contains essays on theoretical aspects that represent essential background knowledge of this thesis.

The initial thoughts which this work is based on are tried to be strengthened by this literature overview.

In order to attain satisfying and predictable results when laser welding, the heat input per unit of length (HI) has to be consciously set. The resulting dilution of the two materials will determine the metallurgical composition of the protective layer, and thus the quality cladding in the end.

The functional gain of the envisaged difficult material combination wants to be maximized. Concerning the steel layer it is intended to not lose good mechanical properties, namely very good wear resistance at elevated temperatures. Speaking of the Cu-substrate material, good thermal properties are intended to stay unchanged. These two demands claim for avoiding strong dilution of the two materials.

However, a certain dilution is necessary in order to guarantee a well established connection at the interface.

The essential for solving this thesis' problematic therefore is to find optimized welding parameters, and thus an appropriate HI and dilution. This compromise is believed to lead to an optimized welding result in the end.

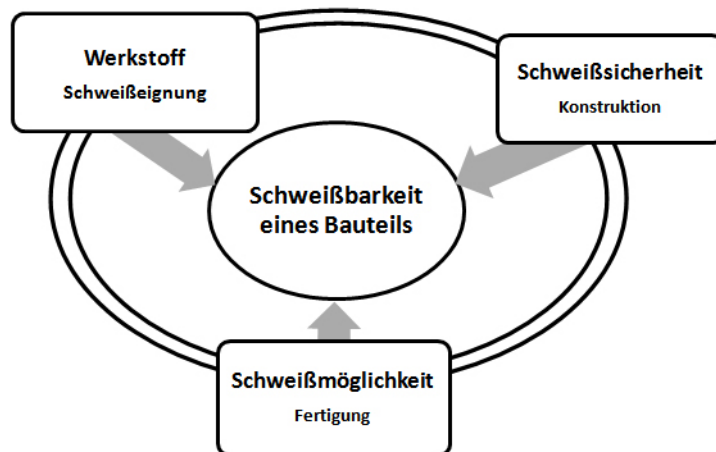


Figure 3: Three aspects of weldability according to DIN 8528 1st part. [2]

2.1 Weldability

According to [3] there is no universally accepted meaning of the term weldability. A definition of the term from the American Welding Society is:

“The capacity of a metal to be welded under the fabrication conditions imposed, into a specific, suitably designed structure, and to perform satisfactorily in the intended service”. [3]

What is interesting to point out in this definition is the consideration of fabrication conditions the weld is imposed to. This question is very relevant to this thesis. All influencing factors, including manufacturing conditions, need to be characterized.

In [2] the definition of weldability from the standard DIN 8528 1st part can be translated like this:

“Weldability of a part of metallic materials is given if a metallurgic joint can be established by welding with a given welding process while paying attention to a certain imposed manufacturing sequence.” [2]

More precisely, the standard defines weldability as a result of three influencing factors as depicted in the fig. 3.

“Schweißmöglichkeit” can be translated to “the possibility of welding” or, more freely the accessibility of the welding spot or the manufacturability of the weld. Therefore this first aspect asks for the abilities of the given welding process and the manufacturing environment it takes place in. The welding possibility is significant throughout the whole manufacturing process of a welded part. Three factors according to such a sequence can be distinguished time-dependently.

- welding preparation:
joint/surface preparation, preheating, filler and other auxiliary materials
- welding procedure:
thermal course, built-up of the weld, heat input, welding sequence
- post welding treatment:
post weld heat treatment, straightening work, acid cleaning, mechanical after work.

“Werkstoff” in stand for material. The “Schweißbeignung”, or freely translated “suitability for welding”, considers the welded material’s properties. Again this aspect of weldability can be divided into three further factors:

- First the chemical composition of the material. It will for example influence the hardening tendency of steel materials by the carbon content. Another example would be the influence alloying elements can have on the susceptibility to hot cracking because of the formation of low melting phases.

2 Theoretical essays

- Second the metallurgic properties of the material. E.g. : grain size, segregations or solubility.
- Ultimately the physical properties are part of the welding suitability of a material. Big solidification intervals are sources for hot cracking as they prolong the presence of liquid phases in between solidified dendrites. Another example would be the thermal expansion coefficient and the thermal conductivity. Both will influence residual stresses.

[2]

The third influencing factor asks for the welded part to fulfill its functional purpose. Here, the weldability depends on the design of the part and where the weldments are placed, as well as the location, direction and sort of applied load the part has to bear.

2.2 Laser deposition welding

This section of the report gives a short introduction to laser deposition welding. As an initiation, statements on welding fundamentals are mentioned. They give a good theoretical foundation of how to approach investigations of this thesis.

“Welding: an operation which unites material(s) by means of heat or pressure, or both, in such a way that there is continuity in the nature of the material(s) which has (have) been joined. Filler material, the melting temperature of which is of the same order as that of the parent metal(s) may or may not be used.” [4]

Only if metallic continuity at the interface is established, the materials are welded. Hence, this very basic statement from the standard can help to define whether two materials are welded or not. It helps to indicate the appropriate welding parameter’s range inside of which one can still consider the applied process as a weldment.

The HI represents an important factor for this work. The source of heat creation influences the HI. It is essential to have a look at the origin of heat creation when laser welding.

Laser is an acronym for **L**ight **A**mplification by **S**timulated **E**mission of **R**adiation which basically describes the physical transaction that is used as energy source when laser welding, refer to page 23. A laser beam is not “hot” by itself, as it is the case for a lot of other heat sources of different welding methods. Neither can it apply forces to the welding spot.

“When laser welding, the energy is transmitted without mechanical or electrical contact via electromagnetic waves, namely the laser beam, from the energy source to the work piece.” [5]

Translated from German standard DIN1910 [5]: “The necessary heat arises from transformation of bundled energy-rich radiation during penetration into the workpiece.”

When laser welding, it is therefore necessary that the laser beam is absorbed at the welding spot and that its energy is transformed into heat in order to increase temperatures high enough for melting the materials. This fact represents a significant difference compared to other fusion welding methods. Instead of heat conduction and/or convection a transformation of energy in form of a beam of coherent electromagnetic waves into heat represents the initial mean for the necessary temperature elevation.

Laser welding is a beam welding process and can be further classified according to its laser producing media, offering different characteristics in terms of power levels and densities, wavelengths, handling of the beam etc. [2]

Laser deposition welding, or laser cladding, is closely related to laser welding, for it uses the same heat source. Instead of connection joints several beads of filler material are flatly clad to a substrate part and are aligned in parallel next to each other in order to form a continuous layer of deposited material. Those coatings aim for different functional goals.

- On the one hand they can serve as repair-welds. Removed material can be replaced or faulty areas can be reworked. An often far more expensive exchange of a part or a whole assembly can in this way be avoided.
- On the other hand laser deposition welding is taken advantage of as surface enhancements in manufacturing. Two purposes can be further distinguished in this case.[6]
 - The weldments serve to increase wear resistance. This application is referred to as armoring.
 - The weldments are surface enhancements to increase corrosion resistance. This application is referred to as plating.

Laser claddings are also used for changing optical, isolating and lubricating properties of surfaces.

Laser deposition welding can be used in manufacturing in fully automated mode and manual mode as well.

For automated application the laser is guided with the help of CAD-data over the work piece. Laser welding machines are at least partially robotized. This method is well suited for single specific purpose weldments as well as for larger deposition welds and for series production.

When welding automatically the deposited material can be supplied in two ways.

- A metallic powder is blown in the weld pool through a nozzle. The laser heats the substrate material creating a weld pool where the filler powder is melt. This technology is also referred to as Laser Aided Direct Metal Deposition.[7]
- The deposited material is supplied in form of a wire. The wire deposition can be done manually or in automated mode.

When manual laser welding an operator guides the laser manually over the work piece. The operator supplies the filler wire manually as well. These manual welding techniques offer great advantage wherever small and flexible deposition welds are produced. The material can be placed very accurately.

The machines used for manual welding application are partly robotized as well. They therefore offer automated or semi-automated welding mode.

Manual laser deposition welding is in general rather suited for special purpose small weldments where it can play on its flexibility.

Both operating modes today can be estimated as common technology in industry. [7] [8]

One great advantage of laser cladding is that it allows for locally exact and flexibly applicable weldments. Because of the possibility of a very fine adjustment of the HI this welding method is used for similar as well as dissimilar weldments.

Dissimilar weldments are used to locally take advantage of the clad material's different properties for armoring and plating. The effectiveness in manufacturing can be increased by placing the right material right where it's specific properties are of use.[9]

A summarizing statement from literature closes this introduction to laser deposition welding. "Considering various factors relevant to the costs of materials, equipment and manufacturing processes, and the quality of deposited materials, laser cladding has demonstrated some unique advantages over others: it can produce metallurgically sound and dense clad layer using a relatively low heat input which minimizes the distortion of the component or tooling being deposited; it produces metallurgical bond between the clad layer and the substrate; and it can control the dilution of cladding material into the substrate to reduce undesired deterioration of mechanical of the base material." [10]

2.2.1 Mechanisms of heat encapsulation

When laser welding two different mechanisms of heat encapsulation have to be distinguished. The following remarks are based on [11].

Heat conduction welding appears at lower energy intensity beams and short contact times. The laser beam is absorbed at the surface of the workpiece which is heated up by transforming the electromagnetic waves into heat. If the energy absorption is high enough a melt pool is formed which enables welding.

Heat is transferred from the surface into the work piece by heat conduction. The transport is supported by convection as well.

A further increasing of the power intensity leads to a stronger local heating and a changing of the geometry of the molten material. The maximum of the welding depth and width is attained as soon as the losses of heat conduction inhibit a further increase of the surface temperature.[5] [11]

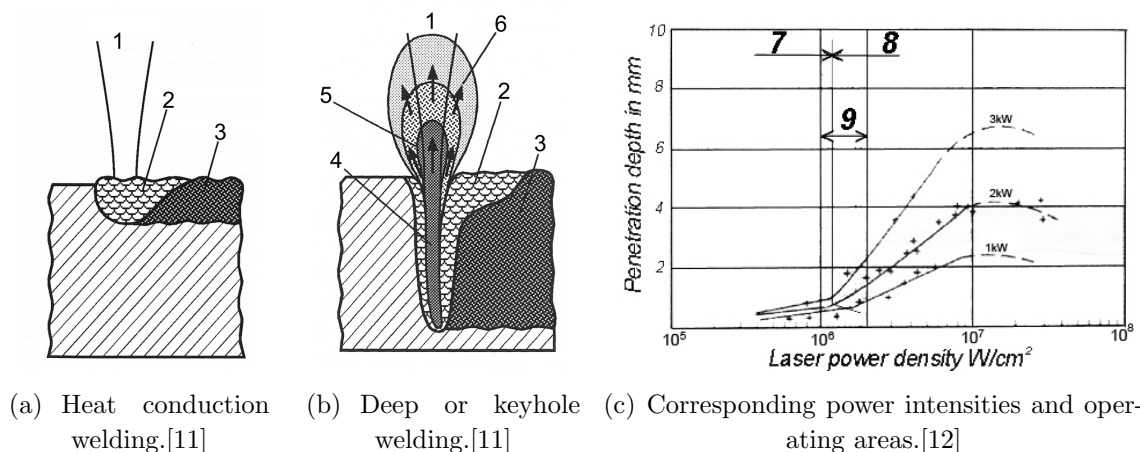


Figure 4: Heat encapsulation when laser welding. **1** laser beam, **2** liquid melting zone, **3** solidified melting zone, **4** vapor/plasma capillary, **5** laser induced plasma, **6** flowing out metal vapor, **7** operating area heat conduction welding, **8** operating area keyhole welding, **9** intensity area at plasma welding.

The second known mechanism of heat encapsulation is deep welding or keyhole welding. If the intensity of the laser beam is increased to such an extent that [13]:

$$I = \frac{P}{\frac{\pi}{4}d_w^2} > 3 * 10^6 \frac{W}{cm^2} \quad (1)$$

the material partly reaches boiling temperature at the welding spot. A bore-hole is formed. It is kept open due to the elevated pressure resulting from evaporation of the metal. This hole is also referred to as keyhole and the corresponding mechanism is therefore also called laser keyhole welding.

In contrast to the above mentioned heat conduction welding the laser beam is conducted optically inside the workpiece where it is trapped. It's energy is absorbed at the liquid walls of the capillary. Hence the laser beam penetrates deeper inside the material which also transfers the location of heat generation deeper inside the material. Two additional effects increase the heat input for this mechanism:[13]

- Multiple reflections of the laser beam inside the keyhole enlarge the area of interaction of energy source and material, namely to the entire walls of the capillary.
- The second effect comes from differing impingement angles of the radiation inside the capillary which's influence can tremendously increase the absorptivity of a metal surface.

Plasma formation influences the heat input as well. A plasma cloud which is formed above the welding spot shields some of the incoming radiation which can therefore not

enter the keyhole. Contrary to that plasma can also absorb some of the radiation, resulting in higher heat input.

The heat creation mechanism becomes more complex when keyhole laser welding appears and happens to a greater extension inside the material.

Fig. 4 depicts the two above mentioned mechanisms of heat encapsulation. The images show in a decent mode where the actual interaction of the laser and the substrate material happens.

The HI changes a lot for the two different mechanisms. “The coupling rate for CO_2 -laser welding changed steeply at the transition from heat conduction welding state to keyhole welding state.” [14]

This fact is graphically depicted in 4(c). On the one hand the great difference of absolute absorbed HI can be derived from the diagram. On the other hand the steeper increase during keyhole laser welding is visible.

Keyhole laser welding has not been encountered during weldments of the presented work. Still, it is important to mention the difference and that this mechanism does not apply for the presented weldments. The presentation of both mechanisms wants to point out the greater importance of absorption for heat conduction welding.

2.3 Dilution

When deposition welding the dilution of the substrate material and the deposited material have a great significance. The intended properties of so created layers are generally deteriorated if the intermixture is too high.[15]

A welding optimization for deposition welds will aim to optimize the dilution. Two contradicting results must be attained:

- Sufficient bonding strength by an intense enough joint at the interface of the materials: A higher dilution will most probably increase the bonding strength.
- Upholding of single materials properties: A higher dilution will most probably have negative influence on this goal. [15]

This asks for a trade-off in terms of dilution.

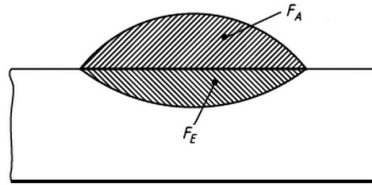


Figure 5: Degree of dilution. D degree of dilution, F_A cross section of added filler material, F_E molten base metal cross section. [9]

Based on planimetric evaluations of a cross section of a weld bead the dilution can be calculated. A definition is given in equation 2.

$$D = \frac{F_E}{F_E + F_A} \quad (2)$$

The dilution defines the intermixture of the two welded materials. The degree of dilution is the relation of the surface of weld penetration and the total weld metal surface, which in turn is the sum of the penetration surface and the added filler material.

It has to be clear that for practical purposes this value can contain a certain scatter of the results for it only depicts the degree of dilution at a certain cross section.

For this thesis' purposes the applied determination mode of planimetric evaluation represented a good method for estimating the degree of dilution. It is used as reference value for characterizing the weldments.

2.4 Absorptivity of laser beams

“When material processing with laser radiation the result is predominantly determined by the energy that is absorbed within a workpiece. A measure of the power, P_{abs} , that is available for the material treatment process is the absorption or absorptivity A . The absorptivity is defined by the ratio of the power that is absorbed within a workpiece and the total power of the incident radiation. The absorptivity can have any value between 0 and 1.” It is also referred to as factor of absorption or degree of absorption.[16]

$$A = \frac{P_{abs}}{P} \quad (3)$$

The degree of absorption plays a determining role in laser welding, especially when heat conduction laser welding. It directly defines the quantity of heat input to the weld pool, respectively the welding energy per unit length of weld bead (HI). Therefore the degree of absorption will determine the dilution of the welded materials and thus the weld quality.

The absorption factor is influenced by several parameters as [17] presents it in his

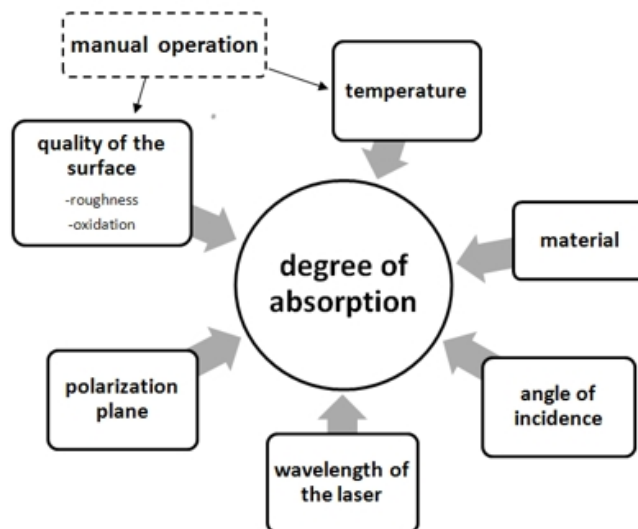


Figure 6: Influencing factors of absorption. [17]

dissertation. In order to perform a welding parameter optimization it is necessary to know and control as many influencing factors as possible. Figure 6 depicts these indicated influencing factors.

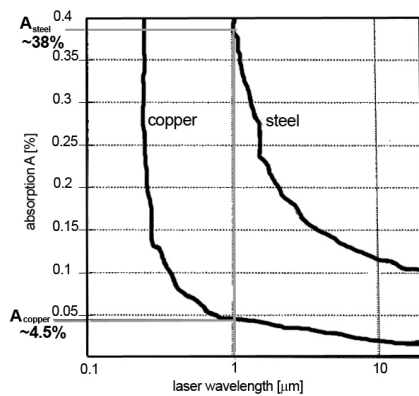
In addition to the rather concrete and general factors from Schneider [17] the specific manual welding method and specific way of manually preparing the probes can be considered as an important influencing aspect for the results of the weldments of this thesis.

Manual operations are influencing the absorption for the presented work via the surface quality on the one hand and via the personal judgment of the operator of the welding process on the other hand. This fact is schematically added to the image in fig. 6.

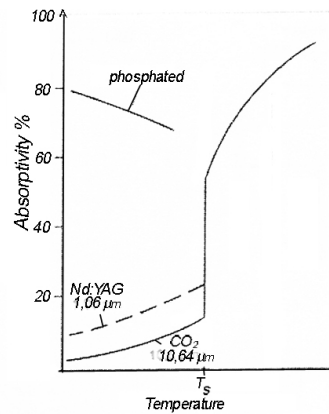
2.4.1 Material properties and laser wavelength

Metals and especially Cu and its alloys show a relatively very low absorptivity to Nd:YAG laser beams. However, Nd:YAG laser's wavelength is still better absorbed than the one of CO_2 -lasers.

Figure 7(a) shows the absorptivity of copper and steel for different wavelengths. Nd:YAG-laser's wavelength of $1.064 \mu m$ is indicated in the diagram. It can be derived that the absorptivity of copper is about 4.5% whereas the one for steel is as high as about 38%. This fact is of course problematic as both materials will be engaged during welding at the same time. The parameters however can only be set to result in an appropriate HI for one of the two materials at a time. Furthermore, it has to be taken into consideration



(a) Absorption of the laser beam as a function of wavelength for copper and steel. [17]



(b) Absorptivity increase at melting temperature and for coated surfaces. [12]

Figure 7: Absorptivity as a function of material characteristics. T_S ... melting temperature

that the absorptivity goes up once the metal melts. The increase is indicated by the graph in figure 7(b).

2.4.2 Polarization

This subsection introduces the term polarization. It points out the difference between a laser beam and common ray of light.

Laser radiation is generated by induced emission. Photons that are released from a induced transition of molecules from the laser medium from higher to lower energy levels form through amplification in a resonator the laser beam. These photons have the same wavelength, Nd:YAG-Laser: $\lambda = 1,064\mu\text{m}$, one unique direction of propagation and the electromagnetic radiation oscillates coherently, in same phase respectively. [18]

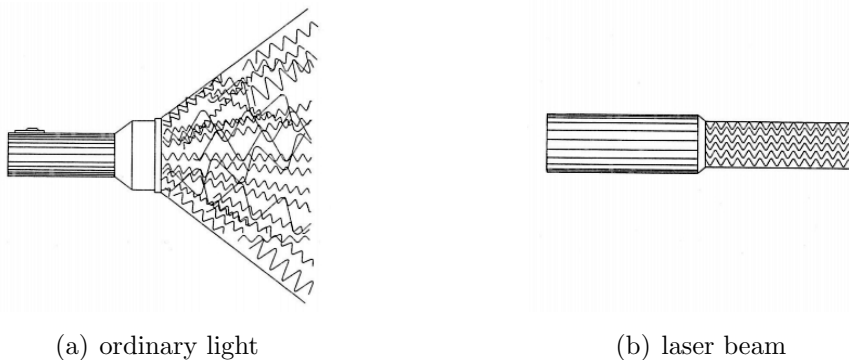


Figure 8: Laser beam vs. ordinary light. [18]

Fig. 8 shows an ordinary unpolarized ray of light in 8(a) and a polarized laser beam in 8(b). As it can be derived from this comparison an ordinary light source produces diverging radiation in terms of wavelength, phase relation and direction of propagation. Therefore an ordinary light beam will loose its intensity after a certain traveling distance. Furthermore it will not show integral reflection behavior when impinging on a surface. In contrast to that the waves of a laser beam will arrive coherently as depicted in the figure. The energy content of the waves is bundled and concentrated. This feature in the end makes lasers a well suited heat source for welding applications.

The propagation of light can be described by using a wave model. Out of that definition light is a transversal electromagnetic wave consisting of a electric and a coupled magnetic field. Both of them are oscillating at the same frequency. The vectors of the two fields are aligned perpendicularly to each other as shown in fig. 9.[19]

This specific oscillation state of the field strength is called transversal polarization. At transversal polarization different forms of oscillation can appear, e.g. linear, circular or elliptic. [20]

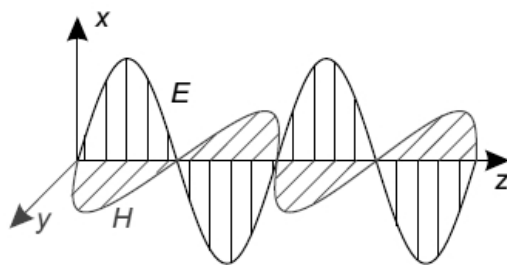


Figure 9: Wave model of light propagation. \mathbf{z} direction of propagation, \mathbf{H} electromagnetic field, \mathbf{E} electric field [19]

The polarization plane is spanned by the vector of propagation direction of the wave of the electromagnetic field. Two different planes of polarization can be distinguished. If the plane in which the electromagnetic wave of the beam oscillates is parallel to the impingement plane, the beam is **p**-polarized, fig. 10(a). If the electromagnetic wave oscillates in a plane perpendicular to the plane of impingement, the beam is **s**-polarized, fig. 10(b).[21]

2.4.3 Angle of impingement

For what regards the interactions with solids, the Fresnel formulae can be used to describe the reflection and the transmission of a plane harmonic wave incident on an infinitely extended ideal plane surface. Polarization of a laser beam changes impingement conditions as it changes the angle of incidence of the waves on the surface. The formulae distinguish perpendicular and parallel polarized waves.[16]

$$r_s = \frac{n_1 \cos \alpha - \frac{\mu_1}{\mu_2} \sqrt{n_2^2 - n_1^2 \sin^2 \alpha}}{n_1 \cos \alpha + \frac{\mu_1}{\mu_2} \sqrt{n_2^2 - n_1^2 \sin^2 \alpha}} \quad (4)$$

$$r_p = \frac{\frac{\mu_1}{\mu_2} n_2^2 \cos \alpha - n_1 \sqrt{n_2^2 - n_1^2 \sin^2 \alpha}}{\frac{\mu_1}{\mu_2} n_2^2 \cos \alpha + n_1 \sqrt{n_2^2 - n_1^2 \sin^2 \alpha}} \quad (5)$$

- r_s : reflection of filed amplitude for perpendicular polarized wave
- r_p : reflection of filed amplitude for parallel polarized wave
- μ_1, μ_2 : magnetic permeability of media
- n_1, n_2 : indices of refraction of media
- α : angle of incidence of radiation

The magnetic permeability μ is the magnetic conductivity of a material. It depicts how much better a material can conduct the magnetic field lines than air.[22] The index of refraction is an optical material specific parameter and depicts the relation of the propagation speed of light in vacuum and in the specific material. A good approximation is to define it to be 1 in air.[23]. Out of equations 4 and 5 it can be derived that the reflectivity depends on those two material specific values and the angle of incidence of the radiation. It has to be added at this point that the indices of refraction can be real values as well as complex ones and that the equations 4 and 5 are valid for both types of indices of refraction. For what regards the presented work it makes sense to set the index of the medium the laser approaches the weld spot n_1 to 1, as it is in a simplified view air or respectively shielding gas. Still, the refraction index of the material to be welded n_2 has to be, in general, set to:

$$n_2 = n + ik_e \quad (6)$$

n : real part of the index of refraction n_2

k_e : imaginary part of the index of refraction or the extinction coefficient

n and k_e depend on the plasma frequency and the frequency of the incident radiation, as well as the electron collision frequency. It is derived in [16].

The diagram in figure 10(c) shows the degree of absorption of a CO_2 -laser as a function of the angle of incidence for perpendicularly, s- polarized and parallel, p- polarized beams. On the one hand it can be derived that the degree of absorption strongly depends on the angle of impingement. On the other hand the great difference because of different polarization planes can be seen as well as the alteration of the difference over different angles of incidence. This diagram was calculated with the help of the Fresnel equations and is taken out of Beyer's book [11].

For what concerns the presented work the influence of polarization direction is not of great significance, especially if looking at the weldment at a macroscopic scale. The polarization of the laser beam as well as the angle of impingement are held constant. Variation in the result of weldments can therefore not be drawn back to polarization nor the angle of incidence. However, if one takes a closer look at the surface of a metal it becomes clear that the described dependence of the absorptivity will play a role for the weldments.

2.4.4 Temperature

The following passages are adapted out of book from E. Beyer [11]. Sections that are copied word by word are put under quotation marks.

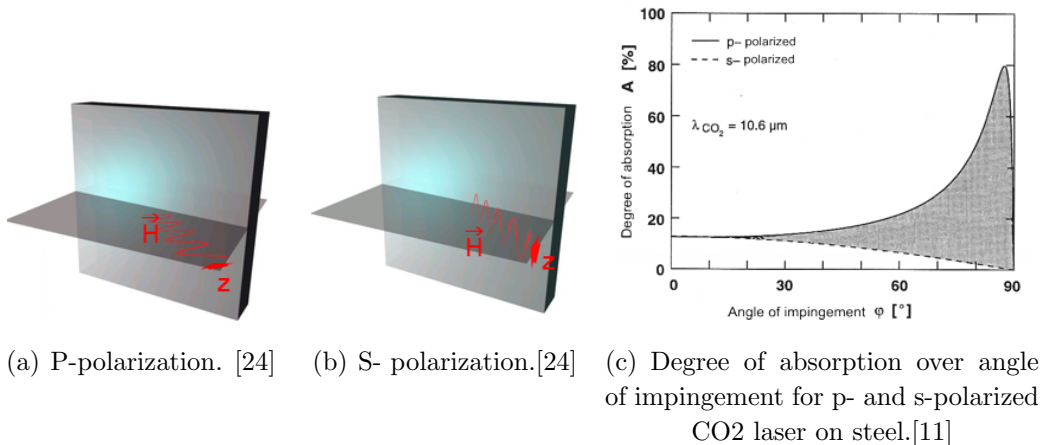


Figure 10: Polarization and the angle of impingement. \vec{z} : direction of propagation, \vec{H} : electromagnetic field

“A certain laser wavelength given the absorption factor is in an area of low absorbed intensities ($I < 10^4 W/cm^2$ for metals) a material specific temperature dependent optical constant. At metallic objects the interaction with laser radiation happens via the electrons in the conduction band. According to the band model electrons of a not replenished band in a solid act like classic free electrons. Because of their very small mass these free electrons of the metal can be moved relatively easily by the electric field intensity of the laser light. The absorption of a part of the laser light happens because the electrons can not move ideally free but collide with other particles and are therefore accelerated inside of the alternating magnetic field. This mechanism is called inverse Bremsstrahlung. Hence energy encapsulation (absorption) into matter happens because of impacts of electrons (in gases with atoms or ions, in solids with grid imperfections and phonons). The dielectric constant ϵ can be derived from the equation of motion of electrons. ϵ goes into the wave equation for the propagation of electromagnetic waves into medium.” [11]

A more exact derivation of why absorptivity is temperature dependent is given in [11] on pages 28 to 31. By summarizing his statements it turns out that the frequency of electron collisions is influencing the absorptivity. The frequency of elastic collision of free electrons consists of two components defined by the obstacles the electrons hit:

- collisions of the electrons with imperfections, dislocations and other lattice defects
- interactions of the electrons with phonons (lattice oscillations)

The elastic frequency of electron collisions is additively composed of these two types of collision:

2 Theoretical essays

$$v_c = v_{St} + v_{Ph} \quad (7)$$

v_{St} : frequency of collision of electrons with defects of the lattice

v_{Ph} : frequency of collision of electrons with phonons

v_{St} depends on the amount of defects of the lattice which is not temperature dependent. v_{Ph} increases with increasing temperature because the density of phonons in solids goes up with increasing temperatures following to 8.

$$v_{Ph} = C_1 T \quad (8)$$

C_1 : material specific constant

These two equations are valid for solid materials. Additionally they can be used as good approximations for metallic melts, for the short range order of the atoms as well as the movability of the free electrons only changes marginally at the phase transition from liquid to solid.

Summing up, an increase of the temperature increases the density of phonons in solids. Therefore the frequency of collisions of electrons with phonons goes up. Hence a change of temperature changes the absorption factor of a material.[11] [25]

This subsection shows that the relevance of the temperature dependence for the presented work is relatively low. The calculation of the absorption factor of high alloyed steel to a CO_2 -laser from [11] as a function of the temperature is exemplarily pulled up. It shows a relatively low influence at temperatures relevant for the presented work. Laser

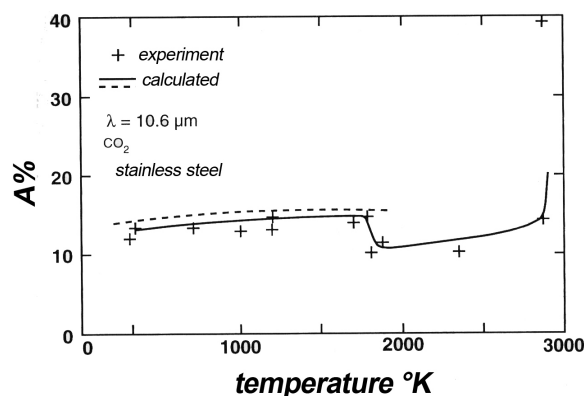


Figure 11: Absorptivity as a function of surface temperature for CO_2 -laser.[11]

welding is known for its very concentrated heat source. Considering this fact and additionally the high thermal conductivity of copper, which will prevent tremendous heating of the probes, the temperature dependence of the absorption factor is considered to not have much influence on the total amount of heat input for the presented work. Combining this fact to the values of E. Beyer's calculation [11] the influence of the substrate surface's temperature for the presented work is estimated to be negligible.

2.4.5 Surface quality

Roughness of a surface will determine the absorptivity. In order to determine the surface roughness of a workpiece the arithmetic average surface roughness R_a can be applied. Table 1 shows exemplarily the absorptivity of 1.6673 steel to CO_2 -laser when laser

Mechanical preparation	R_a [mm]	Absorptivity [%]
polished	0,02	5,15- 5,25
ground	0,21	7,45- 7,55
ground	0,28	7,70- 7,80
milled	0,87	5,59- 6,05
milled	1,1	6,35- 6,45
milled	2,05	8,10- 8,25
milled	2,93	11,60- 12,10
milled	3,35	12,55- 12,65
sandblasted	10,65	33,85- 34,30

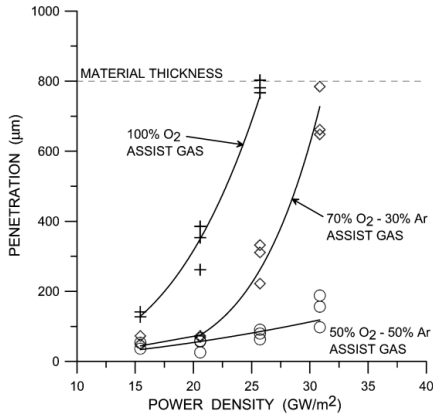
Table 1: Absorptivity of 1.6673 steel to CO_2 -laser radiation as a function of surface roughness R_a . [26]

welding as a function of the mechanical surface preparation and corresponding R_a . It can be derived that with some exceptions the absorptivity goes up with increasing surface roughness. In 2.4.2 the strong influence of the angle of incidence of the laser beam is presented, assuming ideally plane surface. When looking on a mechanically prepared surface with a certain R_a value at a microscopic scale it becomes clear that it is not plane at all. The rougher a surfaces is the more it will consist of differently inclined morphologies. These can be seen as radiation traps for incoming laser beam. Hence a higher R_a is supposedly increasing the absorptivity of a surface.

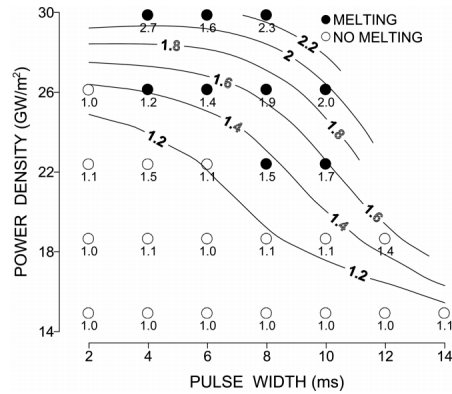
On the other hand coatings on the surface of a metal can increase the absorptivity, as it is indicated by the "phosphated curve" in fig. 7(b).

Oxidation of the surface

Oxidation will as well influence the absorptivity of laser radiation on metals. Investigations by [27] revealed the influence oxygen in the process gas has on the absorptivity when laser welding copper. Two digrams of his publication show the emphasizing influence oxygen has on the absorptivity of copper.



(a) Penetration of bead-on-plate welds with 100%, 70%, and 50% O₂ in Ar assist gases.



(b) Ratio of the effective absorptivity of Cu to 1.06- μ m wavelength light when a 100% O₂ assist gas is used to that when a 100% Ar assist increase of weld penetration with increasing power density gas is used vs pulse width and power density

Figure 12: Influence of oxygen on absorption when pulsed Nd:YAG laser welding. [27]

“It was found that the effective absorptivity of the Cu increased as the oxygen content of the Ar assist gas was increased.” [27]

The absorptivity at this study [27] was measured with an energy meter that detected the reflected laser radiation from the workpieces’ surfaces. Both diagrams in figure 12 are presented for good reasons:

First, fig. 12(b) shows that the use of oxygen instead of argon as shielding gas increases the absorptivity of Nd:YAG laser radiation by a factor of up to 2.7. The absorptivity was measured to always be at least the same and in the majority of cases higher when increased amounts of Oxygen were present at the weld pool. There are no comprehensive investigations of underlying reasons for this augmentation carried out in [27]. With regards to [27] it is believed that the presence of oxygen in the assisting gas causes oxide formation at the weld pool. This is because of high temperatures resulting from welding and the high content of oxygen in the welding spot from the shielding gas.

The second graph in 12(a) points out the strong increase of welding penetration due to an increase of absorptivity caused by the presences of oxygen inside the welding spot.

The intention of accurately hitting a certain degree of dilution in order to obtain qualitatively best welding results was mentioned already in 2.2.1. The welding penetration directly influences the degree of dilution. With the help of the presented graph the great significance of oxide formation on the surface of the copper for the presented work can be depicted.

Summing up, oxidation can significantly influence absorptivity and thus weld quality. This is also because the influence roughness has will disappear as soon as the top layer of the work piece is molten. However oxide particles will still be present inside the melting pool.

2.5 Welding residual stresses

Residual stresses are stresses that remain inside of a workpiece although external loads are removed. The reason why residual stresses exist is always an unbalanced strain situation. The formation of welding residual stress can be accounted to the three events shrinkage, quenching and transformation.[4]

The following remarks are adapted out of R. W. Messler's book [28] and describe the formation of residual stresses during fusion welding.

Residual stresses resulting from fusion welding are thermally induced. Thermally induced residual stresses result from a temperature gradient or a temperature change. Three causes for thermally induced stresses can be distinguished:

1. a volumetric change due to a change of phases: ∂V .
2. a difference of the coefficients of thermal expansion: $\partial\alpha$.
3. a temperature gradient: $\frac{\partial T}{\partial x}$.

The formation of residual stresses throughout a welding sequence is explained in fig. 13(a).

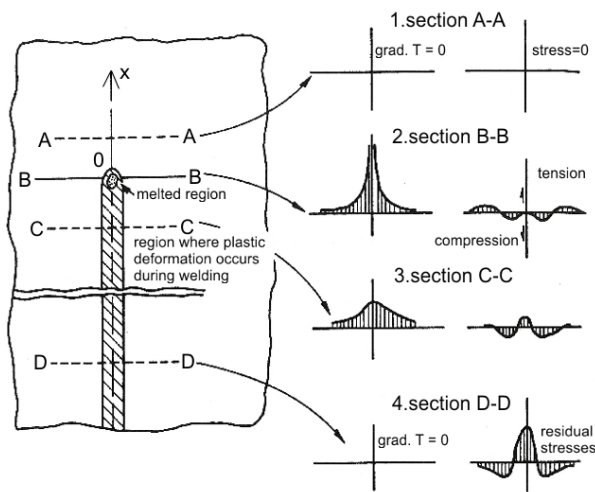
The figure schematically depicts a bead-on-plate weldment. The X-axis is aligned in welding direction. Four cross sections are described. Each represents a certain stage throughout a welding pass. The corresponding temperature and longitudinal stress σ_x profiles are depicted. The origin of the graph is always to be found on the weld center line.

Cross section *A-A* represents unattended base material. No temperature gradient and hence no stress profile appears here. Cross section *B-B* is taken right at the welding spot. The temperature gradient is steep. Right at the welding spot the melting temperature is reached. Hence, no stresses can form as the material is liquid here. Compression stresses appear around the welding spot resulting from thermal expansion. These stresses can not be transformed into strain as this area is countered by surrounding material that is colder and thus still has higher strength. The compression stresses are limited by the tensile strength which is temperature dependent. The weakened material at the center compensates the appearing stresses by deformation. The appearing compression stresses have to be balanced by tensile stresses at the outer ends of the profile to establish a mechanical equilibrium.[28]

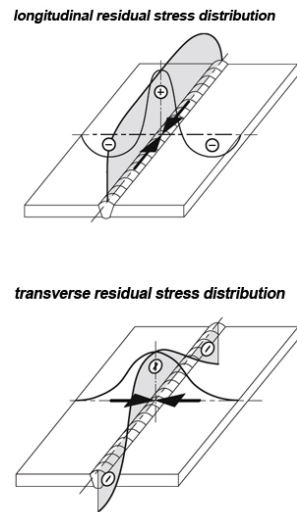
After considerable cooling tensile stresses arise in the center resulting from shrinkage. In this case compression stresses at the outer ends of the profile have to compensate in order to establish mechanical equilibrium. The so attained stress profile is depicted in cross section *C-C*. Further cooling will emphasize the latter described appearance until the temperature gradient finally diminishes, resulting in a final state of residual stresses

which is depicted in cross section $D-D$. High tensile stresses remain in the center of the fusion and heat affected zone. The profile is symmetric to the welding axis and has the its maximum in the center.[28]

Fig. 13(b) shows qualitatively the resulting stress profile alongside a whole welding pass' length in longitudinal (σ_x) and transverse direction (σ_y). It can be seen that tensile stresses in transverse direction are present in the center of the weld. Hence, the weld metal is teared away from the center in lateral direction there.



(a) Formation mechanism of longitudinal welding residual stresses, σ_x , for a bead-on-plate weldment.[28]



(b) Distribution of longitudinal, σ_x , and transverse, σ_y , welding residual stresses.[2]

Figure 13: Welding residual stresses.

2.6 Welding defects

Lange G. [29] divides weld defects into manufacturing and operation caused ones. This section describes the former ones, and therein cracks resulting from welding.

In this section an emphasized consideration is taken of formation mechanisms of hot cracking.

Additionally cold cracking, binding errors and pores are described.

2.6.1 Hot cracking

Hot cracks form during solidification inbetween liquidus and solidus temperature. Hence, the material separation happens in liquid respectively mushy state. According to [4] two types of hot cracks are to be distinguished.

Solidification cracks appear during solidification of the weld pool.

Liquidation cracks appear because of low temperature melting phases in the HAZ.[6]

“The main cause for the formation of solidification cracks is to be found in the metallurgically dependent formation of low melting phases which remain during solidification in the form of a liquid films at the grain boundaries of the primary solidified crystals.” [30]

Following this statement, the metallurgical composition of the weld metal, and especially the composition in front of the solidification front, plays a determining role. C, S, P, B, Nb, Si and Ti are mentioned elements which can favor the formation of low melting phases and eutectics. Therefore a higher content of these alloying elements can result in higher hot cracking susceptibility.[29]

In [31] various interacting factors that affect hot cracking susceptibility are mentioned. The author describes the following metallurgical and mechanical factors, recognizable by the accentuation of the terms in every single paragraph. The following statements are a summary from [31]. Literally overtaken passages are put into quotation marks.

“The *solidification range*, divided by the temperature gradient, gives the extent of the two-phase mushy zone.” An increased mushy zone will experience more shrinkage and hence higher shrinking strain, which in turn will leverage hot cracking susceptibility.

As long as *back-filling* is guaranteed arising material separations can be filled up with liquid. Crack formation can be healed. “The rate of flow is controlled by dendrite tortuosity, liquid fraction, fluidity and surface tension.”

“*Dendrite coherency* refers to the degree of solid-solid bonding between dendrite arms occurring at the ultimate stage of solidification within the mushy zone. An alloy with a large coherent region is expected to have a higher susceptibility to cracking.”

“Alloys with large *solute content*, and hence large *quantity of eutectic*, will be less susceptible to hot cracking. This is because:

1. there is less extensive coherent dendrite structure and
2. shrinkage can be more readily fed by means of back-filling due to a more open dendrite array.”

In the end this means a smaller ΔT during solidification.

The *surface tension* will influence the susceptibility to hot cracking by defining if there is continuity of liquid attained by wetting of the base of the dendrites at the very last stage of solidification. Whereas the two extreme situations, where complete wetting or no wetting at all occurs make cracking unlikely. All situations of partially wetting increase the susceptibility to hot crack formation.

“Solidification cracking normally occurs along weld metal’s *grain boundaries*. This is because segregations of solute or impurity elements preferably gather at grain boundaries. It follows that the grain shape, structure and size should have a profound effect on hot cracking susceptibility.” [31]

Porosity can on the one hand increase the susceptibility to hot cracking because the flattening and elongation of such pores can serve as crack nucleus. On the other hand pores can help to eliminate the need for back-filling and therefore counter crack formation. [31]

[31] additionally gives a summary of theories describing the following mechanical influencing factors.

Out of the *strain* theory of Pellini hot cracking occurs when an intergranular liquid film is strained beyond some critical value. Based on this theory Prokhorov [32] and Senda [33] established models where an experimentally determined critical ductility curve and the deformation curve are put in the same diagram. Cracking will occur where the two curves intersect. Fig. 14 depicts the diagram schematically. What is directly inherent to this model is the *strain rate*. “The slope of the deformation curve in fig. 14 can be related to the strain rate and the cooling rate as follows:”

$$\frac{d\epsilon}{dT} = \frac{\frac{d\epsilon}{dt}}{\frac{dT}{dt}} = \frac{\dot{\epsilon}}{\dot{T}} \quad (9)$$

Finally the *restraint* will influence the susceptibility to hot cracking. It is proven that high restraint does not necessarily result in higher cracking susceptibility. “The interaction of restraining forces and local weld strains, and specifically how this affects strain and strain rate in the vicinity of the mushy zone, is more important.” [31]

Some passages from literature reveal the possibility of hot cracking when dissimilar welding copper and steel.

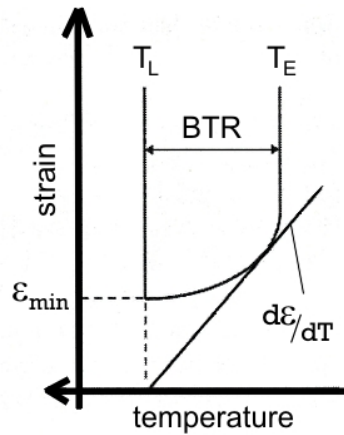


Figure 14: Critical ductility curve and deformation curve vs. temperature after Senda's theory. **BTR**... brittle temperature range, T_L ... liquidus temperature, T_E ... eutectic temperature.[31]

“The thermal expansion coefficient and thermal conductivity of copper are significantly higher than those of the low carbon-steel. Hence, during the welding process the large misfit strain and the residual stresses will be inevitably generated in the joint, leading to solidification cracking of it.” [8]

“When connection welding Cu and steel as well as Cu-plated steel, one has to be aware of the so called red shortness, also referred to as liquid metal embrittlement. In liquid state Cu and Cu-alloys can cause red shortness.” It appears only if there is tensile stresses existent in the steel weld metal during solidification.[34]

However literature reveals that if the welding is done properly crack formation can be avoided or at least reduced. “A copper-steel dissimilar joint free of defects can be obtained when the amount of copper dissolved in the molten steel is very limited.” [8]

Summarizing the hot cracking problematic with regards to the presented work, metallurgical problems when welding together copper and steel are described with the help of the binary phase diagram of Cu and Fe in fig. 15.

Limited solubility of copper in iron, and vice versa, can be derived from the diagram. Additionally the great divergence in melting temperatures can be seen, $T_{MFe} = 1536^{\circ}C$ whereas $T_{MCu} = 1084^{\circ}C$. This constellation results in a big solid-liquid-two-phases-region for alloys with copper contents from about 12% of copper. For alloys that solidify inside this region it can be imagined that liquid copper-rich phases are to be found in between already solidified steel crystals. In combination with solidification shrinkage this situation forms ideal conditions for solidification cracking as described above. According to this derivation three areas corresponding to alloys more or less susceptible to hot cracking are indicated in fig. 15. The classification is made regarding the welding

suitability because of hot crack formation as a function of metallurgic composition of the welding metal.

Area 1 corresponds to a degree of dilution of up to about 8,2 weight-% Cu in Fe. It corresponds to alloys of good weldability because of a very small solid-liquid-two-phases-region.

On the very opposite area no. 3 indicates in the same way bad welding suitability. According to this classification, area no. 2 reaches from about 8,2% to about 15 weight-% Cu in Fe and indicates alloys in-between of medium welding suitability.

The solubility of Cu in Fe is relatively high at about 1400°C but goes back down until Cu solidifies causing probable precipitation of liquid Cu phase. Due to high temperature gradients and high cooling velocities resulting from the specific welding application this apparition it is believed do not happen or to just partly happen. It is more likley that a in copper supersaturated steel matrix will form. Therefore partially weldability is estimated in area no. 2.

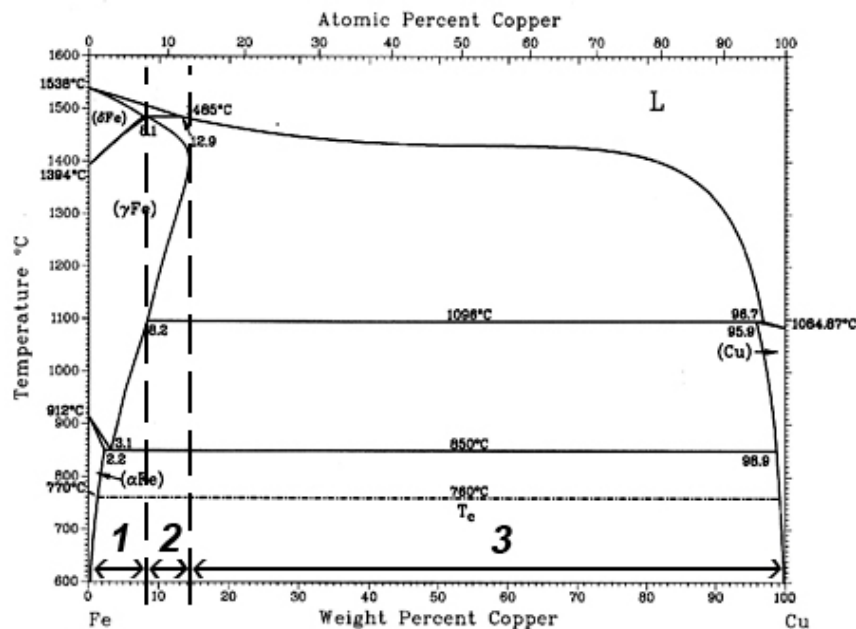


Figure 15: Binary phase diagram of Fe and Cu indicating phases compositions areas of differently good weldability.[35]

2.6.2 Cold cracking

“Cold cracking is one of the most common failure causes of high strength and hardness sensitive steels.” Cold cracks can appear in the coarse grained zone of the HAZ, the weld

metal and the heat affected overlay zone. Hardening cracking and hydrogen-cracking are to be distinguished. [29]

Hardening cracks appear in the coarse grained part of the HAZ where hard and brittle microstructures can not relieve welding residual stresses.[6] [29]

Hence, a crack sensitive microstructure and high enough stress levels are the prerequisites of hardening cracking.

Hydrogen cracking can appear if a over critical H-content has is in the material. H causes embrittlement of the material at the welding spot. If hydrogen diffuses into the coarse grained zone of the HAZ and is draped inside because of too fast cooling the material is supersaturated in H and therefore becomes even more brittle.[29]

A problematic of this cracking type is that it can appear during and some time after cooling down.[4]

Three cold cracking types can be further distinguished [4]:

- shrinkage cracks: appear if deformation is locally hindered.
- kerf or root cracks: appear because of geometric or metallurgic kerfs.
- lamellar tearing: appear in anisotropic and inhomogeneous materials along segregation lines.

2.6.3 Lack of fusion

“When dissimilar welding the danger of the formation of binding flaws is greater than when welding similar materials.” The reason for this can be accounted to the mismatch in melting temperatures and thermal conductivity.[36]

Binding flaws, also referred to as cold spots or as lacks of fusion, are unwelded points, between the base and weld metal, or even between single weld passes.[6]

As there is no metallurgical connection at these areas it is clear that it will cause a deterioration of the strength of the connection.

Dilthey U. [6] names the following causes for lacks of fusion:

- forerun of weld pool because of too high energy per unit length of weld
- welding on slag remains, oxide or tinder layers
- too low energy per unit length of weld

The relevance of lack of fusion for this thesis is shortly discussed in the following lines. The first point from the list has to be seen from this special application's point of view. The great difference in melting temperature of the two materials make the presence of inappropriate energy input per unit of length, if only at least for one of the two, very likely.

The second point emphasizes the already mentioned importance of the surface condition of the welded part, refer to page 28.

The third point is emphasized by the fact that the welding parameter optimization for the presented work is necessarily tried to be performed at the lower limit of necessary HI. The reason for this way of proceeding is mentioned on page 19.

In the end the probability of the forming of these kind of defects will strongly depend on the preparation of the parts to be welded and the manual skills of the welder, as well as an appropriately tuned process setting. This fact needs to be taken into special consideration as both, probe preparation and welding, are done manually for the presented work.

2.6.4 Pores

Pores are globular gas inclusion inside the weld metal. [37] Pores form during welding if dissolved gases can not exit the molten metal because of too fast solidification. These gases precipitate in molecular form inside globular cavities. Metallurgically and mechanically formed pores can be distinguished. [2] [4]

The following influencing factors are mentioned in [2]:

- solidification rate, and hence the welding method and the adjustment of the HI.
- quantity and type of dissolved gases, respectively the in proximities of the weld metal present gases.
- viscosity of the molten metal.
- properties of the welded metal, especially the solubility for gases and how much the solubility changes during temperature changes.
- diffusion coefficient.

2.7 Copper-Beryllium-alloys

This section introduces copper as a material and classifies its commercially available alloys. A more detailed classification and short description of different Copper-Beryllium-alloys (CuBe-alloys), as one of them is used for the presented work's weldments, is subsequently given. The overview is made with the help of the ASM handbook for material selection of non-ferrous alloys. [38].

Copper is known for its reddish color, its very good electric and thermal conductivity and its good corrosion resistance. Copper is one of the major commercial metals. Its application spectrum is very large. Cu-alloys can be found in very differing industrial branches, such as the electric industry as conductor material, applications for heat exchangers or apparatus engineering in the chemical field and wherever there is a need of special corrosion resistance. Copper and its alloys can be classified into five families with regards to their metallurgic composition:

1. copper, meaning commercially pure copper, containing less 0,7% of alloying elements.
2. dilute- or high-copper alloys , containing elements of less than 8% solubility in a Cu-matrix.
3. brasses, containing zinc as major alloying element.
4. bronzes, containing tin, aluminum or silicon as major alloying elements.
5. copper-nickels and nickel-silvers, which from a metallurgic point of view form complete solid solutions.

Cu-alloys can be classified into three groups regarding the applied strengthening mechanisms.

- *Solid-solution hardened alloys*: Inside this group, also modified solid-solution hardened alloys exist where elements are added to form dispersions to cause grain refining and strengthening. E.g. cobalt provides dispersion of intermetallic strengthening particles. This measure can help to increase the mechanical properties without losing too much of conductivity properties. Tin-bronzes are historically known and brass maybe is more common because of its everyday applications.
- *Age-hardenable alloys*: CuBe-alloys are to be found within this. Also referred to as beryllium-coppers, these alloys can be further classified into two groups.

1. beryllium contents reaching from 0,2% to 0,7% and total additions of nickel and cobalt of up 2,7%.
2. Highly alloyed beryllium-coppers can contain contents of 1,6% to 2% beryllium and about 0,25% cobalt.

The beryllium content increases the yield strength of those alloys. However, a higher Be-content reduces the thermal conductivity. Co and Ni addition help to restrict grain growth during annealing with the help of dispersion of beryllide particles in the matrix. Besides the age hardening response is increased and the tendency to overage or soften at extended aging times and higher aging temperatures is decreased.

- Besides there exist copper-alloys that are hardened by a *martensitic-type-hardening* process. Aluminum bronzes are to be rated among this group.

2.7.1 Weldability of copper

The weldability of copper depends on its oxygen content. Desoxidized coppers are generally better weldable. The problem arises from the formation of α -Cu-CuO₂ eutectic that is remelted in the areas that reach temperatures higher than 1065°C during welding. This low melting phases gather at grain boundaries. These films cause an embrittlement of the material. Additionally coppers high thermal conductivity enlarges the HAZ zone and the elevated temperature causes significant grain growth inside a wider range around the welding spot.

The tendency to absorb gases causes problems especially in hydrogen containing atmosphere where a diffusion of hydrogen atoms can cause embrittlement by the formation of vapor inside cavities.[39]

2.7.2 Weldability of age hardened materials

“It is best to weld beryllium-copper in the annealed condition with subsequent precipitation hardening.” [38] The reason for this is described in the following lines.

CuBe-alloys can be age hardened, see 2.7. The weldability of such alloys is according to [2] generally not good. The reason is to be found in the experienced complex ductility reducing structure change during solution annealing and reprecipitating, caused by the welding process. The two deteriorating mechanisms are described according to [2] and are depicted schematically in fig. 16.

1. Within a narrow region next to the fusion line the solved strengthening particles are over-aged, can not precipitate fully or arrange in an unfavorable way due to increased cooling velocity. The consequence of that is a decrease of the strength, hardness and especially the ductility of the material in this region.
2. For multiple alloyed materials it is likely that within the partly liquefied region next to the fusion line low-melting phases form or are remelted. In combination with the stresses due to welding hot cracking in form of solidification and liquidation cracking can appear.

In [2] Schulze recommends to control the HI very exactly in order to avoid the above mentioned problematics when welding age-hardened materials. One possibility would be to reduce HI as much as possible to reduce the reprecipitation in an unfavorable form.

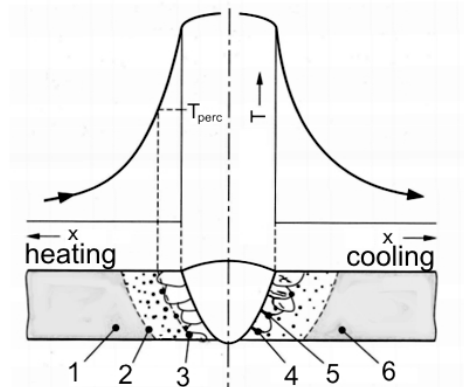


Figure 16: Microstructure changes in HAZ of age hardened material. Initial state: aged. **1** non-affected base material, **2** start of coagulation, **3** precipitations are fully dissolve, **4** reprecipitating of particles in unfavorable way, **5** possible formation of re-melting crack or hot cracks, **6** non affected base material. [2]

2.8 High alloyed steels

The deposition wires investigated in this work are based on high alloyed steels. These steels are special purpose materials with different specific properties such as high strength, corrosion resistance, tempering resistance or possible elevated operation temperatures.

2.8.1 Assorted relevant alloying elements

The microstructure of a high alloyed steel principally contains the same components as other steels, such as ferrite, austenite, perlite, bainite, martensite, carbides and partly intermetallic phases. Alloying elements for steels can be classified into two groups.[40]

- α -stabilizers, such as Cr, Si, W, Ti, V, Al.
- γ -stabilizers, such as Ni and Mn, and also C.

For C-containing steels a further distinction can be made.[40]

- Elements that preferably go into solid solution with the Fe-matrix, such as Si, Ni, Co, Cu, Al and partly Mn.
- Elements that preferably form carbides, such as Cr, W, Mo, V, Ti and partly Mn.

This section gives a discrete presentation of alloying elements which's influence on microstructure of steels are relevant for the presented work.

Chromium

Cr is one of the main alloying elements in high alloyed steels. It is added in contents from 0,3% to 30%. Cr is a ferrite forming element. The Fe-Cr phase diagram is depicted in fig. 19(b). Fe and Cr form a complete solid solution.

Cr and Fe form the intermetallic σ -phase, which forms at elevated temperatures.

Moreover special carbides Cr_7C_3 and Cr_4C form in steel of Cr-content higher than 5%. These carbides can also bind Fe-atoms and are then called mixed special carbides, e.g. $(Cr, Fe)_7C_3$. The advantage out of those carbides is that they can help to reduce diffusion velocity and form temperature resistant obstacles for dislocation movements.

This fact can increase the temper resistance and possible service temperature.

For what concerns mechanical properties, 1% of Cr added increases the tensile strength by 80 to 100 MPa whereas the elongation at fracture only decreases by 1,5%.

Cr decreases the critical cooling speed for martensite formation.

Because of the presented characteristics Cr-steels are in use as tool steels and are also applicable at elevated operation temperatures.[40]

Silicon

Si as a ferrite forming element is added to steels from 0,5% to 4,5%. A part of the Fe-Si binary phase-diagram is presented in fig. 19(f). It can be derived that an intermetallic phase $\epsilon(FeSi)$ forms from the liquid phase and the $\eta(Fe_3Si_2)$ phase in solid state forms at elevated Si-contents of 25%.

Ferrite can dilute Si up to 14 % at room temperature, whereat Si is randomly spread in the Fe-crystal for contents up to 6,5%. For higher contents Si-atoms arrange in a superlattice inside the Fe-matrix which can cause embrittlement. In C-steels only 5% of Si form composite carbides with cementite.

Si increases the tensile strength by approx. 100 MPa per additional 1% alloying content. Furthermore it increases wear resistance and through-hardening. Together with Cr it increases the resistance to forging scale formation. An important point for what regards hot working steels is its decreasing influence on C-diffusion and the so caused enhanced tempering resistance.[40]

Si is a desoxidizing element. It is used for solid solution hardening.[41] Regarding welding applications, Si increases hot cracking susceptibility, especially for austenitic steels. [2]

Molybdenum

Mo is a further γ restricting element. It has positive influence on corrosion resistance and mechanical properties at elevated temperatures.[40]

Mo is a strong carbide former, M_2C , M_6C and MC, and therefore plays an important role for secondary hardening.[41]

Mo forms intermetallic Laves-phase at contents of 2% to 3% and χ -phase. Mo can serve to reduce temper brittleness. [40]

2.8.2 Hot work steel

High temperature materials are used in high temperature operating machines or facilities. It is intended to maintain its mechanical properties at elevated temperatures.[42]

For what concerns a metallurgic classification, three different groups of high temperature steels can be distinguished.[42]

- Low alloyed high temperature mild steel is produced in normalized or annealed condition. This kind of steel is strengthened with the help of carbides and carbon-nitrides of the elements Cr, Mo, V, W, Nb.
- High temperature chromium steels are produced in annealed condition as well. They use the same strengthening mechanisms and are additionally resistant to forge scale forming because of elevated Cr content of 9% to 12%.

- High temperature austenitic Cr-Ni steels.

Tool steels are used for making tools for shape giving operations, such as cutting, drilling, forging or deep drawing as well as injection molding.[43]

A subgroup inside them are hot work steels, defined in the ISO 4948-1 and ISO 6929 standard as alloyed tool steel which's service surface temperature is above 200°C. Their field of application is to be found in forging, die molding and injection molding tools.[43] Hot work steels have medium C-contents of about 0,35% to 0,45%. Typical alloying elements are Cr, W, Si, Ni, Mo, Mn, V and Co. Good mechanical properties, namely strength and hardness for good wear resistance combined with sufficient ductility, and to maintain these properties at elevated temperatures are part of its characteristics. [44] [42]

The microstructure of hot work steels consists of tempered martensite with secondary carbide precipitations. This microstructure guarantees for the demanded properties. It is attained by special hardening and tempering sequences.[41].

Exemplary standard material numbers (AISI) from [43] are:

- Chromium steels: 1.2367 (H10), 1.2343 (H11).
- Tungsten steels: 1.2581 (H21), 1.2625 (H23).
- Molybdenum steel -(H42).

2.8.3 Weldability of high alloyed steels

The weldability of high-alloyed steels is generally worse compared to unalloyed steels.[2] As it was mentioned above, refer to 2.8.2, these steels can have very differing properties and alloying compositions. A general and exact statement on their welding suitability can therefore not be easily given.

Three aspects, all of them negatively influencing the welding suitability of the high alloyed steels, are separately mentioned at this point.

- High C-content and other alloying elements in combination with the high cooling rates resulting from welding will result in a expectingly high hardness of the weld material. The resulting embrittlement is known to be problematic for weldings in general.[2]
- The special properties of hot work tool steels are only attained through a very specialized heat treatment prior to operation.[41]

This heat treatment is not applied by the welding and therefore the deposited material can not be expected to have the same relevant properties.

- The chromium content is likely to cause the formation of the σ -phase. Already little contents of this intermetallic phase can cause embrittlement of the material.[40]

A general statement about weldability of this material is not intended at this point. The weldability theoretically is not good, but not said to be absolutely not existent. Literature reveals that tool steels are weldable if the necessary precautions are taken care of [45], respectively the appropriate and sophisticated welding methods are applied.[46] [47]

2.8.4 Microstructure estimation diagrams

CCT-curves

This section presents two CCT-diagrams in order to estimate the microstructure of the for this thesis used filler wires. 1.2343 hot work steel, which chemical composition is similar to the Laser Mold[®] 50 wire is depicted in fig. 17(a). 1.4718 valve steel is presented in fig. 17(b). Its chemical composition is the same as for Laser Mold[®] 10 wire, refer to page 61. It is intended to reveal the phases and hardness which can be expected with regard to the applied process.

The microstructure for the hot work steel consists of martensite with about 7% pearlite and approx. 27% of bainite and approx. 25% of ferrite and carbide, for a hardness of HRC 55.

For what concerns the 1.4718 steel the microstructure consists of martensite with carbides and less than 20% of ferrite with carbides, for a hardness of HRC 55.

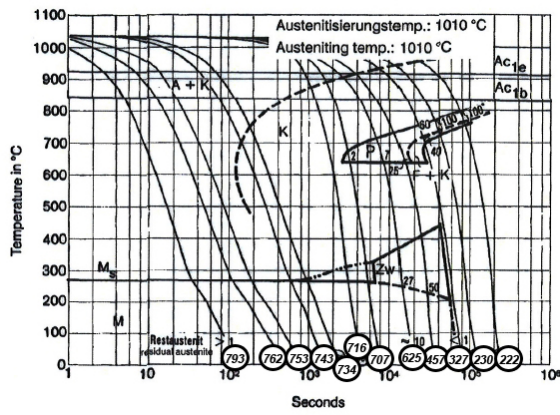
The relatively high content of martensite in combination with the expectingly high thermal stresses from the mismatch in thermal expansion coefficients make the intended cladding of this thesis theoretically prone to hardening cracking inside the deposited weld metal. Because of the same reasons shear stresses at the interface are possible reasons for material failure.

Schäffler diagram

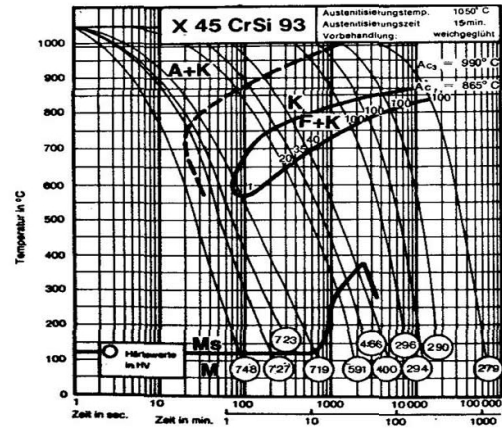
The Schäffler diagram is known as a measure when welding high alloyed steels to estimate the resulting microstructure. Further more it is divided into regions representing different areas of cracking mechanisms. [4]

For the two in the presented work used welding wires the Cr- and Ni-equivalent is correspondingly calculated and the results are depicted in the Schäffler-diagram in fig. 18. The Laser Mold[®] 10 wire is denoted by a square and is to be found inside the austenitic-martensitic region of the diagram. The Laser Mold[®] 50 wire is denoted by a cross and

2 Theoretical essays



(a) 1.2343 [48]



(b) 1.4718

Figure 17: CCT diagrams of 1.2343 hot work steel [48] and 1.4718/X45CrSi9-3 valve steel.

is to be found in the martensitic region of the diagram.

The Laser Mold[®] 10 wire is to be found inside the hot cracking area. The Laser Mold[®] 50 susceptibility to hot cracking can be estimated less. However it is found inside the cold cracking susceptible region of the diagram.

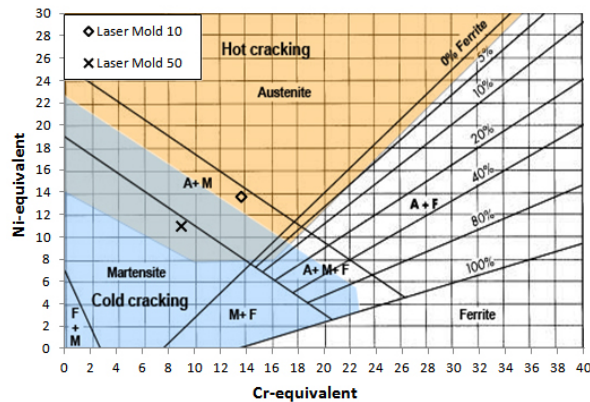


Figure 18: Schäffler-Diagramm for used deposition wires. [2]

2.9 Dissimilar welding of copper and steel

When welding dissimilar materials, as it is done in the presented work, additional aspects compared to welding of similar metals have to be considered.

In [39] it is stated that problems of weldability of dissimilar metals generally arise due to differences in the following physical, thermal and mechanical properties of the metals:

1. melting temperature T_s
2. density ρ
3. coefficient of linear expansions α
4. heat conductivity λ
5. crystal lattice (type and parameters)
6. type of binary equilibrium diagram

Additionally limited miscibility can cause local divergence of the metallurgical composition of the weld pool.[8]

The content of this diploma thesis basically is all about these problematics. Pohle [36] recommends to consider the following influencing factors when planning to realize a weldment of dissimilar materials.

1. Local position of the dissimilar joint within an assembly.
2. Choice of an adequate welding method.
3. Thermal expansion coefficient.
4. Metallurgical compatibility of the materials and of applied filler material.

The first point is anticipated for the presented work. MAHLE's wear problems appear locally on the surface of the core inserts, fig.2(c) p. 6. In order to fulfill their functional goals the weldments have to be placed right where wear appears.

The second point is partly defined, as the initial objective is to prove the applicability of the manual laser deposition process for the intended specific purpose. The welding method is not a parameter that can be adapted. It can be found in literature that welding methods which offer highly concentrated heat sources are best suited for dissimilar welding. Laser welding is clearly to be classified upon these methods and hence is estimated to be suitable. Additionally the used welding machine offers great potential for an accurate laser parameter optimization.

The difference in thermal expansion coefficients in combination with the fact that the

produced parts are used at elevated temperatures will very likely cause stresses at the interface during operation. This fact will as well increase residual stresses in as welded condition.

The last point is discussed more in detail in the following two sections. According to [36] two aspects are worked out:

1. Crystallographic similarities and atomic radii are compared. They will influence the type of interface that forms.
2. The possibility of the forming of intermetallic phases is discussed. This is done on the one hand by considering binary phase diagrams of the main involved elements. On the other hand it is done by introducing the electronegativity as a reference value for the possibility of intermetallic phases to form.

For simplification reasons instead of the specific CuBe-alloy and the specific type of steel the corresponding elements, mainly Fe and Cu are used. This kind of abstraction is believed to offer qualitatively valid statements.

2.9.1 Crystallographic similarities

C. Pohle mentions in [36] that the connection of two materials can be estimated the better the more their physical and chemical properties resemble. “At the interface the atoms of the materials orientate according to chemical and physical properties.”

The physical properties of involved elements are presented in table 2. It can be derived that numerous differences exist.

However, not only the material parameters will determine the connection’s strength. “The metallurgic transition the forms at the interface of two different phases during solidification depends on the temperature cycle resulting from welding and, idealized, on the grid type and the atomic radius of both the material. Solidification mechanisms can be associated to heterogeneous nucleation. The thermal conditions during welding given almost always heterogeneous nucleation occurs.” [51]

With regards to found scientific publications connections between steel and Cu-materials are laser-weldable. Two exemplary statements are depicted:

“A complete metallurgical bond was obtained at the interface between copper plate and the steel plate in the present study.” [8]

“SEM micrography of the specimen showed that both H13 tool steel and 41C stainless

values at room temperature	Fe	Cr	Cu	Be
grid type	BCC	BCC	FCC	HCP
atomic radius CN12 [pm]	127	128	128	112
Mendeleev-number M	61	57	72	77
Pauli-electronegativity	1,83	1,66	1,9	1,57
melting temperature °C	1535	1857	1083	1287
thermal conductivity $W/(mK)$	78	87	390	190
thermal expansion coef. $10^{-6}/K$	11,7	6,6	16,6	11,3

Table 2: Physical properties of relevant elements. [36] [49] [50]

steel were successfully deposited on copper alloy substrate. Sound deposits with crack free and pore free interfaces were observed in both deposits. Both the interfaces show characteristics of sharp transition between cladding and substrate materials.” [7]

2.9.2 Forming of intermetallic phases

When welding two dissimilar metals the formation of intermetallic phases can be problematic. “Based on the location of two metals within the periodic table one can deduct if a homogeneous welding together is possible or if it is likely that intermetallic phases form.” [36]

In terms of chemical properties intermetallic phases are to be placed at a transition point of solid solutions and non metallic bondings. They are therefore also referred to as intermediate phases. The greater the ratio of atomic bonding inside such a phases is the more it is brittle.[36]

Little contents, precipitated as seam on grain boundaries, can make a material completely brittle. That is why problems appear when welding dissimilar metals that form intermetallic phases.[2]

Binary phase diagrams

A good tool to estimate the weldability of two materials is to consider binary phase diagrams. Although these diagrams refer to equilibrium states, which can never be attained during welding because of too fast temperature cycles, it can help to predict solubilities and possible formation of intermetallic phases.

Fig. 19 shows binary phase diagrams of possible combinations of the main alloying elements of the for this thesis used metals . A Si-Fe diagram is added as it represents the second main alloying element of a used filler wire during experimental studies. The diagrams are analyzed one by one regarding welding suitability in terms of solubility and formation of intermetallic phases. Interaction are not taken into considerations at this stage.

- Fig. 19(a) shows the binary phase diagram of Iron(Fe) and Copper(Cu). It can be derived that the solubility of Cu in Fe is limited. Whereas it is still 12% at temperatures of about 1400°C it approaches 0% at room temperature. This fact is to be considered to have negative influence on the weldability, especially when comparing the big difference in T_s of the two elements. However a possible forming of intermetallic phases can be excluded with regards to the diagram.
- Fig. 19(b) shows the binary phase diagram of Fe and Chromium(Cr). It can be derived that the two elements form a complete solid solution. However the forming of the σ -phase is known for Fe-alloy with high Cr content. With regards to an expectingly small Cr-contents in the weld metal of the weldments of this work the formation of the σ -phase is believed to be unlikely.
- Fig. 19(c) shows the binary phase diagram of Cu and Cr. It can be seen that these two elements form a complete solid solution. The formation of intermetallic phases is not derivable. Hence, the welding suitability of these two materials is good.
- From fig. 19(d) it can be derived Fe and Beryllium(Be) have limited solubility in solid state. An ϵ and χ intermetallic form at high Be contents. Again, the relatively even lower content of Be in the weld metal of the weldments of this work are believed to not negatively influence the weldability.
- Fig. 19(e) shows the binary phase diagram of Cr and Be. It can be derived that two intermetallic phases form. $CrBe_2$ forms at approx. 73 weight-% of Be in Cr. $CrBe_{12}$ forms at contents of approx. 33 weight-% Be in Cr. It can be further derived that low melting eutectics form at approx. 1220°C by the Cr and $CrBe_2$, by the two intermetallic phases and by $CrBe_{12}$ and Be as well. This constellation is for sure more problematic when compared to the other phase diagrams that have been mentioned so far. However the intermetallic phases form at relatively high Be

contents and the absolute Be content of the envisaged material combination is low. Hence this problematic's influence on the overall weldability is again considered to be low.

- Fig. 19(f) shows the lower section of the Fe-Si binary phase diagram. Si is the second main alloying element of one of the steel filler wires used. It can be derived that two intermetallic phases form whereas $FeSi$ forms directly from the melt at Si contents of approx. 33 weight% in Fe. It can be furthermore derived that the intermetallic phase forms a low melting eutectic (1195°C) with α -Fe. This appearance can be considered to be problematic during welding. Low melting phases enable the formation of hot cracks. From this point of view the second intermetallic phase is considered to be less critical as it forms in solid state only. Nevertheless embrittlement inside the weld metal because of the two intermetallics can be assumed.

However, the relatively high solubility of Si in Fe is positively influencing the welding suitability.

Summing up this analysis, the weldability of the envisaged material combination is partly given. Because of restricted solubility of Cu in Fe, and the other main alloying elements the dilution is to be kept as low as possible. Out of the other diagrams it can be stated that the formation of intermetallic phases must be considered.

Electronegativity

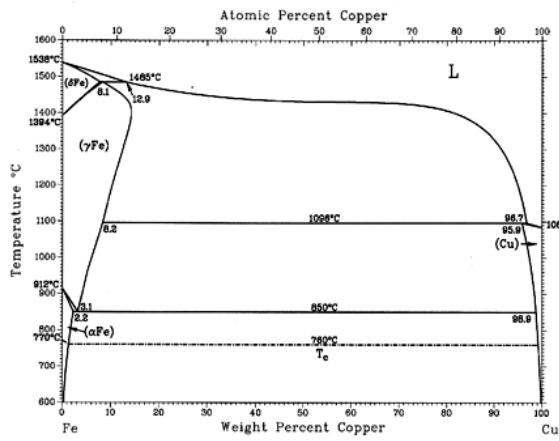
The electronegativity is a structure controlling factor for the formation of alloys. It can help to assess if two materials are likely to form intermetallic phases or to form a solid solution. "The ability of an atom to bind an electron out of the outer shell of a neighbor atom into its own sphere of activity is referred to as electronegativity." [36]

The greater the difference in electronegativity of two elements is the greater is the possibility of a formation of an intermetallic phase. Together with the atomic radius the electronegativity is used to build darken-gurry ellipses. Those diagrams are based on the Hume-Rothery rules and help to assess the solubility of different elements in a reference element. [36]

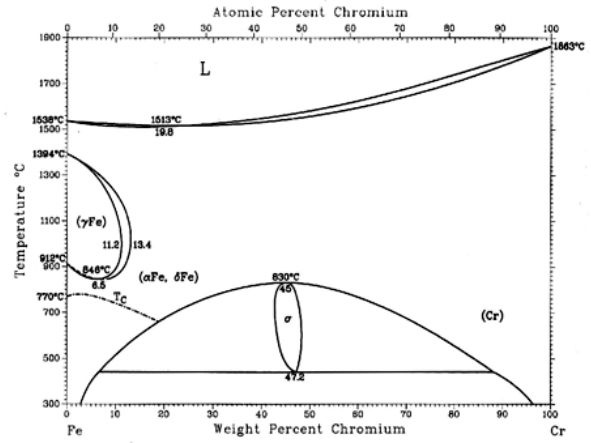
A further development of these ellipses was published by E. M. Sawitzki and G. S. Burcharow. [36] A diagram of this type is presented in fig. 20 for Iron(Fe) as reference element. It displays the electronegativity above the atomic radius and draws two ellipses around the reference element. The smaller one indicates the forming of solid solution and the bigger one elements with restricted solubility. [36]

For what concerns Fe and Cu they can be found inside the smaller ellipse. This fact indicates good preconditions for weldability.

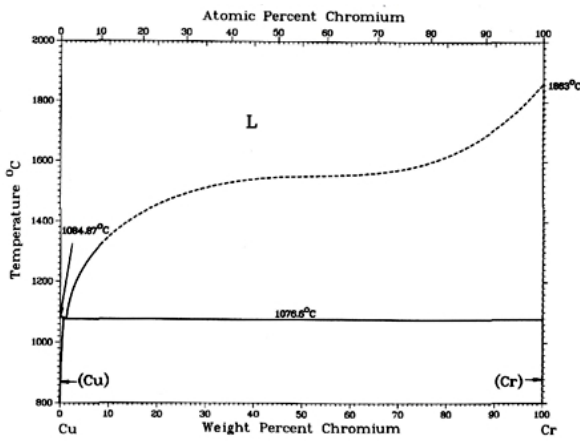
2 Theoretical essays



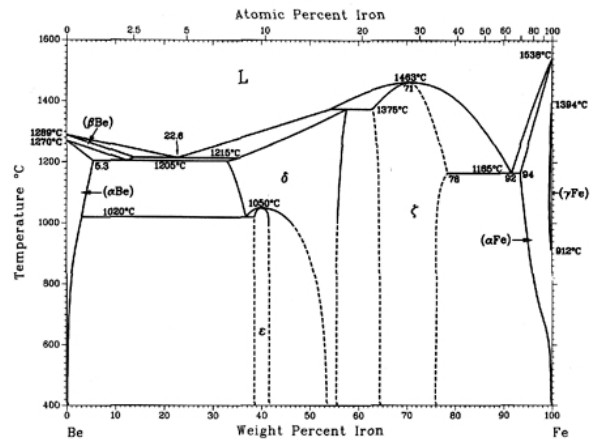
(a) Fe-Cu [35]



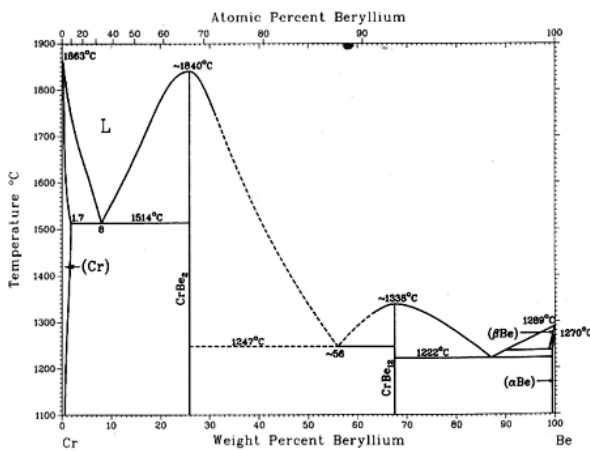
(b) Fe-Cr [35]



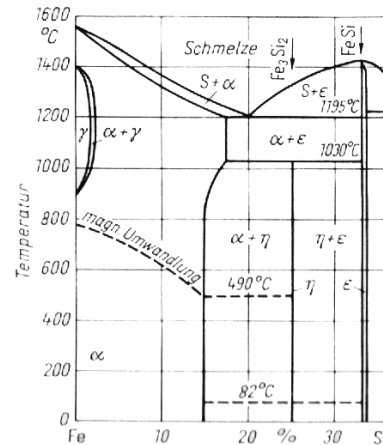
(c) Cu-Cr [35]



(d) Be-Fe [35]



(e) Cr-Be [35]



(f) Fe-Si [40]

Figure 19: Binary phase diagrams of selected main alloying elements. [35] [40]

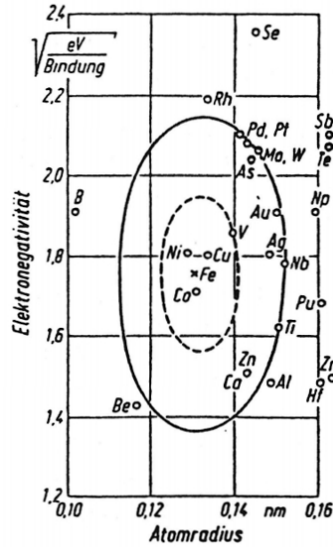


Figure 20: Sawitzki-Burchardow ellipses for Iron. [36]

2.9.3 Buffer layers

A measure to avoid problematics of dissimilar weldments is to apply a buffer layer inbetween the two welded metals. This can help to smoothen the metallurgic and physical incompatibilities. The following appearances can be countered [2]:

- intermetallic phases.
- martensite.
- low melting phases.

FCC materials and especially Nickel and Ni-base materials could prove to fulfill the mentioned improvements. This is because of their fcc lattice, and hence good ductility, and the fact that they form complete or extended solid solutions with a high number of other metals.[2]

Especially for deposition weldments [2] mentions the following advantages of Ni-base buffer layers:

- welding residual stresses can be coped with easier, and crack free, by means of plastification.
- the ductile buffer layer can stop cracks to save the welded part. This is especially valid for hard facing and armoring applications.
- avoidance of brittle intermetallic phases.

The applicability of a Ni-base buffer layer for this work's purpose can also be derived from the Sawitzki-Burchard diagram in fig. 20. Fe, Cu and Ni are to be found inside the smaller ellipse, indicating good preconditions for welding.

However, an example from literature reveals that the application of a fcc steel buffer layer for a tool steel on copper substrate cladding could not bring about improvements in terms of bond strength. "The bond strength was higher in the directly clad H13 tool steel compared to the H13 tool steel clad with 41C stainless steel as buffer layer." [7]

3 Experimental

This chapter describes the experimental realization of this thesis. The applied conceptual approach and way of proceeding are introduced. The descriptions comprise, besides the sequence of carried out experiments and corresponding purposes, the used devices, materials and examination methods for weldability investigations.

This chapter finally also describes the modeling and assumptions for the FEM-simulation carried out for estimating the deterioration of the heat transfer by deposition welded core inserts.

3.1 Welding experiments

The concept for the experimental part of the presented work envisioned an approach that characterizes the process' capabilities in terms of weldability of the dissimilar weld from the very bottom up, and continuously gathers knowledge on its influencing factors. The goal was an optimized weld to serve as a reference for the technology's capabilities. The gained experiences and insights were used right away for incrementally improving subsequent experiments. This results in a methodology that initially uses rather simple "tryout experiments" and becomes more and more systematic in terms of parameter variation on the one hand, and more sophisticated in terms of experimental setup and proceeding on the other hand. Out of that the sequence of the experiments can be divided into two experimental series phases.

1. **VR0-experimental series (VR0)**: An initial process characterization to find a possible laser parameter window, and subsequent studies on additionally the result of the weldments influencing factors.
2. **VR1-experimental series (VR1)**: Basic welding parameter optimization of two different material concepts, based on the finding of VR0-ES. VR1-ES also persisted of the welding of samples for tensile-shear strength measurements.

Table 3 and 4 depict all carried out experiments and corresponding experiment numbers. For each series the purpose of the weldments is mentioned. An additional column in each table indicates where the experiment protocol can be found in the appendix of the report.

The applied numbering system of the welding experiments is finally introduced in this section. Every performed welding was assigned a unique number so it is clearly identifiable afterwards. The system is described by means of an example depicted in fig. 21. The first two letters of the number are only used for symbolic recognition reasons. They

3 Experimental

experiment series no.	description of the purpose of the experiment series	no. of welds	Addendum
VR0.1.	initial parameter tryouts for process' capabilities assessment	6	A1
VR0.2.	further parameter variations based on VR0.1 in order to improve welds' soundness	5	A2
VR0.2.6.	different welding technique try-outs based on VR0.2	5	A2
VR0.3.	welding results repeatability study elevated T_V and welding speed scatter study	8	A3 A4
VR0.3.9. VR0.3.10.	process studies on additional influencing factors	20	A5 A6
VR0.4.1	welding suitability study for 0.4mm X35CrMn7-2 wire	3	A7

Table 3: VR0: process and influencing factors characterization experiments.

experiment series no.	description of the purpose of the experiment series	number of weldments	Addendum
VR1.i.1-19 i=1... 4	parameter optimization for material concept 2 (Ni-base buffer)	29	A8
VR1.j.21-32 j=1... 3	parameter optimization for material concept 1 (steel-direct-to substrate)	23	A9
VR1.5. ...	tensile shear strength testing probes at optimized parameters	6	A10
VR1.6. ...	tensile shear strength testing probes at too high HI and reference steel-to-steel probes	6	A11

Table 4: VR1: parameter optimization experiments.

VR 0. 1.9.1
1. part 2. part 3. part

Figure 21: Applied experiment numeration: an example.

stand for the German term “Versuchsreihe” which can be translated to “experimental series”. The second part of the number indicates the experiment phase this weldment was carried out in, 0 for the initial process characterization phase and factor studies, 1 for the parameter optimization phase.

After a separating dot the third part of the number identifies with the help of an incremental and within one experimental phase unique number the exact weldment. Separating dots inside this third part of the numbers indicate a temporally or by a different purpose caused change over during the experimental proceedings.

3.2 Used materials

3.2.1 Substrate: AMPCOLOY® 88

AMPCOLOY® materials are wrought copper alloys of different alloying compositions, used for MAHLE's injection molding tool core inserts because of their high thermal conductivity in combination with their relatively good tempering and wear resistance. These two characteristics appear contrariwise. Within the for such purposes provided alloys AMPCOLOY® 88 represents a certain trade-off, as it has medium thermal conductivity and medium mechanical properties for wear resistance. Additionally it provides good machinability. It is delivered in age hardened condition in blocks or bars of different dimensions. Its material designation code is C17500 for US ASTM standard [52] and is 2.1285 in DIN 17666 norm [52]. The chemical composition as provided by the supplying company is given in tab. 5. The main mechanical and physical properties are in given in tab. 6.

Be	Co+Ni	Others	Cu
0,5%	2,5%	0,5%	residual

Table 5: Chemical composition of AMPCOLOY® 88. [52]

AMPCOLOY88 age hardened	
Tensile strength R_m	890 MPa
Yield strength R_{p05}	680 MPA
fracutre elongation A_5	14 %
Young's modulus E	130 GPa
hardness	270 HB30
Density ρ	8.75 g/cm^3

Table 6: Mechanical and physical properties of AMPCOLOY® 88. [52]

Substrate plate preparation

This section of the report describes the preparation of the CuBe-substrate probes at MAHLE tool making department. For welding experiments all probes are prepared manually and the same way. Therefore the surface quality in terms of roughness is macroscopically the same. Nevertheless, with regards to the meticulousness of the welding method a certain local scatter of the surface condition in terms of roughness as well as oxidation has to be expected. Due to this microscopic topographic divergence because of manual sandblasting and due to manual cleaning of the probes it is believed that the surface morphology and oxide layer forms stochastically resulting in a surface of locally different absorptivity characteristics.

AMPCOLOY[®] 88 was chosen to be the substrate material of investigation in accordance with the tool design department. The definition of a single substrate material is necessary to reduce the high number of possible influencing factors. Plates of 152mm x 70mm x 2mm are wire cut from an age hardened raw material block. The plates are sandblasted right after cutting to remove pollution from cutting lubricants and manufacturing edges. Just before experiments the plates are sandblasted again to remove possible oxide formation and pollution during storage. The manufacturing department indicates a surface roughness of about $R_a = 12\mu\text{m}$ for this surface finishing method. This corresponds roughly to what was found in literature and is presented in tab. 1. Besides a cleaning function this method can help to increase the low absorptivity to laser light as well.

After that the areas for deposition weld are marked with the help of a metallic scriber. During welding the temperature increases at the welding spot and the nearby areas. This will emphasize the oxide coat formation around the weld bead and therefore even more increase absorptivity for subsequent welding in areas of the HAZ. All beads are distributed equidistantly on the plates with enough distance to avoid metallurgical change of the substrate material from previous weldments.

During the final preparation step before welding the plates are cleaned with 70% alcohol to remove fat films and other pollutions.

An exemplary documentation image of VR0.2 welding series is presented in fig.25(d). Besides the placing of single welds on the substrate it is also shown how metallography probes are subsequently extracted.

3 Experimental

C	Cr	Si	Mn	Fe
0.45%	9%	3%	<1%	residual

Table 7: Chemical composition of λ aser Mold[®] 10 wire.

C	Cr	Mo	Mn	Fe
0.35%	7%	2%	< 1%	residual

Table 8: Chemical composition of λ aser Mold[®] 50 wire.

3.2.2 0.5mm λ aser Mold[®] 10 wire

This wire is recommended to be used for reparation weldments of broke out edges and surfaces of blanking dies, and drawing and bending as well as injection molding tools. It's hardness in as welded condition is 55-60 HRC. [53] The same alloy is known from gasoline engines to be used as inlet valve shaft material and has the DIN material number 1.4718.[42] The yield strength of this steel is approximately 1200 MPa. It is resistant to shock-loads and harsh environments. [42]

This wire was used for all VR0-ES weldings. The reasons for its choice were its availability and mainly the high hardness. Its chemical composition is given in tab. 7.

3.2.3 0.4mm λ aser Mold[®] 50 wire

This wire is recommended to be the ideal material for repair-welds of injection molding tools. It's hardness in as welded condition is 50-58 HRC. [53]

This wire was chosen for VR1-ES weldings because it only had little less hardness in as welded condition compared to λ aser Mold[®] 10 wire and was, according to the supplier less susceptible to hot cracking. Its chemical composition is very similar to a typical hot work steels. The chemical composition is given in tab. 8.

3.2.4 0.5mm JOKE[®] Fill 120 wire

This wire is a Ni-base filler material that has good crack resisting properties. It is recommended to be used for ductile and high-strength base and buffer layers for similar and dissimilar joints. Its hardness in as welded condition is 220-250 HB. The max. breaking strain is 46%. The tensile strength is 700-780 MPa. Its chemical composition is given in tab. 9

C	Cr	Mn	Nb	Fe	Si	Ni
0.2%	19.5%	2.8%	2.5%	1.9%	0.5%	residual

Table 9: Chemical composition of JOKE[®] 120 Fill Ni-base wire.

3.3 Weld bead structures

This sections introduces the structures of the produced multi-pass welds and the two material combination concepts that are applied for the parameter optimization in VR1-ES.

All for initial weldability estimation reasons produced weldments of VR0-ES are welded like it is schematically depicted in fig. 22(a). The numeration corresponds to the sequence the beads are placed during welding.

For the influencing factor studies of VR0-ES single pass weldments direct steel cladding were performed with the λ aser Mold[®] 10 wire.

For VR1-ES a smaller bead built-up was done. It is introduced in fig. 22(b) and fig. 22(c).

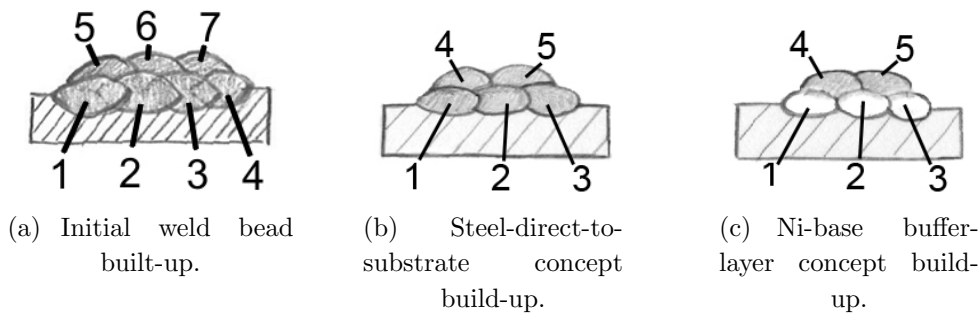


Figure 22: Schematic sketches of weld bead structures. **shaded gray** protective steel layer, **white** Ni-base *JOKE*[®] *Fill 120* bead, **light gray ruled** *AMPCOLOY*[®] 88 substrate plate.

3.4 Laser welding device

In this section of the report the laser device that is used for welding experiments at MAHLE's tool making department is described. Technical specifications of the machine as well as a detailed step by step description of the proceeding and handling of the operator during welding is given. A major part of this thesis' experimental realization consists of the characterization of the welding process. More detailed knowledge of the specific way of manually operating can help to understand some of the findings. A more detailed description is therefore assumed to be relevant.

The type designation of the welding apparatus is *AL Flak 300 mobil*. *AL* stands for **A**lpha **L**aser which is the manufacturing company. *Flak* describes as an abbreviation the intended field of application of the device. '**F**lexibler **L**aser zum **A**uftrags- und **K**onturenschweißen' means in English 'Flexible Laser for Deposition and Contour Welding'. *300* depicts the medium output power of the device in Watt. The apparatus is flash lamp pumped and works in pulsed mode. A Nd:YAG (neodymium-doped yttrium aluminum garnet) crystal is used as solid-state laser generating media. One advantage of it generally lies in its mobility and flexibility. The machine is basically intended for manual operation and is mainly used for repair welding at MAHLE's tool making department. However the *AL Flak 300 mobil* can also work in semiautomated mode by disengaging single axis from manual control to constant numerically controlled feed motion. Moreover it exists the possibility of fully numerical controlled operation mode by communication with a suitable software and CAM routine via an electronic interface. The device can basically be used like a robot. Even complex geometries can be welded. Its automated mode is not in use yet.

The following lines describe the procedure for manual operation in more detail. This represents the modus operandi during most of the experiments of this work. Contrary to weldments with the help of automated machines, manual operation causes scatter. This fact plays an important role for this welding method and represents a main field of interest for this thesis.

With one hand the operator controls the movement of the laser over the work piece in three independent linear axis with the help of an analog joystick. The degree of inclination defines the moving velocity in the corresponding direction. Welding speed of the process depends on the welder's individual evaluation of the weld pool formation. A built-in stereo microscope is used for the observation of the process. The magnified image allows for accurate positioning within some tenths of millimeters. The focus of the microscope corresponds to the laser's which the operator takes advantage of to adjust the height of the laser's focus on the surface to be welded.

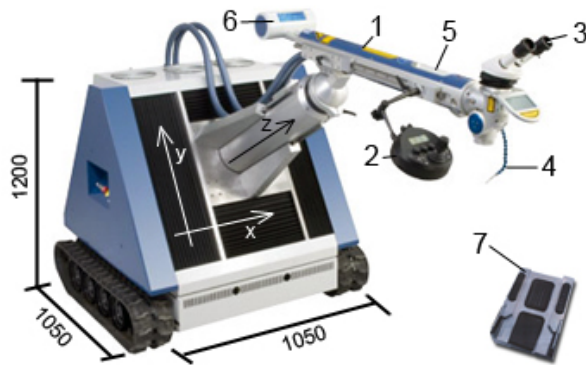


Figure 23: AL Flak 300mobil. **1** laser arm, **2** analogical joystick, **3** stereo-microscope, **4** shielding gaz nozzle, **5** laser parameter input panel, **6** process info display, **7** foot-switch [54]

With the other hand the operator applies the deposition wire. Counter-pressure exhibited by the weld pool lets the operator judge the right amount of wire to be deposited. Preliminary the gas nozzle has to be adjusted manually as well. The nozzle is flexibly mounted on the laser arm. Therefore it follows it's movement during welding and therefore constantly protects the weld bead and the surrounding area. Welding is initiated by triggering down a foot pedal. First, shielding gas starts flooding the welding spot, and subsequently the laser starts operating.

During experiments of this thesis the welding is done bead by bead. After a weld bead is finished the operator cleans the surface of the weld with the help of a glass fiber brush. A second bead can be welded after that. Normally weldments are done at 50% overlap. Deposited beads are about 0.1mm to 0.5mm of height and width, depending on the welding parameters and the diameter of used wire. These numbers shall emphasize the understanding of how meticulously this welding method works. This welding method allows for a very accurate optimization of the weldments by adjusting the HI. However, the high number of variable parameters represents a challenging task for a parameter optimization.

Fig. 23 shows the apparatus and the mentioned components as well as the main dimensions of it. The three controllable linear axis are displayed. The X-axis represents the main welding direction for the experiments. The y- and z-axis are used only for correction of the intended weld bead's direction. Fig. 24 shows the operator during welding.

parameter	range	adjustment step
laser-lamp-condensator voltage (U_L)	200V-500V	+/- 2 V
impulse length (L_I)	0.5ms -20ms	+/- 0.5ms
impulse frequency (F_I)	0Hz-25Hz	+/- 1Hz
impulse form (I_F)	0-100 % of max. power	lin. adjustable curve over impulse length
welding spot diameter (D_{WS})	0.2mm-2mm	+/- 0.1mm

Table 10: Adjustable laser parameters for AL Flak300 mobil.

Laser parameter adjustment

Via an input panel the heat input per unit of length (HI) can be accurately adjusted on the used device. The heat input per laser impulse can be set very accurately via the parameters presented in table 10. The welding speed together with the parameter setting of U_L , L_I and I_F , which will define the energy per laser impulse, will result in a defined HI. The laser diameter D_{WS} defines the energy density at the weld spot. The manufacturing company recommends to set this parameter to the double of the diameter of the used filler wire for standard weldments.

A major part of this work consists of finding a proper combination of the welding parameters for this specif intended application. For VR0-ES initially U_L , L_I and F_I are varied to find a first appropriate parameter window. For weldments of VR1-ES only U_L is used for further optimization of the appropriate HI.

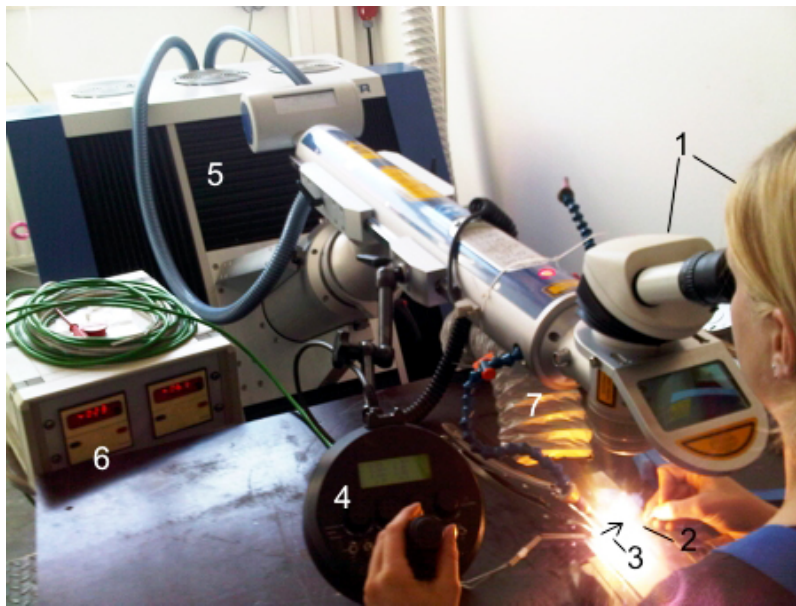


Figure 24: Handling of AL Flak mobil 300. **1** operator surveilling weld on stereo microscope, **2** right hand filler material provision, **3** welding spot and welding direction, **4** control joystick and axle velocity adjustment panel, **5** laser source, **6** two channel temperature measuring, **7** fumes suction system

3.5 Welding experiment setups

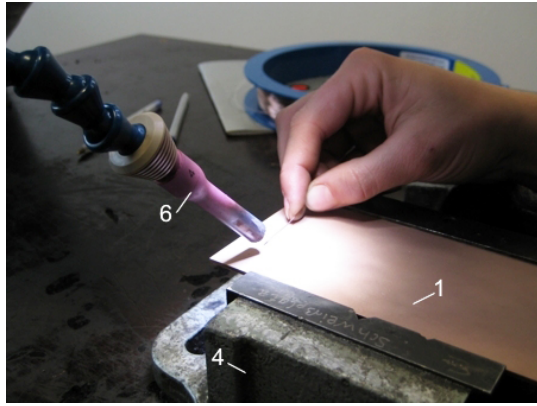
This section of the report describes the welding setups that are established for the single experiments. Different setups are applied corresponding to the attained knowledge of external influencing factors and the purpose of the intended investigations. The substrate plates are clamped. For initial welding experiments no further settings are used, fig. 25(a). Temperature measurements of the substrate's surface are carried out manually with the help of a pyrometer for this setting.

After a first set of experiments a preheated stainless steel plate and later a controlled heated plate is used as support to investigate the influence of preheat temperature T_V . The latter of the two settings is shown in fig. 25(b). A thermocouple is clamped in between the substrate plate and the heating plate to measure T_V .

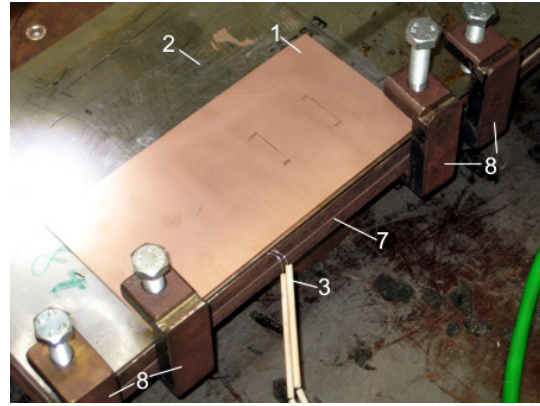
Once T_V 's influence evaluated, the setup is again readapted in terms of temperature measurement. A more accurate two channel temperature measuring device is installed to measure the temperature at the surface of the substrate online from the provided display during welding, fig. 24. Two thermocouples are clamped between a stainless steel plate and the probe plates. The setup is presented in fig. 25(c). The temperature was measured at two corners of the welding plate and twice during one welding pass, first right before the beginning and right after the end of the weldment. A maximum T_V can be estimated with the help of this setup.

Besides their functions as a clamping aid for the thermocouples the stainless steel plates act as insulator. If T_V is increased too high due to the welding heat the steel plate can be exchanged.

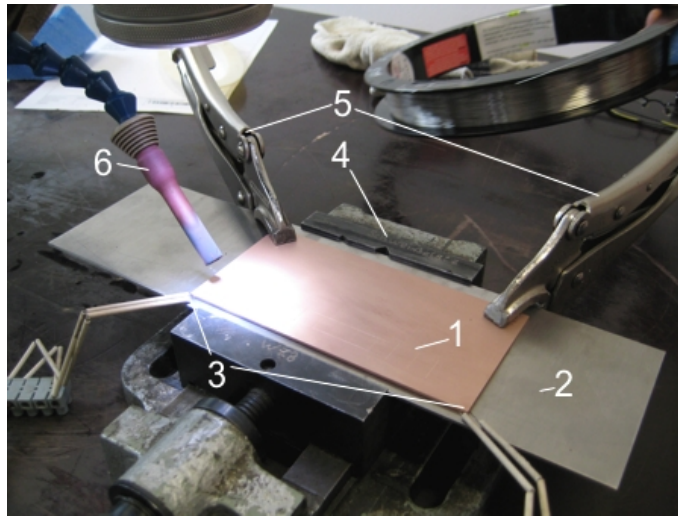
3 Experimental



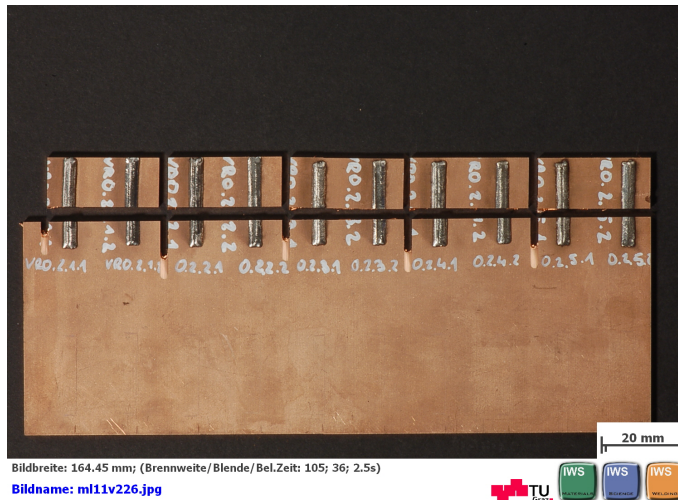
(a) Initial experimental setup.



(b) Experimental setup for T_v study.



(c) Improved experimental setup during VR1.



(d) VR0.2: Sample extraction.

Figure 25: Experimental setups at MAHLE and metallography probe extraction. **1** substrate plate, **2** heat storing stainless steel support plate, **3** thermocouples, **4** vice, **5** gripping pliers, **6** shielding gas nozzle, **7** controlled heating plate, **8** screw clamp.

3.6 Investigations

This subsection describes the examination methods of the produced welding samples.

3.6.1 Metallography probe preparation

The welded samples are extracted from the substrate plate and cleaned. At randomly chosen spots, however rather in middle of the weldments, in order to avoid influence from transient conditions, the beads are cut perpendicularly to weld direction to form cross sections, fig. 25(d).

The welding samples are hot embedded in Struers Multifast BlackTM. Metallography cross sections are prepared by standard procedures which are not explained in detail. Only the used devices are mentioned and especially developed proceedings that were necessary because of the specific materials are described.

Grinding

Principally, grinding and polishing was done in standard automated mode with the help of Struers Tegra Pol-31 equipped with a Struers Tegra Force-5. A main difference compared to conventional probe preparation is that starting grinding disk's graining needed to be of P500 maximum, due to the inhomogeneity of the samples, resulting from the divergence of the mechanical and chemical properties of the welded materials. Furthermore the grinding forces were reduced to "small" values (approx. 20N to 60N per sample) and the grinding time on the other hand was increased to 3min.

This procedure was necessary because otherwise deep scratches in softer the Cu-substrate material which could not be removed with grinding disks of smaller granulation later on are inevitable. In order to determine and accurately measure defects in weldments a kindly blank surface is necessary.

Polishing

Polishing was realized with $3\mu\text{m}$ and respectively $1\mu\text{m}$ polish pastes in automated mode at again low forces (approx. 15 N to 35N). The same device as for grinding is used. The finish is done with UPS-polishing liquid, directly spilled on the polishing disc in small splashes. For the final 15 seconds of polishing a small splash of ammonia solution is added to the polishing disk. For the very last few seconds the polishing disk was intensely cleaned by rinsing with a water sprinkler for the last few revolutions. After polishing the probes are immediately cleaned with alcohol to stop chemical attack. This procedure leads to best results in terms of residual scratches inside the Cu-substrate.

Etching

In tab. 11 different etching approaches are summarized. The etching was partly problematic because of various materials present in one single sample that react differently to the single etchants.

etchant (mixing succession)	application	purpose
50ml HCl (4.) 10ml HNO_3 (3.) 5g $FeCl_3$ (2.) 100ml H_2O (1.)	3-6s. bath etching at room temperature	microstructure of weld metal of X45CrSi9-3 and CuBe-alloy at short exposure time macro etching structure of -"- at longer exposure time
V2A stain 0,2-2ml Sparbeize (4.) 10ml HNO_3 (3.) 100ml HCl (2.) 100ml H_2O (1.)	up to 30s bath etching at approx.60-70°C	macro etching of X35CrMoMn7-2 and CuBe-alloy
20ml glycerin (3.) 20ml HNO_3 (2.) 50ml HCl (1.)	50s up to 1min 30s batch etching at room temperature	macro etching of X35CrMoMn7-2 Ni-Base-alloy and CuBe-alloy revealing mainly the boarder line inbetween the different materials and slightly the micro structure of Ni-Base-alloy

Table 11: Etching methods for metallography.

3.6.2 Optical microscopy

A ZEISS Observer.Z1m is used for optical microscopy of the cross sections. Axiovision software is used to set color, brightness and white balance adjustments automatically. To reveal some specific details these adjustments are partly done manually. This is the reason why the same probes may show different optical appearance, especially in terms of reddish colors. Diverging contents of red color make it difficult in some pictures to display exactly equal color impression. An exponential saturation curve was partly used to increase visibility.

3.6.3 SEM

For SEM investigation a *Leo 1450 VP* is used. For material contrast images *PE* recording is used. For topographic images a *SE*-detector is used. The specific adjustments is written in the information bar at the bottom of the presented images. The SEM-device is equipped with a EDX sensor from *Bruker* which is used for element mappings and line-scans.

SEM imaging is used twice throughout the presented work.

First, fractography of opened crack surfaces was made. A cut is manually made with an ordinary saw from the bottom of the substrate material up to approximately beneath the crack initiation at the interface. After that the probes are trenched in liquid N_2 and broken open along the crack. The low temperatures enable brittle fracture of the steel layer. With the help of this method it is possible to expose the crack surface alongside welding direction. The proceeding is schematically shown in fig. 26. A macroscopic view with topographic details of the formation at the interface is available, as well as an EDX-analyses from inside the weld metal. Partially EDX-mappings and SEM topography images are overlaid.

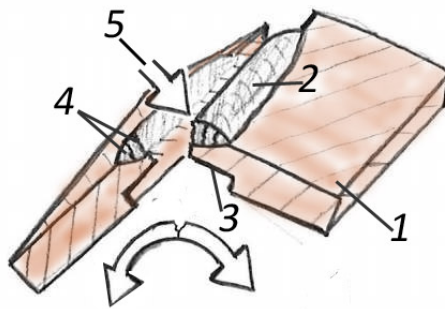


Figure 26: Schematic sketch: Exposure of crack surface. 1 substrate plate 2 deposited weld 3 sawed notch 4 cracks in cross section 5 viewing direction for SEM.

Second, topographic views of the fracture faces on the substrate plate of the sheared off mechanical testing sample are produced.

EDX analyses are made of the above mentioned broken open crack surface as well as of cross sections of weld of different degrees of dilution. The fracture surfaces are EDX-scanned as well to reveal whether the material separation happens in the weld metal or in the substrate material.

3.6.4 Weld defects measurement

Metallographic images from various cross sections of VR0-ES are loaded into the freely available software *Datainf Measure 2.1.2.22 Demo* [55] for defects measurements in the weld metal. The surfaces of defects inside the cross sections are measured by manually fitting of polygons on the image. After defining the right scale, which is given from the microscope's image automatically the software delivers the corresponding μm^2 . Besides assessing the defects also the dilution can be estimated by using this approach.

In order to obtain more data, same welds are partly examined several times. On the one hand both cross sections that result from the above introduced cutting method are embedded. Furthermore by grinding off at least 1 mm of the already investigated samples it can be used for an additional examination. The subsequent metallographic "re-preparation" opens up a different cross section of the same weldment.

Three different error types are distinguished for assessing the amount of defects inside the weld metal:

1. cracks reaching to the surface
2. cracks not reaching to the surface
3. lacks of fusion

Pores were besides some single exceptions not encountered inside the weld metal and were therefore not taken into consideration during defect measurement. Surfaces of every single defect type are summed up and the total surface is calculated. In order to have comparable values those absolute surface values are put in relation to the total surface of the weld metal. In that way a comparison of the single weldments is possible. The purpose of this proceeding is to determine the a possible connection of the weld's soundness, determined by the amount of defects in the weld metal and the degree of dilution. Furthermore it is intended to differentiate between different types of defects. The overall goal of this actions is to identify optimized welding parameters. Fig. 27 shows a screen-shot of the used software during an exemplary measurement.

3 Experimental

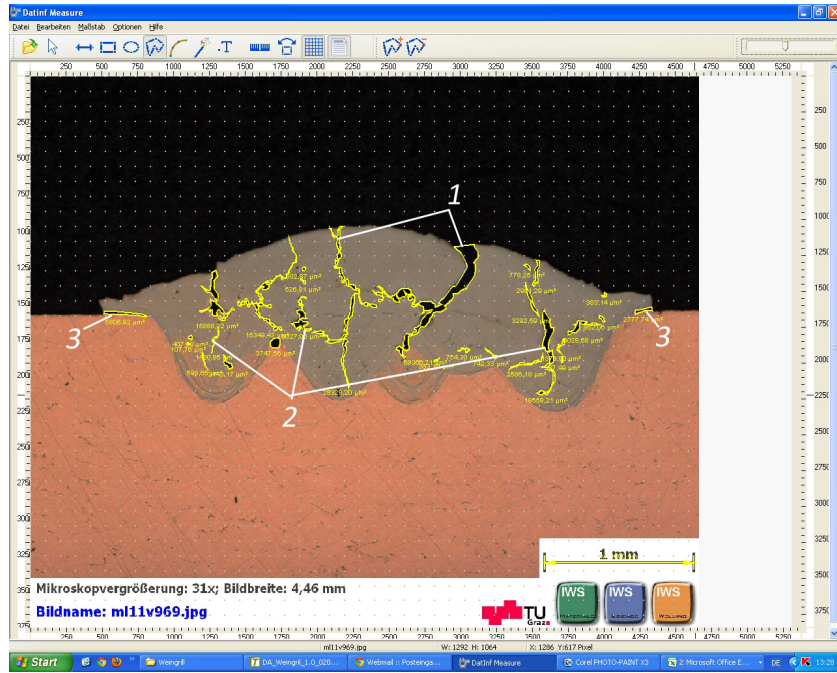


Figure 27: Screenshot: *Datainf Measure* manual measurements of defects in weld metal. **1** cracks reaching on the surface **2** cracks not reaching on the surface **3** binding errors.

3.6.5 Macro hardness testing

Single HV1 hardness measurements are carried out with the help of a *EMCOTEST MIC 010* automated hardness measuring device. Measuring with small load is necessary because of the small weld beads.

As MAHLE's hardness demands are given in HRC scale a converting software is used, [56] [57] The software exists in two versions, using different standards (DIN 50150:1976 / ISO 18265:2003). The differences are identified to be negligible for the purposes of this work.

3.6.6 Hardness line testing

Hardness lines are drawn on welding beads, reaching from the top of the beads down into the substrate material. This is done with the help of a Reichert and Jung MEF3 light microscope and a MHT-4 Microhardness tester from Paar. The lines are drawn manually and their exact location measured afterwards manually with the help of Axiovision[®] software. The results are finalized in MS Excel worksheets.

3.6.7 Shear test

Shear strength measurements are carried out for the presented work. A *Zwick Typ:RMC 100* tensile testing machine is used. A special purpose shearing jig to be mounted in the machine was designed. The jig is adapted from an ASTM-standard for mechanical properties measuring of deposition welds on boilers.

The experiments were chosen to be done like this instead of a common tensile test in order to measure the mechanical properties of the deposition weldment right in the interface. The probes are clamped with the help of a force closure into the tensile testing machine, fig. 28(a).

Tensile shear testing jig

This subsection introduces the functionality of the specially designed jig for testing the shear strength. Fig. 28(a) shows the jig mounted in the tensile testing machine. The fixation and shear off loading of the weld sample can be seen more in detail in 28(b).

The jig consists of two cuboids milled from raw material blocks of 1.2312 steel. The cuboids are steppedly milled and fixed together with the help of two screws. A gap is left in-between at the top which is steppedly narrowed at the top. This feature forms a rectangular sharp edge with a guiding slot for the probes. The guiding slot is manufactured 0.1mm wider than the probe's thickness. The edge at its lower end is used as the shear off counter part. The load applying half of the jig is hardened to guarantee form stability.

At the lower end of both the cuboids 25mm holes are drilled and chamfered. A bolt is slid through the holes of the jig and the fixture of the tensile testing machine for mounting the jig. The resulting pivot joint allows for vertically straight positioning and avoid bending moments during loading. For the experiments the lower cross beam of the tensile testing machine moves downwards. Hence, a vertical force is applied to the weld, resulting in a shear stress inside the interface. The movement of the cross beam is continued until the weld bead is sheared off. This is considered as the maximum attainable shear stress, the shear strength in the interface.

Tensile shear testing probes

The substrate plate for the tensile shear strength testing probes are prepared out of AMPCOLOY®88 and equally manufactured and treated like the probes for metallographic investigations of the welds.

After welding the deposited beads are partially removed by milling parallel to welding direction. The milling cutter is guided right on the surface of the substrate plate. The remaining weld metal forms a perpendicular edge on the surface of the substrate. This

3 Experimental

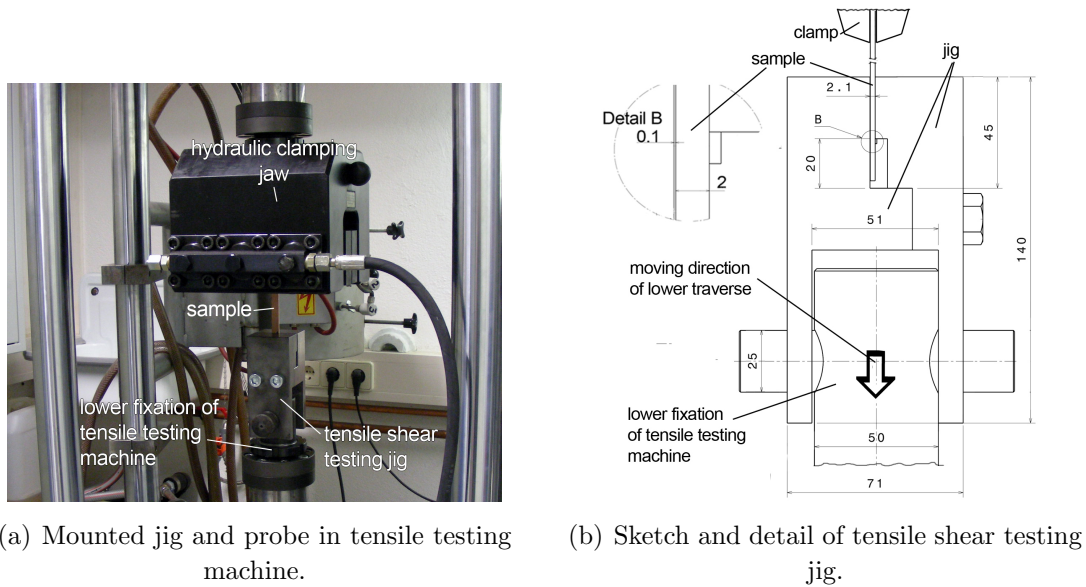


Figure 28: Tensile shear strength measuring.

geometric edge was used to apply the shear-off force from the jig's edge mounted on the tensile testing machine, as described above. Out of the so obtained plate stripes of equal width are cut out.

Before the experiments the exact dimension of each interface was measured for stress calculation later on.

Fig. 29(a) depicts schematically the procedure for probe preparation and where cross sections are examined for corresponding metallography examinations. Two samples which were accordingly prepared for a test run are presented in fig. 29(b).

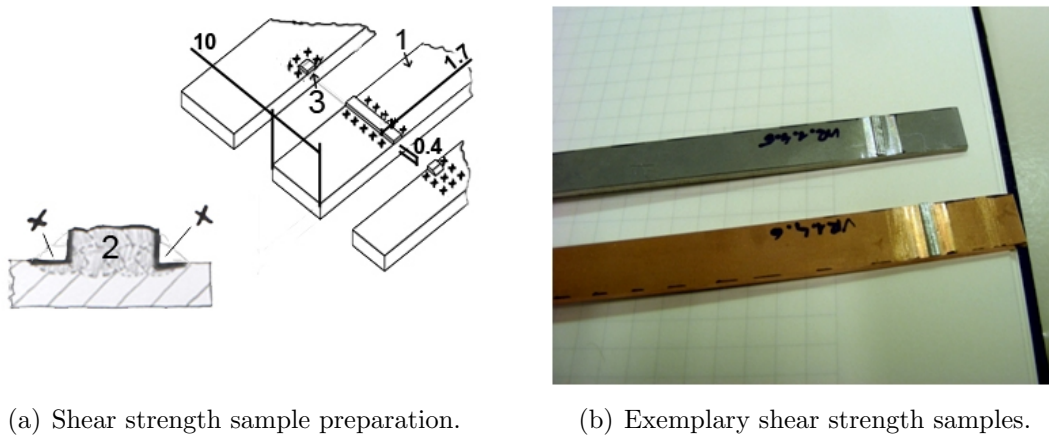


Figure 29: Shear strength samples. **1** strip of substrate material, **2** deposited and machined weld material, **3** cross section examinations, **X** by machining reduced weld bead.

3.7 Heat transfer simulation

A FEM-simulation is carried out in order to estimate the deterioration of heat transfer of the AMPCOLOY[®] core inserts caused by a steel deposition weld. The simulation is realized with MATLAB[®]. The applied routine is taken out of the course “Ausgewählte Kapitel aus Numerische Methoden in der Physik” held by Prof. H. Sormann from the Institute of Theoretical and Computational Physics of TU Graz and is implemented for this work’s purpose.

3.7.1 Modeling

Fig. 3.7.1 depicts how the simplification from a real core insert to the final simulation model is done.

The real part is simplified in a first step to a 2D rectangular geometry. In the center a cooling channel is modeled. On the outside of the rectangle a layer of injected PA66 plastic mold is modeled. The dimensions are adjusted to data from MAHLE’s tool design department.

In a second abstraction step the model is simplified to a 1D geometry. The cooling channel is modeled at the bottom boundary edge. On the upper side the PA66 layer is still present as the heat source. The FEM-mesh is refined at the core insert surface to allow for varying steel layer thicknesses.

This final simplified model is used for the MATLAB[®] simulation.

The exact heat transfer coefficient from the plastic mold to the core insert’s surface is not known. Therefore in-between the PA66-layer and the surface of the core insert a 1mm “ α -layer” is modeled. This layer’s thermal conductivity and density is set to half of the values of PA66. This measure should depict the decrease of heat flux in this area.

3.7.2 Assumptions

Boundary conditions

- The thermal properties are assigned to the corresponding elements in the mesh. A PA66(30%GF)-, a 1.2343- and AMPCOLOY[®] 88-layer is accordingly modelled.
- The edges limiting the core on the lateral sides are defined to be adiabatic.
- The outer edges of the PA66 meshes are as well defined to be adiabatic.

3 Experimental

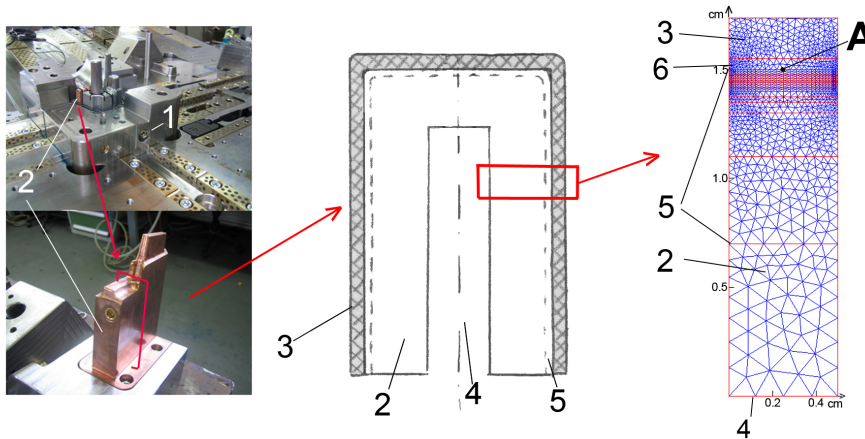


Figure 30: Modeling of the heat transfer simulation. **1** opened injection molding tool, **2** AMPCOLOY® core inserts, **3** PA66 (30%GF) layer, **4** cooling channel, **5** clad steel layer, **6** modeled heat transfer- “ α ”- layer.

- One time step of the simulation corresponds to 0.1s of time.
- The simulation is run in total for 60 seconds allowing the injection process to become constant.

Initial conditions

- The meshes of the plastic mold on the outside have an initial temperature corresponding to the injection temperature in real production 300°C.
- The temperature of the cooling channel edge is set to initial and also during simulation constant temperature of 20°C.
- The initial temperature of the core is set to a temperature of 20°C.
- The specific layer thickness is defined. (0.0mm, 0.1mm ... 1.0mm, 1.5mm, 2.0mm, 4.0mm)

3.7.3 Simulation procedure

The simulation is run for several cooling cycles to establish a constant temperature distribution inside the core insert. The first injection is simulated by initially setting the temperature of the PA66 layer to injection temperature. The simulation runs unattended until the highest temperature inside the PA66 layer has cooled down to 170°C, which marks the ejection temperature of the plastic parts according to MAHLE’s production.

After that the temperature of the PA66 layer is set to 300°C again. The next injection cycle is started. A further cooling inbetween two injection cycles is not taken into consideration. The simulation is run for 60s in total, allowing to process to become constant.

Different simulations are carried out at different steel layer thicknesses, refer to the defined boundary conditions in 3.7.2.

3.7.4 Output

The temperature history of point *A*, refer to fig. 30, is extracted. Point *A* is located in the middle of the model on the surface of the core insert.

Additionally the injection cycle times are extracted.

4 Results and discussion

This chapter of the report presents the results from carried out experiments.

For what regards weldability investigations, the structure of the chapter reveals six sections.

To start off, results from initial VR0-ES, which was engaged for a basic examination of the weldability, are presented. A second section contains the results of a series of seven process studies that are carried out in order to identify additional the welds' soundness influencing factors. After that these first two experimental phases are subsumed and the findings are described in a concluding section.

This marks the change-over to VR1-ES as the starting point for the additionally carried out experiments. Two sections present the results of a welding parameter optimization and second, the corresponding investigations of the weld's mechanical properties. Again a short concluding section of VR1-ES is added.

Finally in a separated section the results of the FEM heat flow simulation are presented.

4.1 VR0: Weldability and process characterization

Fig. 31 shows 7 initial welding tryouts which served as a preliminary determination of weldability. These weldments should help to identify a suitable heat input per unit of length (HI) domain for the following experiments. The laser pumping lamp's voltage is directly influencing the laser beam's energy and is therefore varied for the presented weldments. Higher voltages result directly in higher HI. All other laser parameters are held constant, refer to page 67. All beads are single pass welded. Tab. 12 shows the corresponding laser pumping lamp voltages.

"Bead 4" indicates the lower limit of applicable HI as the wire did not properly melt at this voltage setting. The reddish color of "bead 5" indicates strong intermixing and therefore can be seen as the upper limit of HI, for intermixing is not purposeful for the intended application. "Beads 1, 2 and 6" indicate intermediate dilution. Compared to those three, HI at "bead 2" is higher which can be derived from the flat arching of the bead's surface. "Beads 3 and 7" show qualitatively good results.

According to this comparative judgment of bead surfaces the applicable welding parameter domain is estimated in between 250V and 350V laser pumping lamp voltage. Moreover best results are attained at voltages of about 280V to 290V.

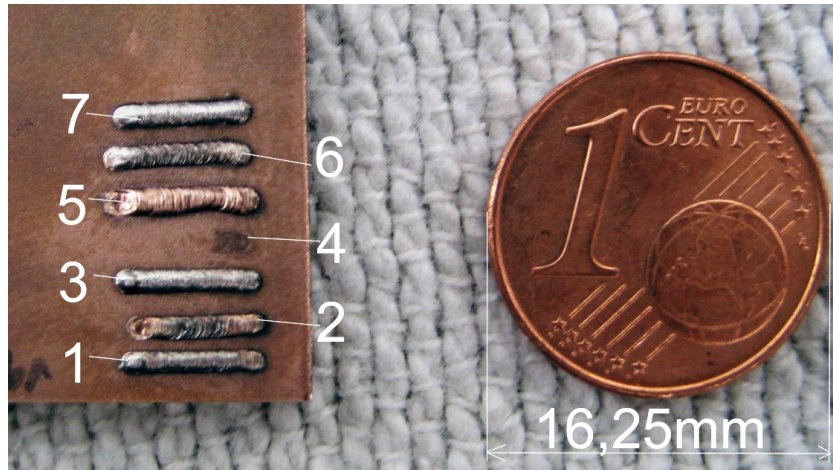


Figure 31: Initial welding tryouts.

bead no.	1	2	3	4	5	6	7
U_L	300V	330V	290V	250V	350V	320V	280V

Table 12: Laser pumping lamp voltage U_S for each bead.

4.1.1 Weld quality

This section contains a qualitative comparison of welding beads of 11 welds from VR0.1 and VR0.2. All of these welds are carried out at different laser parameter settings. However all settings entirely result in a HI that is inside the initially identified appropriate domain.¹ The appropriate HI here is defined in terms of defect-free weld metal on the one hand and a continuously good connection at the interface, and medium weld penetration, on the other hand. Hence this experimental series represents a more detailed identification of appropriate HI after weldability was elementarily proven.

Initially 2 tables are presented in order to give an overview of the performed weldments and to depict the connection of cross sections and bead surfaces.

For the first cycle VR0.1, tab. 13, the optimum result, regarding the cross section of the bead, was attained at experiment VR0.1.2. Based on these settings the laser parameters were further varied. The optimum result of the second tryout cycle was VR0.2.3.

For what regards the bead surface it can be derived that a decent bead surface does not necessarily mean the best welding result. For the first cycle the nicely arched and most

¹The exact welding parameter settings of all carried out welds are documented in experiment protocols which are depicted in the addendum of the report. The corresponding weld is distinctively identified by its experiment No. This is valid for all further welds presented in this report, except the 7 initially presented ones in 4.1.

decent bead surfaces did not reveal the best results. These beads were welded at too low HI and showed lacks of fusion at the interface.

Inside the optimum domain of dilution it is difficult to differentiate the welding result by the bead's surface. A connection of bead surface and welding result can not be derived. Too high HI, refer to bead VR0.1.6, can be derived from the scraggy border line of the two materials.

Three cross sections in fig. 32 indicate in a more detailed way the lower and the upper limit of appropriate HI, as well as the optimum result that was reached within the first two experimental series.

In the cross section depicted in fig. 32(a) the degree of dilution is $< 1\%$. Multiple lacks of fusions can be observed alongside the interface. For these parameter settings HI is too low for sufficiently melting the substrate material.

Additionally pores can be observed inside the weld metal, indicating the single deposited beads. It can be derived that the temperature was too low. The single beads are not properly fused. Additionally it can be derived that these air gaps are starting points of crack formation.

Fig. 32(b) shows a cross section of high dilution. This weld shows continuously good connection alongside the interface and the single beads inside weld metal are no more distinguishable. The crack formation is emphasized when compared to the weld metal in fig. 32(a). Cracks form at deepest penetration points, indicated by wave bases of the interface. Cracks reach through both welded layers and partially reach up to the surface of the bead.

Besides crack formation lateral material lift-off can be derived from the image.

Fig. 32(d) shows a detail of the interface of VR0.1.6 . Dynamically distributed precipitate copper rich phases near the interface inside the weld metal indicate a high Copper content. The too high dilution resulting from too high HI causes this appearance.

All these facts identify the HI to be too high for VR0.1.6 . The upper limit can therefore be defined to be just below these parameter settings.

Fig. 32(c) shows a cross sections of a weld of decent quality. The HI is just fair enough to have no remarkable lack of fusion along the interface. Furthermore the weld metal is almost defect free. Some little flaws can be seen in the center of the weld metal. Regarding their size and amount their influence on possible functional constraints is estimated to be negligible. The HI of VR0.2.3 is therefore assumed to be appropriate for this weldment in first place.

4 Results and discussion


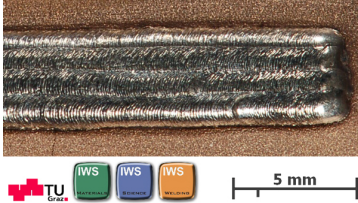
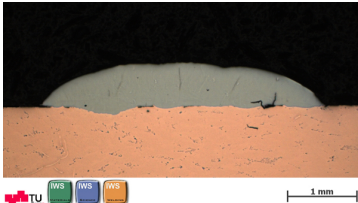
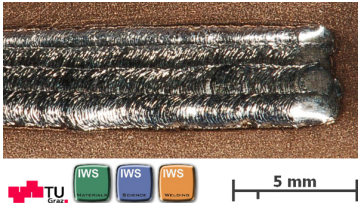

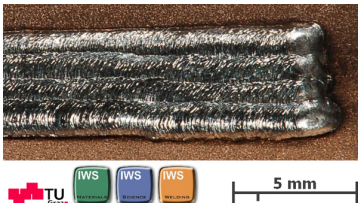
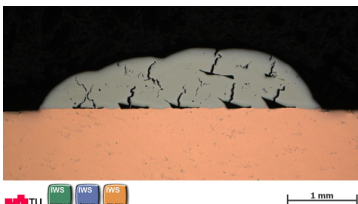

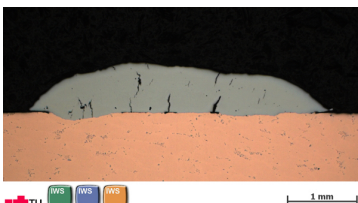
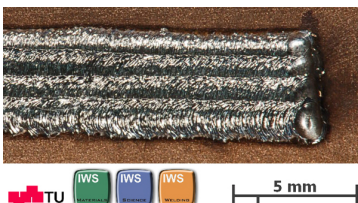
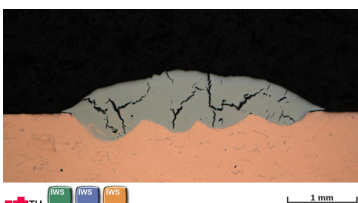
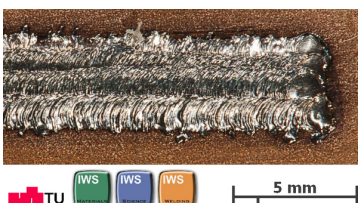
exp. no	U_L	L_I	F_I	cross section	bead surface
VR0.1.1	300V	5ms	10Hz		
VR0.1.2	300V	7.5ms	8Hz		
VR0.1.3	300V	5ms	8Hz		
VR0.1.4	300V	7.5ms	10Hz		
VR0.1.5	320V	5 ms	8Hz		
VR0.1.6	320V	5 ms	10Hz		

Table 13: First cycle (VR0.1): weld bead comparison.

4 Results and discussion

exp. no	U_L	L_I	F_I	cross section	bead surface
VR0.2.1	300V	6ms	10Hz		
VR0.2.2	300V	7.5ms	10Hz		
VR0.2.3	300V	9ms	8Hz		
VR0.2.4	300V	7.5ms	9Hz		
VR0.2.5	300V	6 ms	11Hz		

Table 14: Second cycle (VR0.2): weld bead comparison.

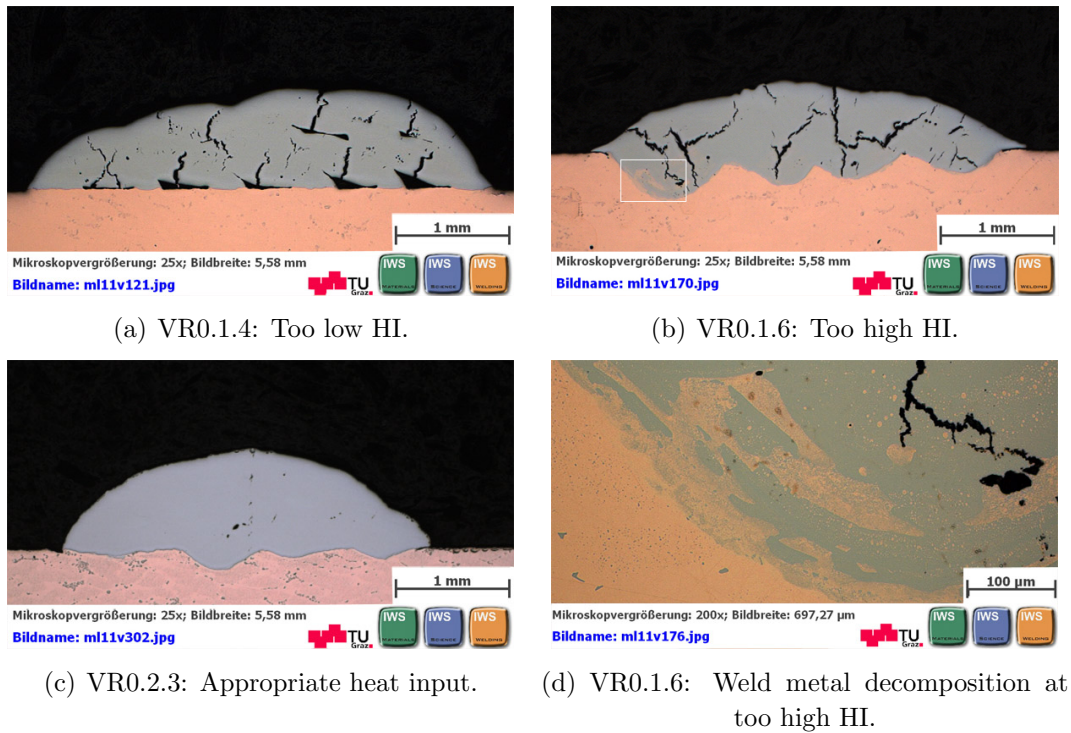


Figure 32: Limits of appropriate HI.

4.1.2 Interface

This section contains results of investigation of the microstructure that forms at the interface for appropriate dilution. In 4.1.1 it is shown that for weldments with appropriate HI a complete connection along the interface is formed. The interface then shows a waved shape along the fusion line, which results from the single parallel weld passes, where the energy density in the center of the laser beam is higher and hence the deeper penetration is formed.

The interface following investigations are presented:

- Mappings of the main alloying element, fig. 33.
- Linescan over the interface, fig. 34.
- Light microscopy of etched detail at the interface VR0.3.3, fig. 35(a).
- SEM topography image coupled with EDX-measurements as of an opened crack surface of weld VR0.3.7, fig.35(b).

Five zones can be distinguished in terms of microstructure, alloying contents and crack surface topography. In order to facilitate the description, these zones are numbered from the top of the bead down to the substrate material and are introduced in the according sequence, refer to fig. 35.

1. *Steel weld metal*: In this area dendritic structures can be observed. Depending on the section plane these dendrites appear in longish or globular form, fig. 35(a). The structure indicates the solidification direction, which runs in bevel upwards direction. The same structure can be observed in the SEM-EDX overlay image in fig. 35(b). This area represents finely cast structure as it is known from weld metal. Within this zone the EDX-analysis shows no copper content. The main element found is Fe with Cr as primary alloying element equally dispersed inside the weld metal. Si as second important alloying element is also found finely dispersed inside the weld metal. However there are Si-rich zones which can be derived by the lighter areas inside the weld metal, indicating possible phase segregations inside the weld-metal.
2. *Transition zone inside weld metal*: In this area no details of the microstructure can be observed in the light-microscopy image. The line scan indicates a low but compared to the cladding augmenting Cu content in this area. Little reddish dots in the light-microscopy image indicate that there is a phase separation of a steel matrix with spheric Cu-rich precipitation. This decomposition is believed to result from the limited solubility of Cu in Fe. These precipitations are also visible inside the weld metal where the penetration goes deeper, refer to area 2a. The crack surface shows a finer structured morphology. However it is difficult to exactly define a transition line to the weld metal.
3. *Transition zone inside substrate*: This zone marks the change-over from the steel to the Cu-rich part of the interface. This zone shows finely dispersed gray dots in a reddish matrix. It is believed that this appearance is due the corresponding decomposition mechanism that is encountered in the cladding's transition zone and that the gray dots are Fe-rich spheric precipitations. The line scan shows augmented Fe-content in this zone. For what regards the SEM topography of the crack surface this zone is finely structured and shows towards the transition line parallel terraces.
4. *Heat affected zone*: This zone is distinguishable by its lighter reddish color in the light-microscopy image. The line scan shows that the Fe content goes down to zero in this area. Furthermore the gray dots, that can be observed in regular distribution in the unaffected substrate material, are present in lower numbers, in smaller size and in less regular distribution. This appearance shows that the welding heat has a strong influence on the precipitations in this zone. However

this does not equally mean that the age hardening effect is destroyed in this area. Age hardening precipitations are not visible at this resolutions.[41]

The crack surface of this zone shows a fine dimpled structure.

5. *Unaffected substrate*: This zone consists of the unattended Cu-matrix with regularly distributed spheric Co and Ni rich precipitations, as indicated by the line scan.

The crack surface of this zone shows a more coarse dimpled structure compared to the heat affected zone.

It must be pointed out that for none of the investigated cross sections of varying dilution the formation of intermetallic phases can be found.

Summing up, the more detailed investigation of the interface shows, that significant interaction can be observed at the interface of performed welds at relatively high degrees of dilution. Five different zones can be distinguished in terms of microstructure and chemical composition, indicating a sound and continuous joint.

In combination with the complete missing of intermetallic phases it can be stated that a metallic connection of good quality can be formed between the two materials. Furthermore, only a small heat affected can be observed.

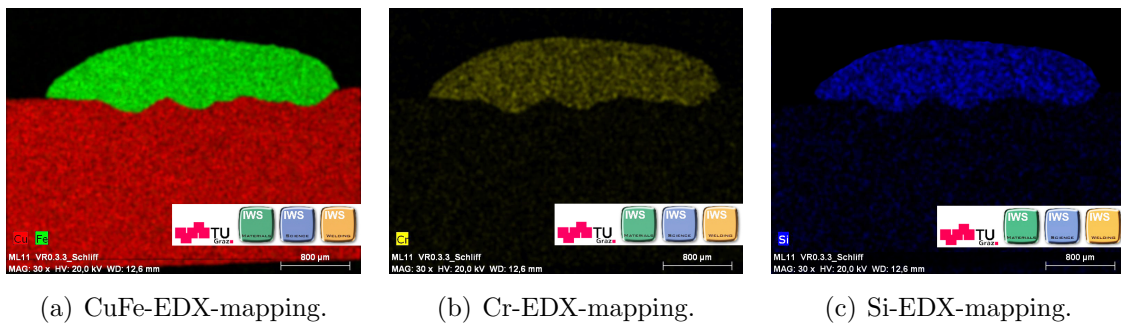
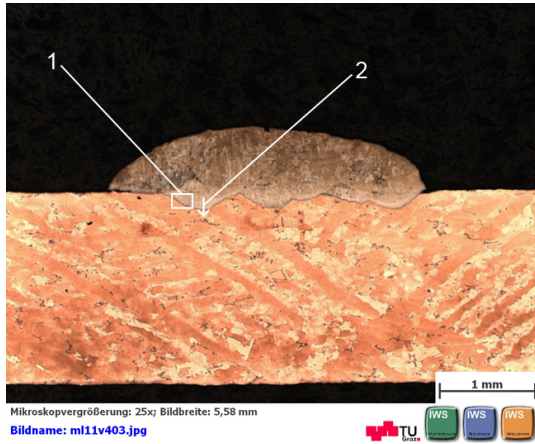
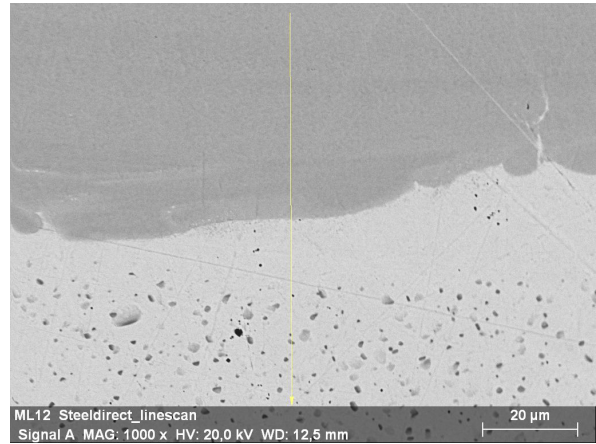


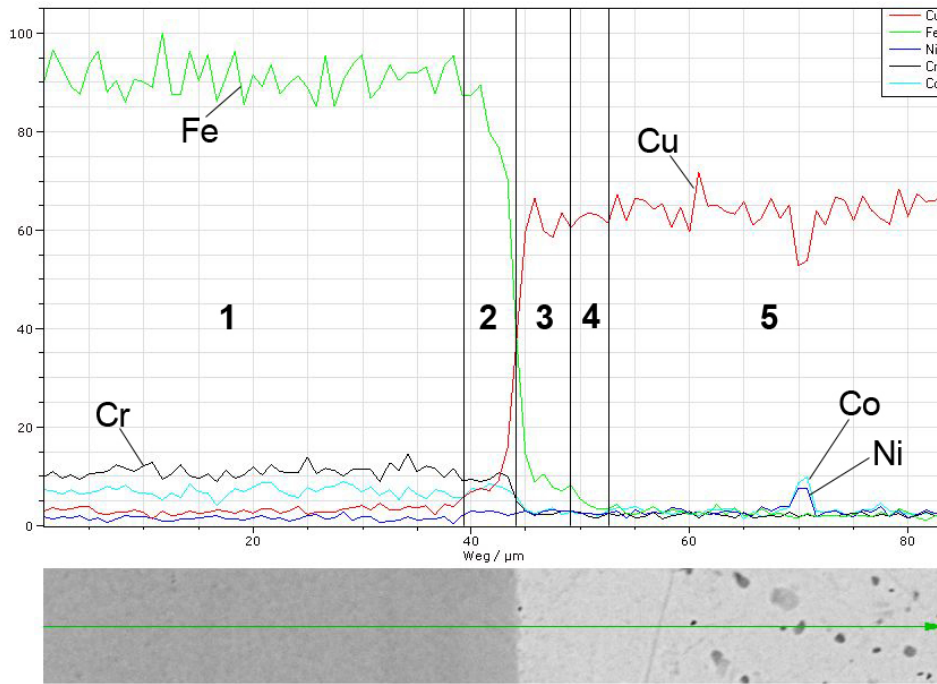
Figure 33: VR0.3.3: main elements EDX-mapping.



(a) VR0.3.3: overview interface investigation.



(b) VR03.3: location line-scan.

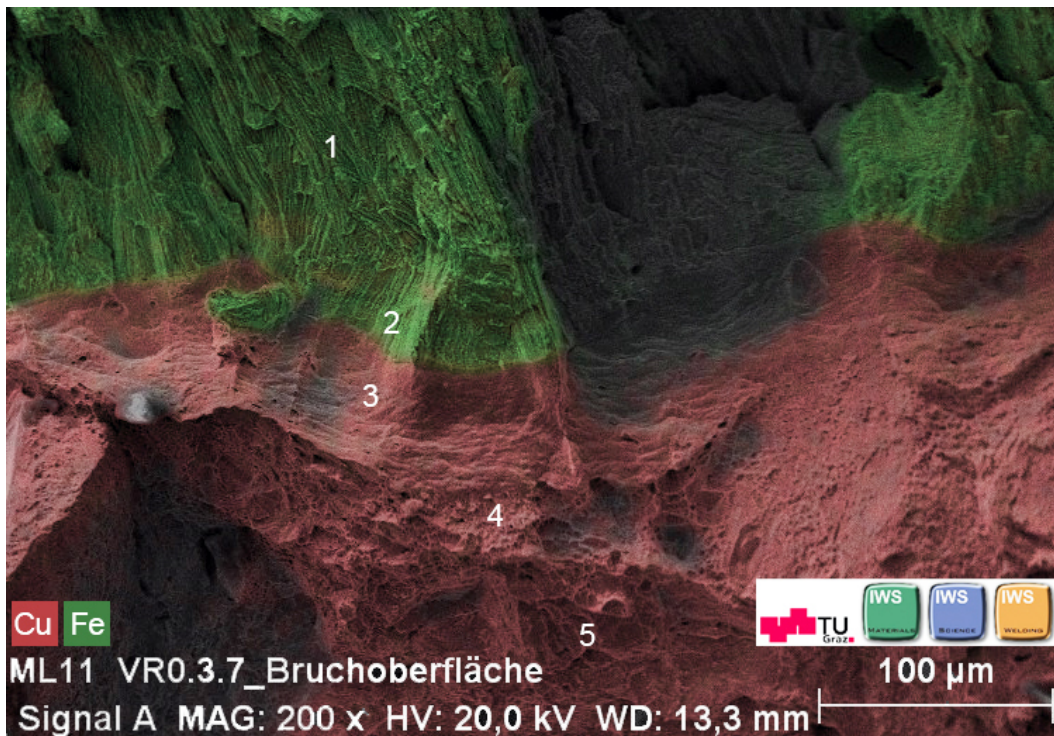


(c) VR0.3.3: interface line-scan.: Fe: green, Cr: black, Cu: red, Co: light blue, Ni: blue.

Figure 34: VR0.3.3: line-scan interface. **1** detail interface fig. 35(a), **2** location linescan fig. 34(b).



(a) VR0.3.3: optical microscopy of microstructure at the interface.



(b) VR0.3.7: SEM-topography and laid over EDX of broken open crack surface at interface.

Figure 35: VR0.3.3, VR0.3.7: interface zones.

4.1.3 Weld metal

Microstructure and defects

With the help of light microscopy images of cross sections the weld metal microstructure and its defects are introduced in this section. Two weldments, VR0.3.3 and VR03.7, which were part of a reproduction tryout of the optimum welding results of the initial weldability studies are representatively investigated.

VR0.3.3 is an example for a good weldment showing moderate dilution and an almost defect free weld metal.

VR0.3.7 represents a too high HI and hence bad welding quality. It is presented to show the typical crack appearance inside the weld metal which was observed for such high dilutions.

The overviews of the two investigated weldments are presented in fig. 36. The penetration basins' form corresponds to the in parallel deposited beads, refer to weld bead structure on page 65, where the laser beam's focus is pointed to.

VR0.3.3 shows a decent and homogenous weld metal, fig. 36(a). The optically measured dilution of this weldment is 16%. No defects can be observed at this magnification level. The higher dilution (63%) of VR0.3.7 can be observed in fig. 36(b). Compared to VR0.3.3 the weld metal is less homogeneous. The weld bead to the very left side of this weldment has a different structure and color, indicating a different chemical composition. The bead's surface is more flat which is due to the higher HI.

Cracks can be observed in the middle of the penetration basins, appearing at regular distances.

Fig. 37(a) shows the lower part of the weld metal and the interface of weld VR0.3.3. The weld metal shows fine cast structures. Grain boundaries are partially visible. The fusion line of the first and second bead can be observed. The microstructure above this fusion line has a darker color. A crack can be observed at the transition zone of the weld beads.

The heat affected zone of the substrate material can be distinguished by the missing of the Ni-Co rich precipitations which are found inside the unattended substrate.

Fig. 37(b) shows the mentioned crack and the weld metal of VR0.3.3 at higher resolution. Two phases are distinguishable inside the weld metal. A dark gray matrix is pervaded by lighter laths of different sizes. These laths partially have a zigzagged structure. Their size is bigger on the lower right side of the fusion line and they are therefore better perceivable in this area.

Inside the crack a small reddish, Cu-rich, inclusion can be observed. The crack's location at the end of the fusion line of two welded layers and the Cu-rich inclusion can be seen as an indications that this defect was caused by hot cracking.

4 Results and discussion

Low melting phases form because of impurities and changed chemical composition on the solidification front.[30] Hence this zone is more susceptible to hot cracking. However this crack is very limited in size.

Fig. 38(a) shows a more detailed view of one of the typical cracks appearing at high dilution in VR0.3.7 . These cracks form inside of the weld metal and reach from the interface all the way up to the bead surface. All cracks of this type do not exceed the interface.

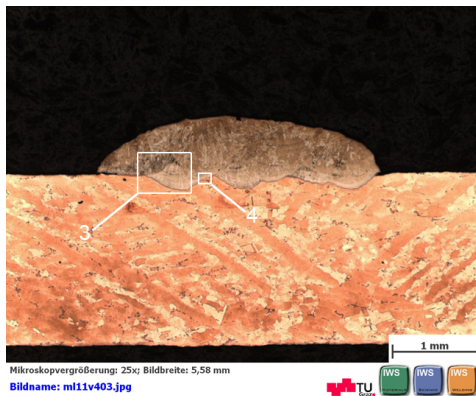
It's width is relatively constant in the range of $17\mu\text{m}$ and $19\mu\text{m}$. In the lower area of the weld metal the crack divides into smaller branches.

Little pores and rounded cavities, which are filled with Cu-rich phase, leaving a pore empty at the upper end can be seen in fig. 38(a).

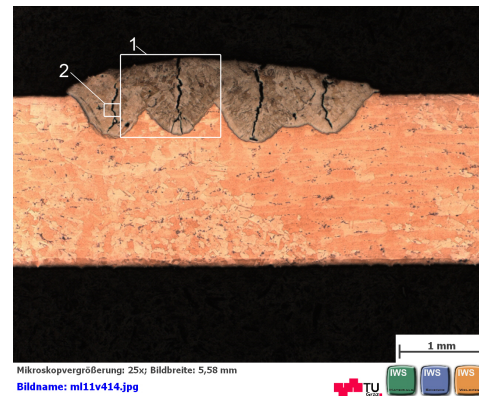
Fig. 38(b) shows the ramification of the above described crack. It can not be clearly determined whether the crack is intergranular or not.

Finally a more detailed view of the penetration basin to the very left of fig. 36(b) is given in fig. 39.

It can be observed that the microstructure is different in this part of the weld metal. Compared to fig. 37(b) and 38(b), no more pervading laths and grain boundaries can be seen. Instead, globular copper precipitations can be observed. The images reveal the problematic of the limited solubility of Cu in Fe as indicated in the phase diagram. For higher dilution weldments this fact causes an inhomogeneous weld metal.

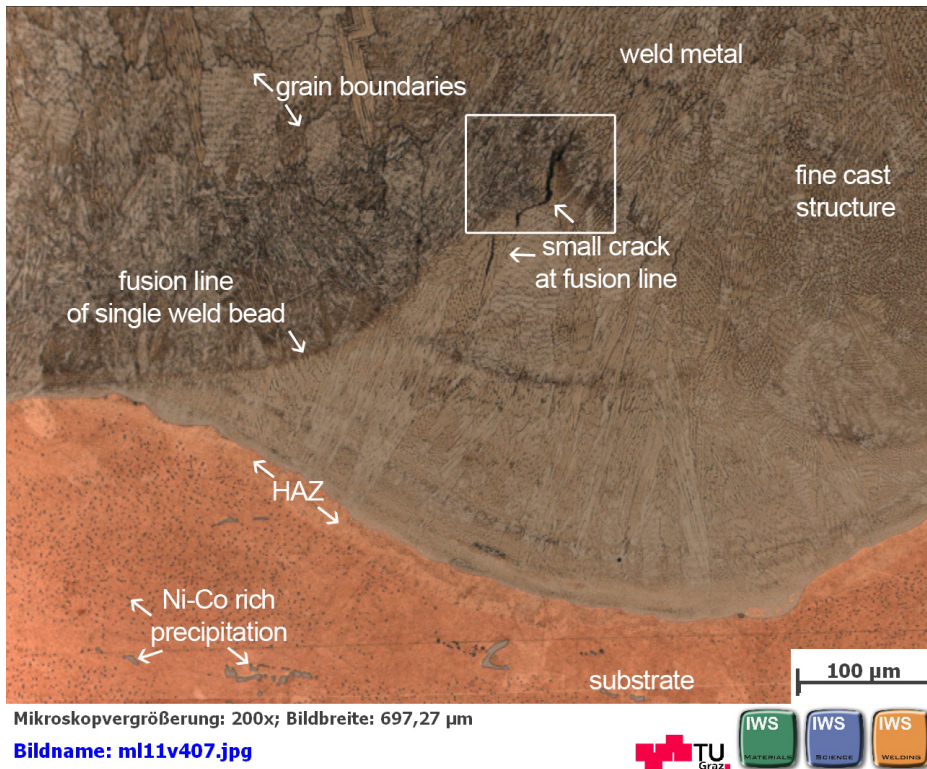


(a) VR0.3.3: Good welding quality, overview.



(b) VR0.3.7: Bad quality weld, overview.

Figure 36: VR0.3.3 and VR0.3.7: Weld metal overview. 1 fig. 38(a), 2 fig. 39, 3 fig. 37(a), 4 fig. 40(c).

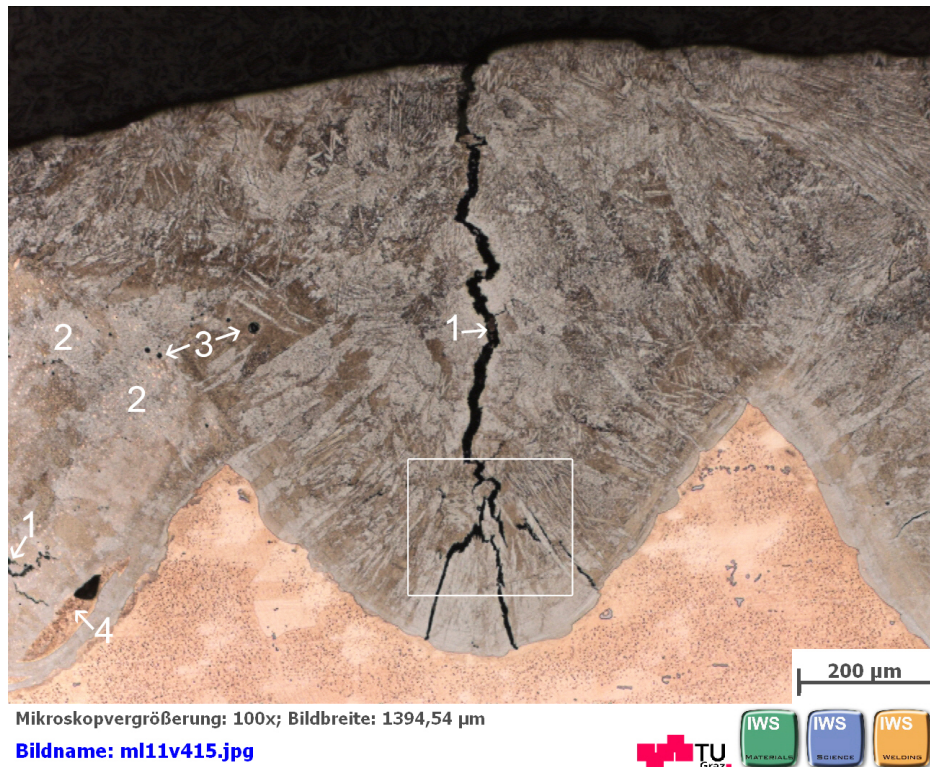


(a) VR0.3.3: Weld metal microstructure

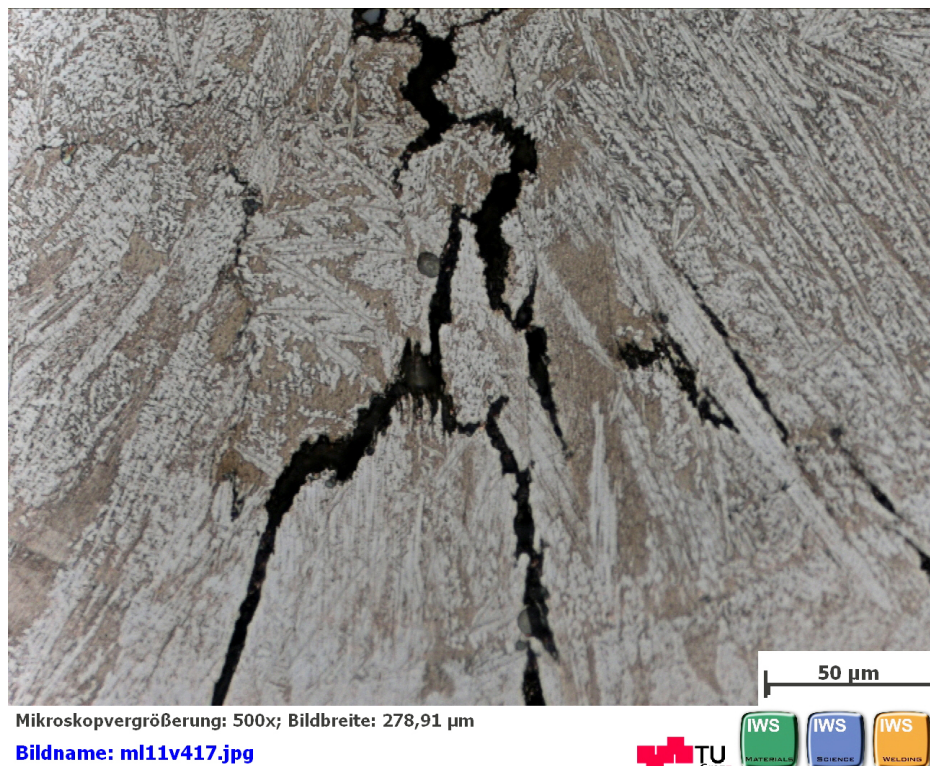


(b) VR0.3.3: Weld metal microstructure and crack detail

Figure 37: VR0.3.3: Light microscopy of weld metal microstructure. 1 reddish inclusion inside crack, 2 “zigzagged” lath-structure inside weld metal.



(a) VR0.3.7: Typical crack type at higher dilution.



(b) VR0.3.7: Crack fragmentation and weld metal structure at magnification

Figure 38: VR0.3.7: Light microscopy of crack appearance. 1 crack, 2 copper rich precipitation/inclusions, 3 pores, 4 copper rich inclusion with cavity.

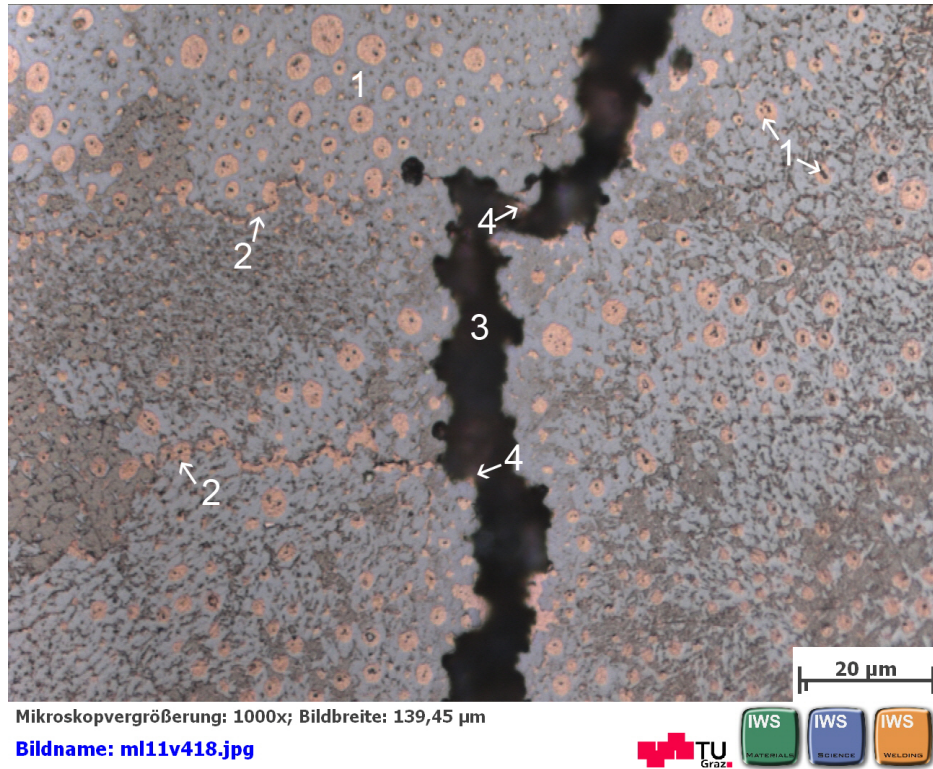


Figure 39: VR0.3.7: Inhomogeneous weld metal, Cu-rich inclusions. **1** globular copper precipitations in weld metal, **2** fused copper precipitations in weld metal, **3** crack, **4** copper rich inclusion on crack surface.

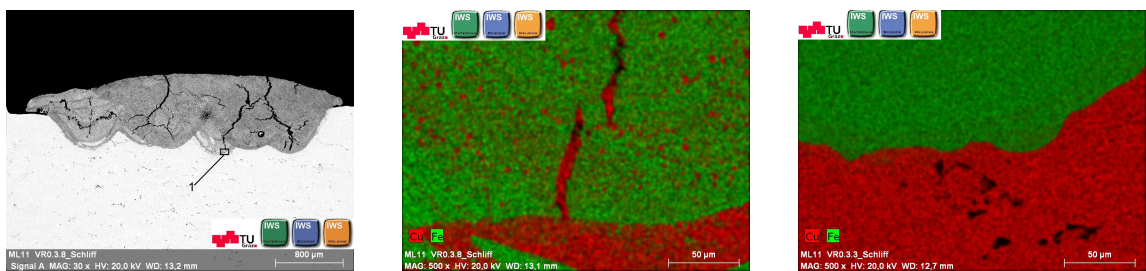
Cracking mechanism

This section shows the results of investigation of the typical crack appearances observed in weldments of relatively high dilution, refer to fig. 36(b) on page 96. Fig. 41 shows SEM images of an opened crack surface of sample VR0.3.7. Fig. 41(a) shows the overview image of the weld overlaid by an EDX-mapping of the same spot to facilitate orientation.

Fig. 41(b) shows a magnified view of Pos. 1. The image depicts freely solidified surfaces. Dendritic solidification structure is present, where the dendrites' main branches reach in upper diagonal direction. Similar topographies can be found on various locations all over the crack surface. Fig. 41(c) depicts a further and distinctive example of such a dendritic solidification surface which was found fa a lower spot inside the weld metal. This topography is a clear sign for hot cracking. The inclination of the dendrites becomes more vertical the more one approaches the upper interface of the weld indicating the varying solidification direction. It is caused by different cooling conditions.

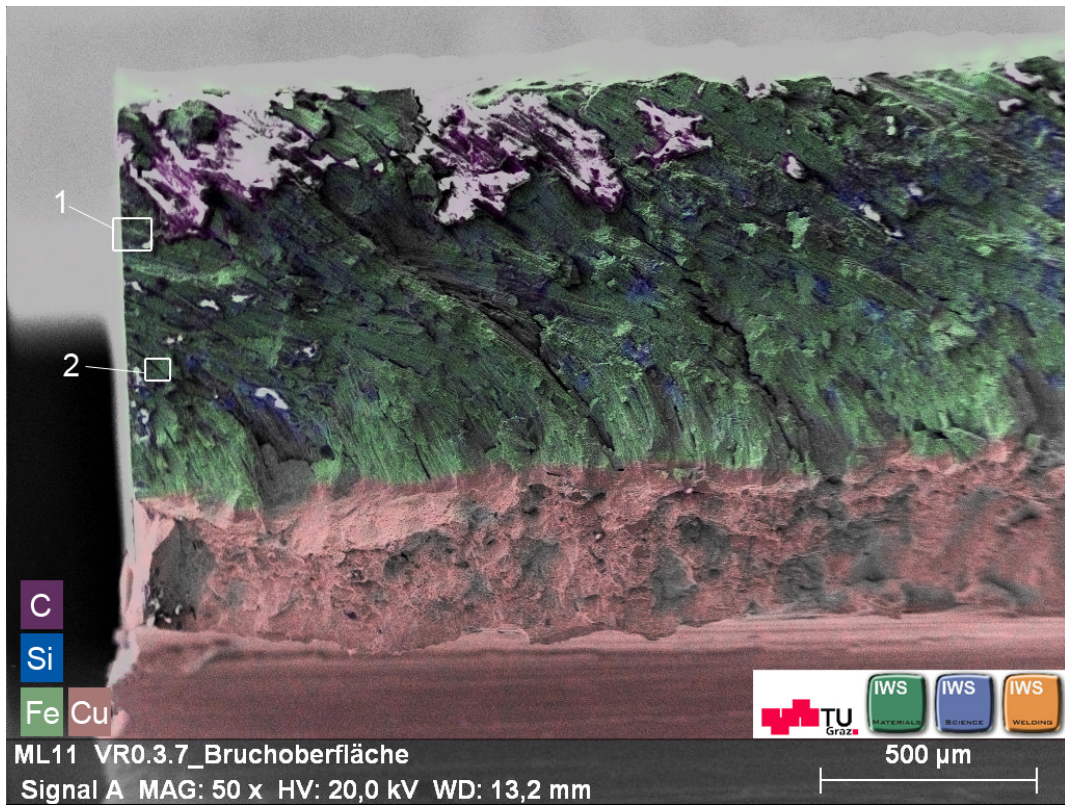
For what regards EDX-analysis, at the top of the bead C-rich areas can be observed. These areas penetrate from the surface into the weld metal. It is believed to be pollution that is draped inside the weld metal because of rapid solidification. The Si rich areas furthermore indicate an inhomogeneous weld metal.

There is no elevated content of a distinct element found near the dendritic surfaces that would indicate a low melting phase. The problematic of limited solubility and different T_M which forms a large liquid/solid two phase solidification range, refers to page 36 is revealed by the following images, fig. 40. For high dilution Cu-rich phases can be observed inside cracks. For appropriate dilution a clear transition line at the interface can be observed. Copper is therefore believed to be the main cause for the observed hot cracking.

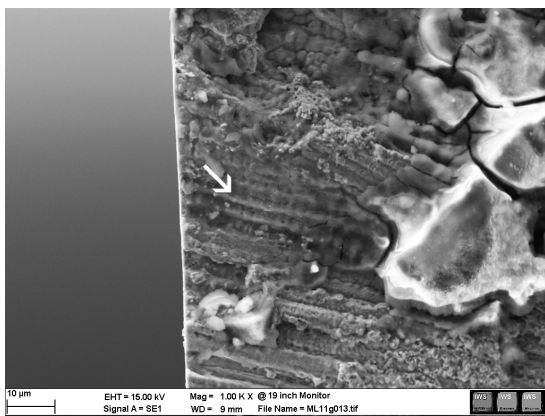


(a) VR0.3.8: dilution = 52%: overview. (b) VR0.3.8 position 1: Cu precipitations in weld metal and Cu inside cracks. (c) VR0.3.3: dilution = 12%. refer to fig. 36 on page 96

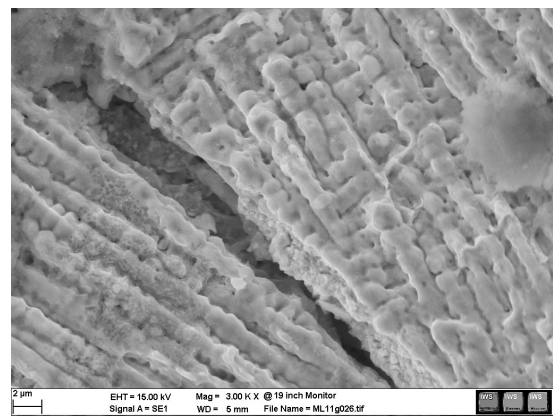
Figure 40: Interface EDX at different dilution.



(a) SEM SE-image overview weld bead



(b) Pos. 1: Dendritic solidification appearance on crack surface.



(c) Pos. 2: Dendritic solidification appearance on crack surface.

Figure 41: VR0.3.7: SEM topography of crack surface.

Hardness

Table 15 and 16 show macro hardness measurements of twelve different welds. These samples are welded at different welding parameter settings which resulted in different dilutions. For multi pass weldments three measurements were carried out inside the weld metal. For single pass weldments one measurement was carried out. The locations are presented in corresponding cross section images.

Hardness values are compared to 55 HRC reference, as required by MAHLE.

The measurements show that the hardness of the weld metal in as welded condition is not constant. The values scatter inside one and the same weldment and in-between different weldments. Hence, the hardness of the deposited weld is influenced by the welding parameters, respectively the dilution. It is believed that this is a result of different chemical composition of the weld metal and varying solidification velocities. The scattering hardness values are an indication for an inhomogeneous weld metal.

However, a trend of decreasing hardness for increasing dilution is perceivable from the gathered data. The decrease of hardness is depicted in fig. 42.

For what regards the required hardness values, none of the measured probes shows constantly the intended 55 HRC. Only 4 out of 27 measuring points reach hardnesses the required hardness. The chosen deposition wire does not produce a cladding of constant values greater than 55 HRC in as welded condition. Rather shows the majority of measured points hardness values below 55 HRC. The decreasing trend of hardness is believed to be caused by higher dilution and slower cooling rates resulting from higher HI. However, the measurements show that up to a certain dilution ($< 10\%$) the hardness of the weld is still in the area of the required 55 HRC.

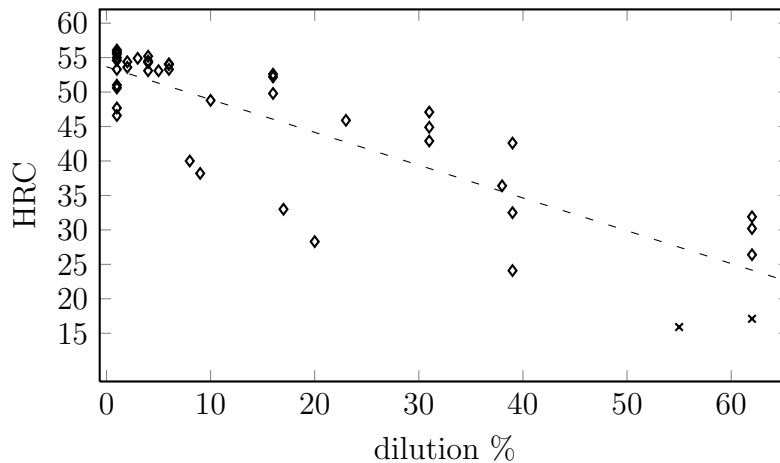


Figure 42: Hardness is a function of dilution. x below HRC scale, equivalent calculated by hardness measuring device, refer to page 77.

4 Results and discussion

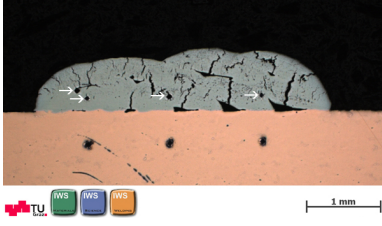
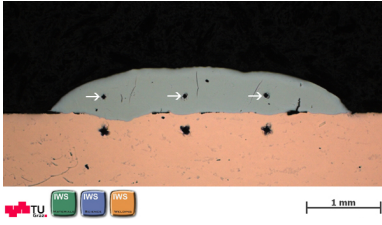
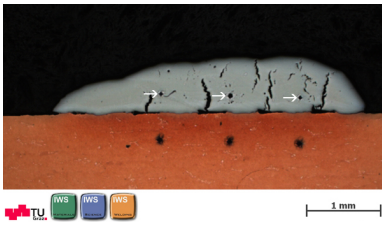
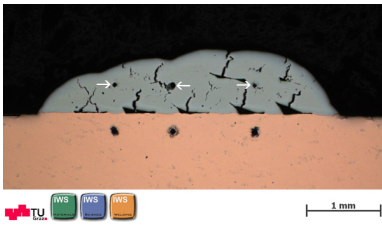
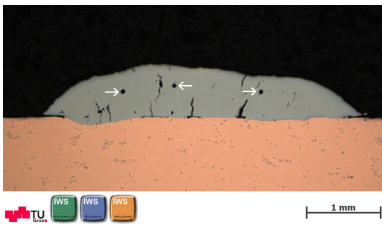
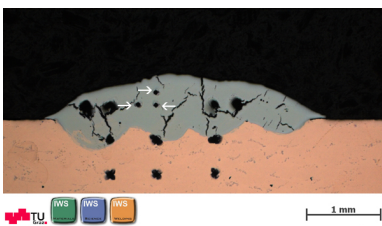
exp. no.	measurement location	HRC	average HRC	dilution
VR0.1.1		51	50.7	< 1%
		46.6		
		54.6		
VR0.1.2		54.3	54.0	4%
		54.5		
		53.1		
VR0.1.3		55.8	54.0	< 1%
		50.6		
		55.5		
VR0.1.4		53.3	53.4	< 1%
		47.7		
		56.1		
VR0.1.5		53.3	53.8	6%
		54.0		
		54.1		
VR0.1.6		42.9	45.0	31%
		47.1		
		44.9		

Table 15: Macro hardness measurements of VR0.1 welds.

4 Results and discussion

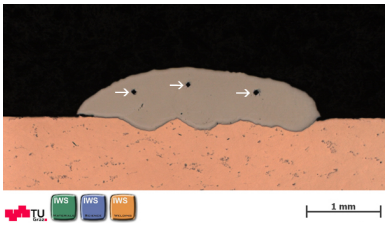
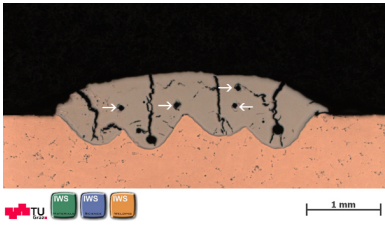
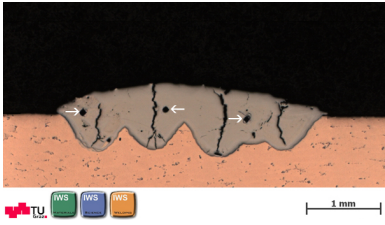
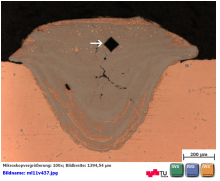
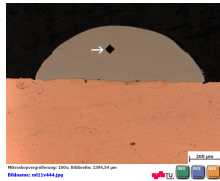
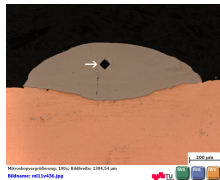
exp. no.	measurement location	HRC	average HRC	dilution
VR0.3.3		52.2	51.5	16%
		52.6		
		49.8		
VR0.3.4		42.6	36.4	39%
		34.1		
		32.5		
VR0.3.7		17.1	26.4	62%
		30.2		
		31.9		
VR0.3.9.2		15,9	15,9	57%
VR0.3.9.3		55,0	55,0	2%
VR0.3.9.4		42,9	42,9	26%

Table 16: Macro hardness measurements of VR0.3 welds.

4.1.4 Weld defects

Four graphs in fig. 43 depict the results from manual defect measurements of 49 randomly chosen cross sections out of all multi-pass welds (17) of VR0-ES. In terms of different defect types, cracks and lack of fusion has been considered for the measurements. Pores were not included in defect measurements. Compared to the two other defect types pores appearance was not significant. Four different aspects of the measured defects are depicted in diagrams as a function of corresponding dilution, refer to 43 on the next page .

The first so attained diagram in fig. 43(a) shows the surface fraction of defects inside the weld metal in % above the dilution. The surface fraction consists of the defect types cracks and lack fusion. It can be derived from the diagram that appearing defect surface fractions in the weld metal can be divided into three areas regarding different degrees of dilution.

- I Inside this area of very low degrees of dilution the amount of defects is high. The max. defect surface fraction in the weld metal of $S_E = 8.7\%$ inside this area is reached at a degree of dilution of $D < 1\%$.
- II For an area of slightly higher dilution of about 5% to 20% the defects' surface fraction drops down steeply. The area is limited at the lower side by a minimum defects' surface fraction of $S_E = 0.4\%$ at $D = 6\%$ dilution and at the upper side of $S_E = 0.3\%$ at $D = 17\%$. Non of the defect fractions measured inside this second area is above $S_E = 2\%$.
- III Continuing further towards higher dilution S_E increases again. The max. value inside this area is $S_E = 7.4\%$ at 31% dilution.

The graph presented in fig. 43(c) shows the fraction of lacks of fusion in the total defect fraction. It can be derived that it is high at low dilution and continuously goes down with increasing dilution. Combining the information gathered from these two graphs it can be subsumed that defects inside the weld metal at low degrees of dilution result mainly from lacks of fusion, whereas for higher dilution the main proportion of defects can be accounted to cracks.

Furthermore in-between these two areas of high S_E there is an area of medium degree of dilution that shows optimum weld quality results.

For what regards absolute defect size, it is more difficult to deduct a direct relation to the degree of dilution. The maximum value of $F_R = 11386 \mu m^2$ is attained at a very low dilution of $D < 1\%$ and the minimum value of $F_R = 681 \mu m^2$ is attained at a degree of dilution of $D = 17\%$.

However, it can be derived from the diagram that the scatter in defect size becomes

smaller for higher dilution. This fact indicates that the defect formation mechanism is more constant for higher dilutions.

The fourth graph in fig. 43(d) depicts the fraction of appearing cracks that reach the weld surface. This information is estimated to be more interesting from a functional point of view. Except three outliers, the measured points depict a almost directly linear trend. Inside an area of +/- 25% scatter, which is also depicted in the graph, the fraction of cracks reaching to the surface is lowest at low degrees of dilution and gets continuously higher at high degrees of dilution.

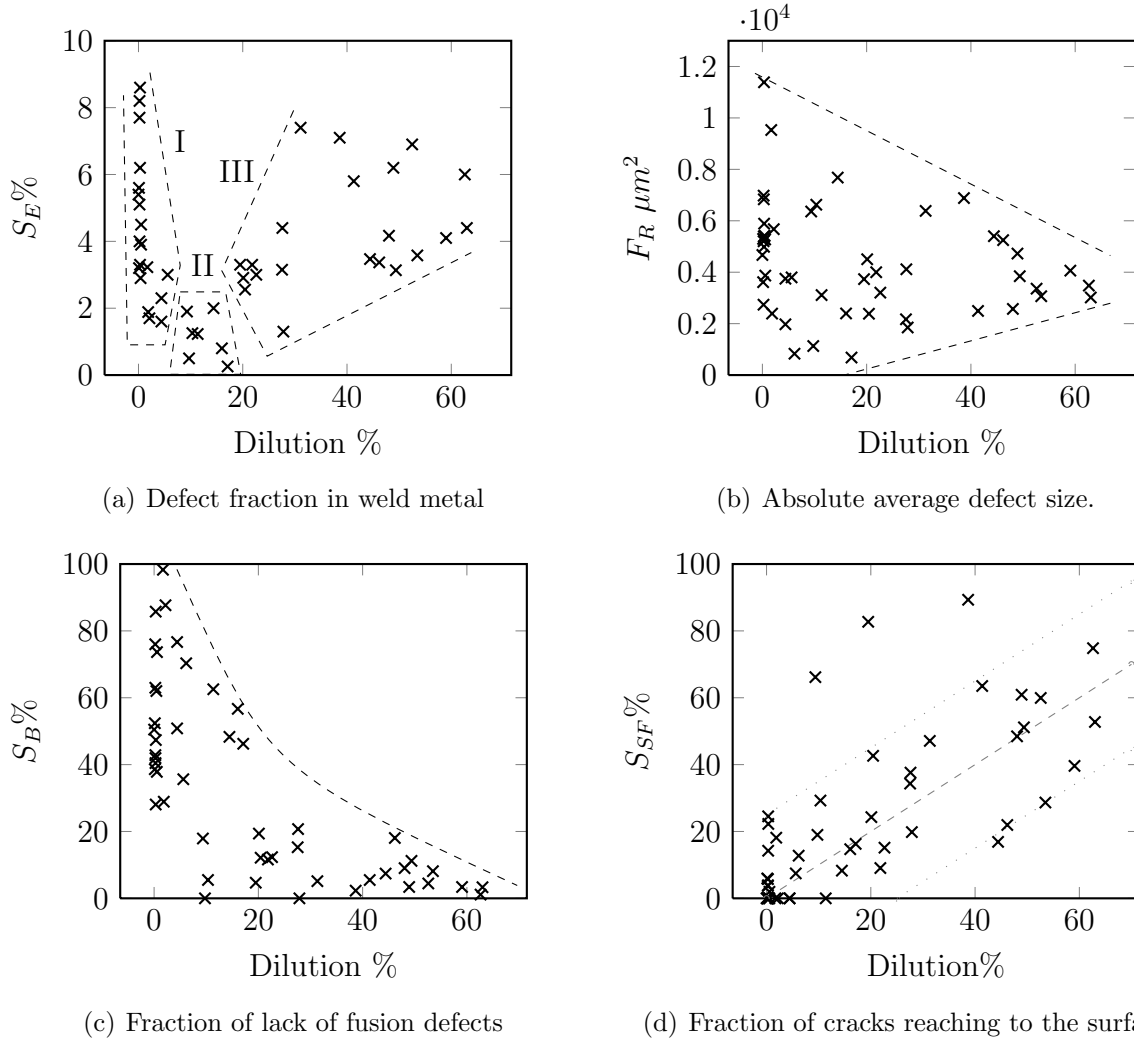


Figure 43: Defects in weld metal as a function of dilution. S_E defect surface fraction in %, S_B fraction of lacks of dilution in defect surface fraction in %, F_R average absolute surface size of defects in μm^2 , S_{SF} fraction of cracks reaching to the weld surface in %.

4.2 Process studies

This section presents a series of seven process studies that are carried out to characterize additional influencing process factors. The so attained process knowledge is intended to increase the consistence of the experimental environment.

4.2.1 Welding velocity

This first study is performed to determine a possible scatter in welding velocity v_s that results from manual operation. The operator is instructed to do the weldments as she/he personally judges them to be “well done”, without especially caring on v_s . The weldments are video recorded. The net average v_s for every single bead is measured by means of video studies.

Three weldments are carried out at the very same welding parameters. Every one of the three weldments consists of seven beads, as depicted in fig. 22(a) on page 65, resulting in 21 investigated weld beads.

Fig. 44 shows average v_s for every single bead of the three weldments performed. It can be derived that there is an increase in average v_s in two ways.

On the one hand v_s increases from one bead to another within one weldment. On the other hand the v_s increases from one weldment to the next. The average welding speed increases by 30% from the first VR0.3.6 to the third VR0.3.8 weldment of this study. Hence a certain training effect can be observed. The biggest difference in welding speed in-between two single beads is $\Delta v_s = 0.68 \frac{mm}{s}$, meaning an increase of 76% from v_{smin} to v_{smax} . The average welding speed of all 21 beads is $1.21 \frac{mm}{s}$.

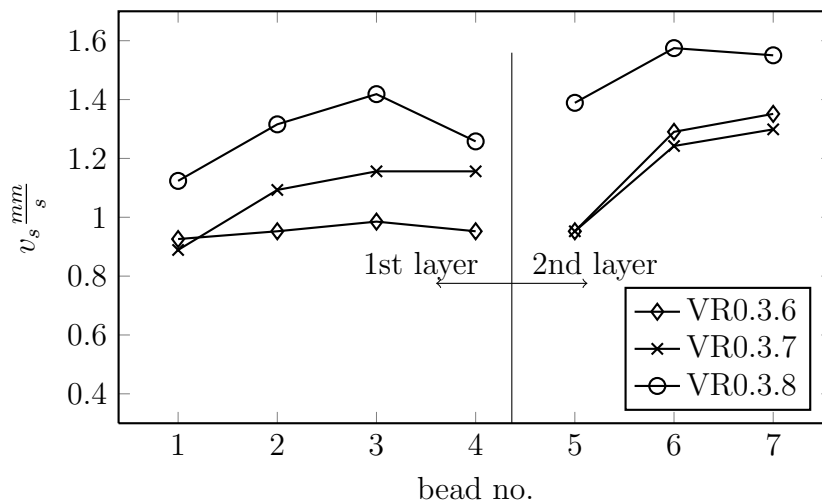


Figure 44: Change of welding speed. v_s welding speed in $\frac{mm}{s}$

experiment no.	VR0.3.6	VR0.3.7	VR0.3.8
1st layer average speed	0.95	1.07	1.28
2nd layer average speed	1.20	1.27	1.50
overall average	1.07	1.17	1.39

Table 17: Average welding speed in $\frac{mm}{s}$ of welding speed study.

4.2.2 Influence of welding speed

For this study six weldments were performed. For two different laser pumping lamp voltages ($U_L = 300V$ and $U_L = 290V$) weldments at three different welding speeds are carried out. All other welding parameters were constant. The welding speed is numerically controlled by switching the x-axis of the welding machine to automated mode. Out of each weldment two cross sections are prepared and compared. The degree of dilution and the hardness measured at single points are depicted in tab. 18.

This study shows no remarkable trend in variation of dilution nor the hardness that can be drawn back to a change in welding speed.

For $U_L = 300V$ it can be deduced that there is a relatively high scatter within one single weld bead in terms of dilution as well as in terms of hardness. The results of the weldments at $U_L = 290V$ are significantly more constant. A more constant and lower dilution and higher and more constant hardness can be observed for lower U_L .

This study reveals that for the given welding speed interval the laser pumping voltage has a much stronger influence on the welding results. This study shows that welding speed is not a dominating influencing factor.

4.2.3 Wire deposition rate

When welding manually in pulsed mode the filler wire deposition rate is defined by the operator. By feeling the counterpressure from the weld pool it is possible to increase or decrease the deposition rate. For this study the filler material consumption wire is measured for 20 single beads. These welds are done at different welding parameters but the length of the beads was constant 10mm.

The measured lengths of deposited filler wire per bead are displayed in the diagram in fig. 45. The average deposited length of 22.85mm per 10mm bead length is marked by a horizontal line. The maximum value of 30mm is attained at bead no. 16. For this weldment the operator was asked to push as much wire as possible into the welding pool.

4 Results and discussion

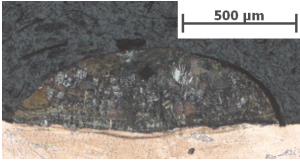
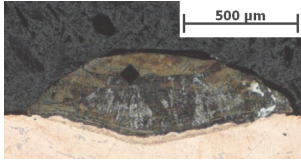
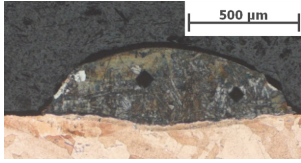
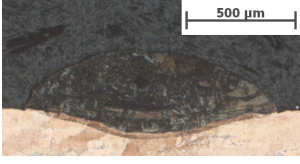
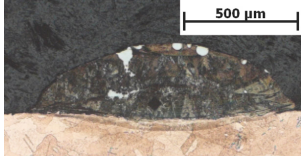
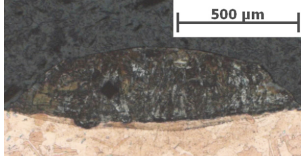
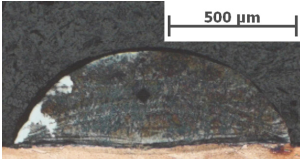
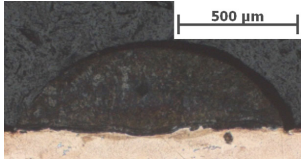
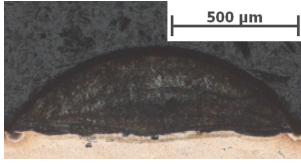
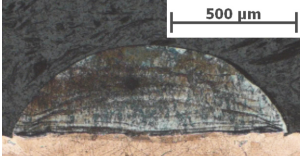
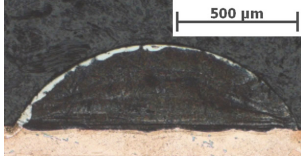

	$v_s = 1.4 \frac{mm}{s}$	$v_s = 2.0 \frac{mm}{s}$	$v_s = 2.4 \frac{mm}{s}$
$U_L = 300V$			
cross section:			
dilution:	8%	20%	9%
HRC	40.0	28.3	38.2
exp. no.:	VR0.3.9.1 1	VR0.3.9.4 1	VR0.3.9.5 1
cross section:			
dilution:	23%	10%	17%
HRC:	45.9	48.8	33.0
exp. no.:	VR0.3.9.1 2	VR0.3.9.4 2	VR0.3.9.5 2
$U_L = 290V$			
cross section:			
dilution:	2%	4%	5%
HRC:	54.4	55.2	53.1
exp. no.:	VR0.3.9.6 1	VR0.3.9.7 1	VR0.3.9.8 1
cross section:			
dilution:	2%	3%	3%
HRC:	53.6	54.6	54.9
exp. no.:	VR0.3.9.6 2	VR0.3.9.7 2	VR0.3.9.8 2

Table 18: Influence of welding speed: weld bead comparison.

4 Results and discussion

Therefore this single value has to be considered as a reference value for maximum possible deposition but can not be taken into consideration for a representative comparison. It is therefore also not included for the average and standard variation calculation. The minimum deposited length is 17mm per 10 mm bead length for bead number 7. The maximum different compared to average therefore is $+7.15\text{mm}$ and -5.85mm or $+31\%$ and -26% . The average wire deposition is $\mu_{W_d} = 22.47$ mm wire per 10mm bead length. The standard deviation is 3.10mm wire per 10mm bead length. ²

The scatter in wire deposition can be seen as a reason for scatter in welding results although welds are performed at equal welding parameters.

However it is believed that the operator, by its personal judgment, unconsciously retains balance of the two varying parameters v_s and wire deposition rate. The measured dilution from other experiments however shows that this external evaluation is not sufficiently accurate in order to constantly produce the same welding result.

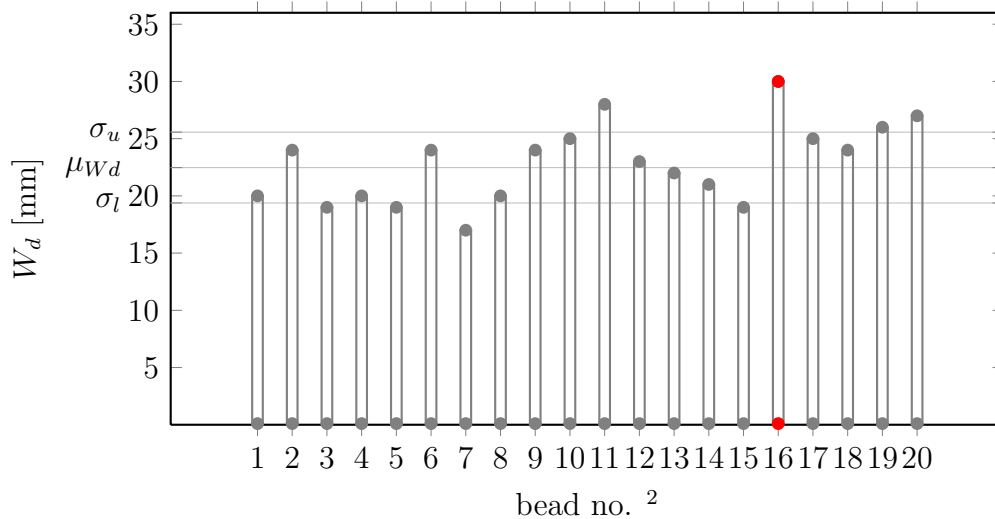


Figure 45: Wire deposition rate. W_d mm of deposited wire per 10mm of bead length.

²beads no. 1-9 correspond to VR0.3.9.1 to VR0.3.9.9. in addendum A5. Beads no. 10-14 correspond to VR0.3.10.1 to VR0.3.10.4 and beads no. 15- 20 correspond to VR0.3.10.6 to VR0.3.10.11 in addendum A6.

4.2.4 Welding sequence

For this study three welds are produced at constant welding parameters.

- one single-pass weld (fig. 46(a)).
- one two-pass weld at 50% overlap (46(b)).
- one three-pass weld, with two equally welded beads in first layer and the third bead in second layer (fig. 46(c)).

The welds are compared to each other in terms of weld quality and dilution. By incrementally depositing single beads the influence the sequence of deposited beads has on the welding result can be observed.

From the images it can be derived that the dilution continuously increases, from first 28% to 36% from the single-pass to the two-pass weld of one layer, and further to 43% for the two layer weldment.

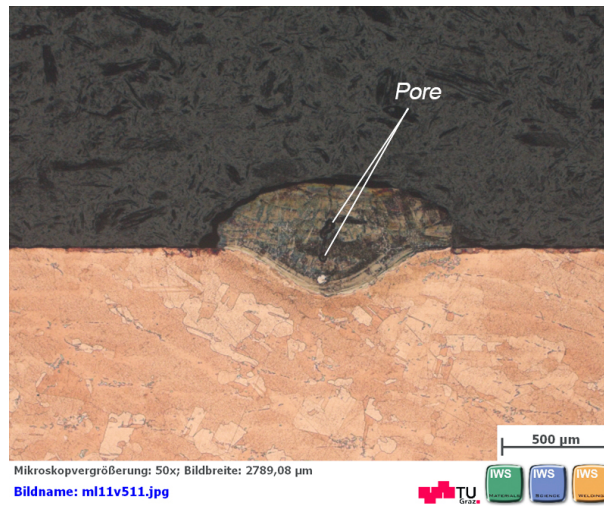
For what concerns defects in weld metal the single bead weld does only show a relatively small amount of defects inside the middle of the weld metal. The weld surface is not attained. For the two-pass and three-pass weld the above described typical crack formation in the middle of the penetration basins, with cracks partially reaching to the the bead's surface, can be observed.

Furthermore, in the cross section of fig. 46(c) the third deposited bead in second layer can be distinguished from the rest of the weld metal in terms of color and microstructure. At the very right ending of the weld this third bead forms a bulge over the substrate. Beneath this bulge a gap between substrate and deposited bead is visible. Because of this solidification form it is believed that this bulge forms by lateral flowing of the molten filler material out of the area of the laser heated zone as a result of too much wire deposition and too low HI. It solidifies on the surface without fusing with the substrate material because the amount of heat inside the melt is not sufficient.

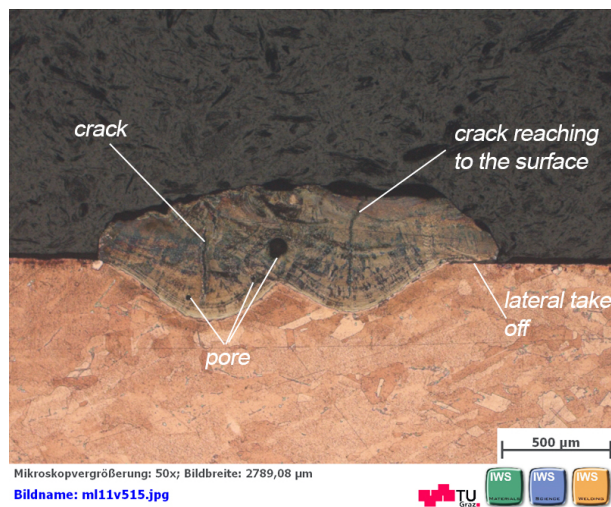
The same lack of fusion problem can be observed in bead 2 in fig. 46(b) for the two pass weldment.

Summing up, for all the three weldments of this study the HI is above the appropriate HI domain indicated by the too high dilution. The investigations showed that the HI needs to be adjusted accurately for every sinlge bead of a weldment. Furthermore, this study showed higher dilution and higher amount of defects for multi-pass welds. It can not be determined whether these cracks form because of the increased dilution or because of the reheating and remelting of the already deposited beads.

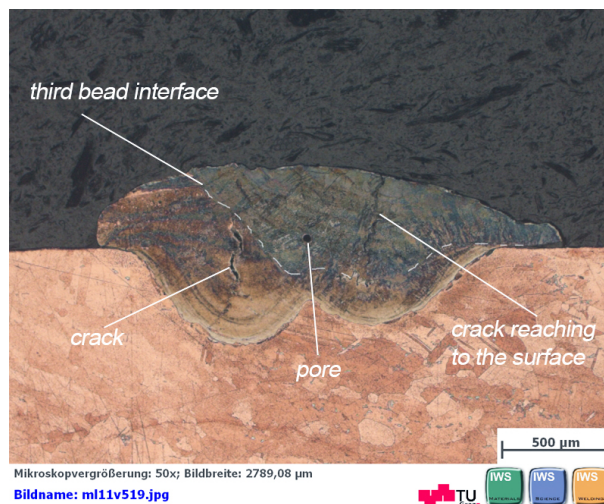
4 Results and discussion



(a) VR0.3.10.2: dilution = 28%



(b) VR0.3.10.4: dilution = 36%



(c) VR0.3.10.5: dilution = 43%

Figure 46: Welding sequence study.

4.2.5 Substrate preparation

For this study three substrate plates are equally prepared as presented in 3.2.1 on page 61. However the timespan to the actual welding experiment after preparation is varied.

1. welding right after preparation.
2. welding four hours after preparation.
3. storage for one week at room temperature under the conditions present in the MAHLE tool making department.

All welds are performed at the same welding parameters, including automated v_s . Of each weld two cross sections are presented in tab. 19 with corresponding dilution. It can be observed that there is no remarkable change of the degree of dilution for the two probes of shorter storage times. The change of dilution is inside a certain scatter that can be accounted to manual operation, from prior weldments known to be inherent to this process.

However, there is a significant increase of dilution for the weld that is performed after one week of storage time. The observed dilution is four times higher.

It is assumed that the reason for this appearance can be found in a time dependent change of the surface quality of the substrate material. An oxidation reaction with the environment is a possible reason. A layer of adherent reaction products forms on the surface increasing the absorptivity and hence the HI. Therefore the dilution increases. This reaction occurs obviously rather slow as there is no change identified for relatively short storage time.

A characterization of this possible layer formation was not realized for the presented work. The knowledge created can be stated like that: There is a time dependent change of the material's surface absorptivity characteristic. The way and moment in time of the surface preparation is important for good and reproducible welding results.

4.2.6 Substrate initial temperature

For this study seven weldments were performed at again constant laser parameters. However the initial substrate surface temperature was varied.

- For VR0.3.6, VR0.3.7 and VR0.3.8 the substrate is clamped to a controllable heating panel, s. fig. 25(b). The substrate was constantly heated to 75°C prior to and during welding.

4 Results and discussion






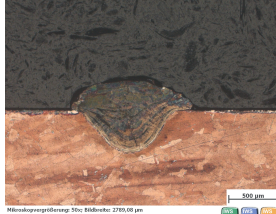
time to weld:	right after preparation	4h after preparation	1 week after preparation
cross sec.:			
dilution:	5%	20%	54%
exp. no.:	VR0.3.10.1 1	VR0.3.10.3 1	VR0.3.10.9 1
cross sec.:			
dilution:	20%	10%	48%
exp. no.:	VR0.3.10.1 2	VR0.3.10.3 2	VR0.3.10.9 2

Table 19: Influence of substrate preparation: weld bead comparison.

exp. no.	T_v °C	average dilution(*)	average dilution	S_E :flaw fraction	S_E :flaw fraction
VR0.2.3	room temp.	8% (2)	8%	0.5%	0.5%
VR0.3.3	59	17% (2)		0.5%	
VR0.3.4	59	39% (1)		7.2%	
VR0.3.5	61	20% (5)	25%	3.0%	3.6%
VR0.3.6	75	52% (3)		4.9%	
VR0.3.7	75	62% (3)		4.9%	
VR0.3.8	75	50% (1)	53%	3.1%	4.3%

Table 20: Influence of initial substrate temperature on weld quality. **number of measured cross section for average calculation*

- For VR0.3.3, VR0.3.4 and VR0.3.5 the substrate was clamped on a steel plate, immediately after this support plate had been heated to 70°C. The surface temperature of the substrate material plate was measured with the help of a pyrometer prior to welding and was approximately 60°C.
- For VR0.2.3 the welding the substrate initial temperature was at room temperature.

To evaluate the results the defect fraction inside the weld metal was measured and depicted with the corresponding dilution. The purpose of this study is to identify a possible influence of the substrate's surface temperature T_V on the absorptivity and hence the result of the welds.

Table 20 contains the data and is classified according to the three different preheating conditions. It can be derived that the dilution increases at higher T_V . Whereas it is as low as 8% at the weldment without preheating, it significantly increases to 25% in average at weldments with the substrate plate on the priorly preheated supporting plates. A further increase to constant 75°C T_v results in a significant additional increase of average dilution to 53%.

Hence it can be derived that T_V has a significant influence on the dilution and weld quality.

With regards to [27] and the two process studies in 4.2.5 and 4.2.6 it is believed that oxidation has great influence on absorptivity of the substrate. It is known that copper materials start to oxidize when exposed to an oxygen containing atmosphere. The reaction is basically slow. At elevated temperatures it will occur more significantly.

The studies show that it is best to weld the substrate at room temperature. Furthermore, it was shown that a relatively small increase of temperature influences the absorptivity significantly. Therefore the heating of the substrate as a side-effect of the welding heat will influence the weld quality.

4.2.7 Welding spot diameter

For this study three single weldments are carried out at different welding spot diameters, reaching from $D_{WS} = 0.8mm$ to $D_{WS} = 1.2mm$ at $\Delta D_{WS} = 0.2mm$ steps. All other welding parameters are kept constant. The weldments are compared in tab. 21 by means of cross sections and corresponding dilution. For each weld one HRC hardness measurement is added to the table. This study's purpose was to assess the laser spot diameter's influence as forth laser parameter on the welding result.

It can be derived that the degree of dilution goes down with increasing welding spot diameter. The penetration into the substrate material is high at the smallest welding spot diameter, resulting in a high dilution of 57%, respectively 56%. For this parameter setting the weld metal is inhomogeneous. A reddish phases can be distinguished. This phase is inconstantly dispersed in size and location inside the weld metal. It partially can even be observed on the top of the weld surface. This appearance again indicates the limited solubility of Cu in Fe and the consequent decomposition of phases inside the weld metal. The structure of the weld metal becomes finer and homogeneous with increasing D_{WS} . The reddish phases are no more distinguishable.

The hardness for weldments of high dilution is significantly lower. Inside the Cu-rich areas of the weldments with $D_{WS} = 0.8mm$ areas the hardness is compared to that again significantly lower. It is even below the HRC scale and is therefore given as 198 HV01. The hardness increases with increasing welding spot diameter.

For what regards crack formation, the cross section welded with $D_{WS} = 1.0mm$ shows the best quality welds. The cross section welded with D_{WS} resulting in lowest dilution shows cracks which reach from the interface all the way up to the weld surface.

Additionally a change in solidification geometry can be derived from the images. The beads show a more arched top surface at increased welding spot diameters.

The size of the welding spot diameter influences the thermal cycle of the weldment as the energy density changes. A larger welding spot diameter will increase the cooling rate as the same amount of heat is dispensed to a larger area. This is emphasized by the high thermal conductivity of copper. For smaller D_{WS} the heat impinges in a more concentrated way at the surface and therefore the dilution is higher. This fact can be

4 Results and discussion

seen as a reason for the found difference in weld metal structure and hardness as well as in the solidification geometry.







D_{WS} [mm]	0.8	1.0	1.2
cross sec.:			
dilution:	57%	16%	2%
HRC:	15.9	42.9	55.0
exp. no.:	VR0.3.9.2 1	VR0.3.9.1 1	VR0.3.9.3 1
cross sec.:			
dilution:	56%	10%	3%
exp. no.:	VR0.3.9.2 2	VR0.3.9.1 2	VR0.3.9.3 2

Table 21: Influence of D_{WS} : weld bead comparison.

4.3 VR0: Conclusion

In this final section a conclusion of the first phase of this these is given. A summary of to this point presented results of the work is done. This includes also the introduction of a model of changing absorptivity throughout a typical welding sequence and an outlook for the second experimental series VR1.

The initial weldability studies can be summarized as follows:

Weldability of a two layer direct cladding with the 0.5mm laser Mold[®] 10 wire on AMPCOLOY[®] 88 substrate with the AL Flak 300 mobil in manual operation mode is conditionally given. The weld quality significantly depends on the dilution respectively the HI. Appropriate HI given a complete joint along the interface is formed where transition zones on both side give indication for metallic bonding. The heat affected zone is small.

However VR0 shows that the process has multiple influencing and that welding results are scattering. Additionally the weld metal shows defects. For too low HI this defect are mainly lacks of fusion. For higher dilution these defects were identified to be hot cracks. Appropriate dilution given the defects can be reduced but not completely avoided. Best results could be observed in-between dilutions of 6% to 20%.

The 0.5mm laser Mold[®] 10 wire can not constantly produce a cladding of 55 HRC. Furthermore for high dilutions the hardness is significantly below 55 HRC.

A simple laser parameter adjustments is not a sufficient mean to produce reproducible good quality welds of the envisaged material combination with this welding process.

The during process studies identified additional influencing factors need to be taken into consideration in order to improve the process control. Improved welding preparation would consist of the following precautionary measures:

- Automated surface preparation and welding immediately after preparation.
- Defined surface starting temperature T_V of the substrate to be below 35°C.
- Accurate adaption of the HI for every single bead of a weld. A model of changing absorptivity is presented below.
- Automated filler material deposition and laser feed motion to guarantee for constant deposition rate and welding speed.
- Thorough post weldcleaning of every single bead.

4.3.1 Changing absorptivity throughout a welding sequence

The laser beam encounters different surfaces during a welding sequence. Fig. 47 shows schematically the variation of absorptivity that is caused by that. The sketch shows weldments from top view indicating the laser welding spot, substrate material and already deposited weld beads. The reflections are qualitatively represented by arrows of different sizes. Big flashes indicate areas of high reflexion. Small arrows indicate areas of low reflexion. According to the welding sequence of two layer weldment four different situations can be distinguished in the model.

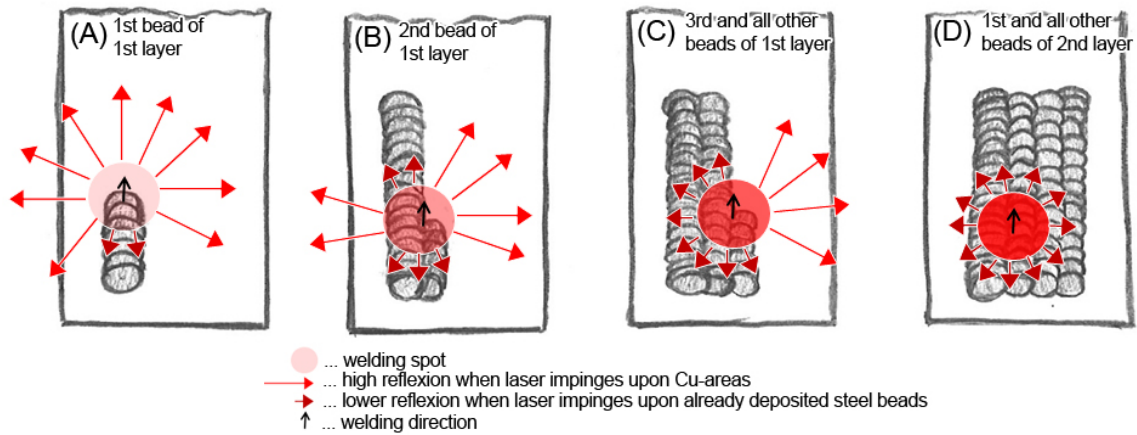


Figure 47: Reflexion of the laser beam during welding sequence, **white**: Cu-Be-substrate material, **shaded dark gray**: deposited steel beads

- A: The first bead is laid on the prepared substrate material. The laser beam fully hits copper material. Copper has a low degree of absorption. The surface roughness depends on the preparation method.
- B: The second bead is welded parallel to first bead at 50% overlap. A major part of the laser beam impinges on already deposited beads. Given the fact that laser welding spot diameter is set by standard to double the wire diameter, it still can encounter some copper material at the left side of the welding spot. The reflection is already a lot lower than for the first bead because the absorptivity of filler material is higher. The already deposited welding beads will show a rougher surface than the unattended substrate surface which can increase absorptivity and hence HI with same laser parameters even more.
- C: The third bead is welded parallel to the second bead with 50% overlap. The laser encounters even more deposited steel when impinging at the workpiece surface. Compared to the second bead it will not encounter copper on the very left side.

Regarding surface roughness the same as mentioned at B applies. The reflection for this bead is even lower when compared to the second bead. This constellation is valid for all additionally added beads of the first layer.

D: The fourth case represents beads on a second layer. The laser beam does only encounter deposited filler material. The reflection is therefore low.

4.3.2 Outlook HI optimization

The necessity of achieving a certain dilution in order to produce good quality weld is shown in 4.1.4. Best quality welding results are limited to a small area of the degree of dilution of about 6% to 20%. A successful HI optimization will depend on the capability of prodding welds inside this dilution domain.

Hence, in order to perform a reliable welding parameter optimization the varying absorptivity has to be taken into consideration. The laser impulse energy has to be adapted throughout a welding sequence according to the above described model. This would involve detailed characterizations of the attained surfaces in terms of absorptivity. This is not done for this thesis. Because of the complex interactions of multiple influencing factors a bead by bead optimization procedure is necessary. The proceeding is based on a trial and error strategy.

The different situations described in the model determine the structure of the weld beads to be optimized, refer to the schematic sketch on page 65.

Two reasons necessitate a change of used deposition wires.

- The Laser Mold[®] 10 wire could not constantly reach the required hardness of 55 HRC.
- The hot crack formation was not clearly identify to only result from the dilution with copper. The chemical composition of Laser Mold[®] 10 wire itself is known to increase susceptibility to hot cracking.[53]

Therefore a Laser Mold[®] 50 wire is used for the steel layer for the HI optimization of VR1 experimental series. Besides a direct steel cladding also a cladding with a Ni-base buffer layer is optimized. The Ni-base buffer layer is expected to improve the weld quality in terms of defect and connection strength.

4.4 VR1: optimized welding

This section depicts the results from the HI optimization for the two material combinations that are presented on page 65. The quality of the welds in terms of appearing defects and the mechanical properties of the optimized welds are presented in this section.

The proceeding during welding is based on the findings from VR0 experimental series and can be described like that:

- Two two layer welds are optimized which's structures correspond to the presented ones in fig.22(b) and 22(c) on page 65.
- The HI for the weldments is optimized bead by bead according to the attained dilution.
- U_L is the only varied laser parameter.
- Welding speed v_s is held constant by means of automated x-axis of the welding device.
- T_v is below 35°C.
- Welding is started right after substrate preparation.
- Enhanced cleanliness.
- The wire deposition is still manual.

4.4.1 Weld quality

Table 22 and 23 show the final optimization results for both material concepts wherein for the direct steel cladding three, and for the Ni-base buffer welds four different laser settings for the second layer were performed. Out of each weldment two cross sections are presented together with corresponding laser pumping voltage for each bead, dilution and defect fraction.

The defect fraction of the optimized weld compared to all VR0 weldments is significantly lower. However, some defects still can be observed for both material combinations. Defect fractions are as follows:

- Optimized welds: average $S_E = 0.7\%$.
- VR0 welds: average $S_E = 3.6\%$.




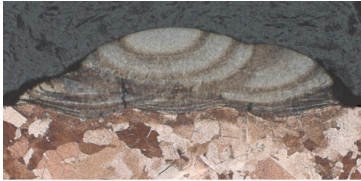
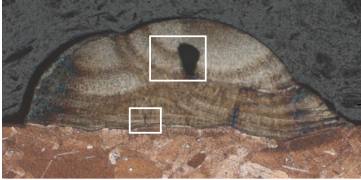

	bead	U_L [V]	cross section 1	cross section 2
VR1.3.21 dilution defect fraction	1	256		
	2	256		
	3	254		
	4	250		
	5	250		
			12% 0.7%	5% 0.4%
VR1.3.22 dilution defect fraction	1	256		
	2	256		
	3	254		
	4	236		
	5	236		
			12% 0.9%	10% 0.6%
VR1.3.23 dilution defect fraction	1	256		
	2	256		
	3	254		
	4	220		
	5	220		
			7% 2.3%	8% 0.8%

Table 22: Optimized direct steel cladding: weld bead comparison.

4 Results and discussion

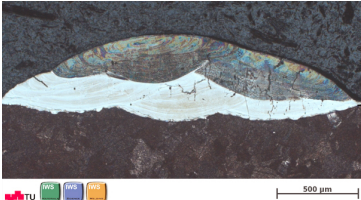
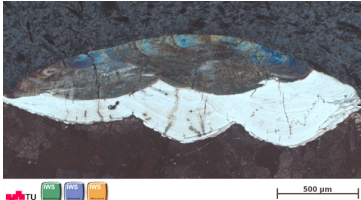
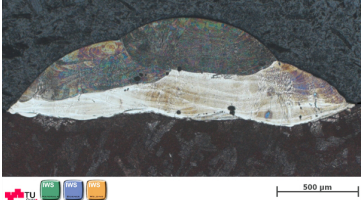





	bead	U_L [V]	cross section 1	cross section 2
VR1.4.1	1	292		
	2	292		
	3	290		
	4	250		
	5	250		
dilution defect fraction			19% 0.35%	32% 0.6%
VR1.4.2	1	292		
	2	292		
	3	290		
	4	236		
	5	236		
dilution defect fraction			14% 0.2%	< 1% 0.3%
VR1.4.3	1	296		
	2	296		
	3	294		
	4	250		
	5	250		
dilution defect fraction			14% 0.6%	23% 0.5%
VR1.4.4	1	296		
	2	296		
	3	294		
	4	236		
	5	236		
dilution defect fraction			16% 0.6%	< 1% 0.2%

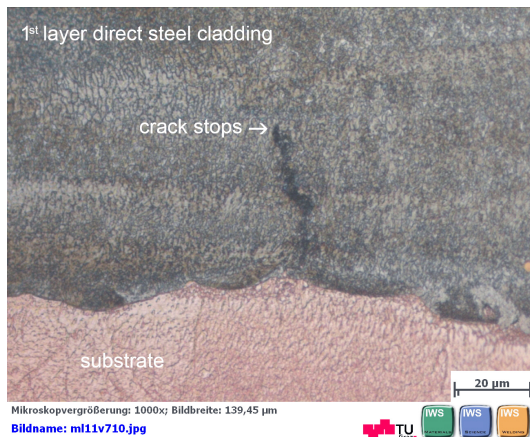
Table 23: Optimized Ni-base buffer cladding: weld bead comparison.

Direct steel cladding

The weld metal of the optimized welds generally show good quality. From tab. 22 it can be derived that all welds are performed at the right amount of HI, as depicted by the appropriate dilution. Because of reduced HI the second layer does not melt the substrate material.

For what concerns defects, it can be observed from the images that cracks still appear. However, the cracks stop at the interface from first to second layer and don't reach the surface, fig. 48(a). Hence, for the direct steel cladding the defects fraction is low, except for one investigated cross section, VR1.3.23. This cross section shows a relatively big pore at the fusion line of the two layers. Because of the relatively big size of this defect the fraction is outstandingly high for this single cross section. Additionally multiple micro pores are found. Micro pores have not been found in any of the other cross sections. This layer of VR1.3.23 was welded at low U_L . The resulting reduced solidification duration is believed to be the reason for pore formation.

The cavity and the micro pores are presented in more in detail in fig. 48(b).



(a) Cracks stop inside first layer.



(b) Cavity and micro pores in second layer.

Figure 48: Defects in weld metal of optimized direct steel cladding. 1 micro pores.

Ni-base buffer

The images from tab. 23 reveal that the weld quality of the Ni-base buffer layer weldments is scattering. The dilution is not constant for given laser parameters. Inside a certain area of scatter, no direct correlation of HI and dilution can be derived. For the same HI the dilution varies from approx. 0% (VR1.4.2) to 32% (VR1.4.1) and 0%, refer to table 23.

Although the HI was higher at VR1.4.3 and VR1.4.4 the dilution was maximum in VR1.4.1. Furthermore the dilution scatters even inside one and the same weld. In VR1.4.4 the dilution changes from $< 1\%$ at minimum to 16%. It is pointed out that this two cross sections are within some millimeters inside of the same weld bead.

For what concerns defect fractions inside the weld metal the images reveal that crack formation could not be avoided with the help of the Ni-Base buffer layer. However the Ni-base buffer layer weldments show constantly low defect fractions because cracks are narrow, below 1% for all investigated welds. Compared to the direct steel cladding this is a slightly but still remarkably lower amount of defects can be observed:

- average S_E of optimized direct steel claddings: 0.95%
- average S_E of optimized Ni-base buffer claddings: 0.42%

The cross sections of welds VR1.4.1 and VR1.4.3, representing high dilution show the biggest amount of defects. Cracks of these welds do not stop inside the first layer, but partially reach the weld surface.

Additionally pores can be observed, whereof the biggest of them appears in VR1.4.3 with a diameter of $85\mu\text{m}$.

It can be stated that the Ni-base buffer layer weld does not necessarily show a better result in terms of the weld quality when compared to the direct steel cladding. Rather, because of cracks that reach to the surface of the weld bead the Ni-base buffer layer's quality can be estimated to be worse compared to the direct steel cladding.

Furthermore it shows more instability in results when compared to the direct-steel-to-substrate welds. Moreover the spread in resulting degrees of dilution inside one weld of this second material concept is greater than the entire area of identified appropriate degree of dilution. Hence a in terms of welding possibility necessary process stability is not given.

4.4.2 Hardness lines

Direct steel cladding

Fig. 49 depicts a hardness line over a cross section of one of the optimized direct steel claddings.

Within the second layer the hardness values are subject a certain scatter. Inside the first layer the hardness stays at a rather constant value of about 660 HV0.05 (HRC 58 [56]). Overall the hardness of the cladding decreases constantly towards the interface. The maximum hardness of the cladding 746 HV0.05, equivalent to 62 HRC according to DIN50150:1976 [56], is attained in the very upper area of the second layer. The minimum hardness of the cladding is 621 HV0.05 (56 HRC [56]) which means that the required 55 HRC is constantly reached by this weld.

Inside the substrate the hardness increases again to 300 HV0.05 (21HRC [56]) and finally evens out inside the substrate material to almost constant 276 HV0.05 (27 HRC [56]).

The investigation shows on the one hand that the optimized deposition weld exceeds the required hardness of 55 HRC in the entire weld metal.

However there is a very steep drop of hardness in the HAZ. The low hardness can be accounted to an inappropriate heat treatment of the substrate due to welding heat, refer to 4.1.2 on page 90.

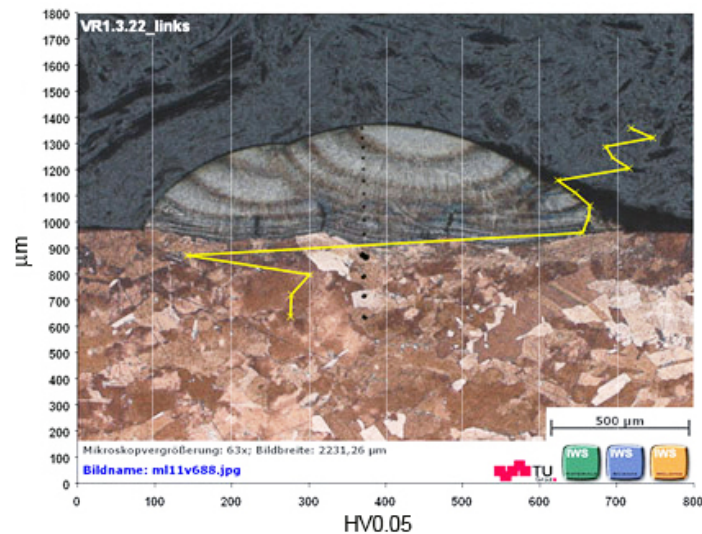


Figure 49: VR1.3.21: Hardness line on direct steel cladding.

Ni-base buffer layer cladding

Fig. 50 shows a hardness line of one of the optimized Ni-base buffer-layer claddings.

It can be derived that the hardness inside the steel layer is constantly on a very low level. The maximum hardness inside this layer is 233 HV0.05. The minimum hardness is 212 HV0.05. The average hardness of the steel layer is only 222 HV0.05.²

The average hardness inside the Ni-base buffer is 249 HV0.05, wherein the maximum is 270 HV0.05 (26 HRC [56]) and the minimum right beneath the fusion line of the two layers is 225 HV0.05.

The same steep drop of hardness to 121 HV0.05 just below the interface can be observed. It equally represents the soft HAZ. The absolute drop is compared to direct steel cladding less. However this measuring point represents the absolute minimum hardness found within this investigation.

The hardness inside the steel layer of the Ni-base buffer layer concept does not reach the intended hardness of 55 HRC by far. Moreover the steel layer is softer than the substrate. Therefore the concept is improper in terms of the attained hardness and the material combination fulfills the weldability demands worse than the direct steel cladding. The same problem of a soft HAZ zone in both welds shows that this appearance is inherent to the welding of this age hardened alloys and appears independently of the actual HI.

The following passages reveal a probable cause for the softening of the steel layer.

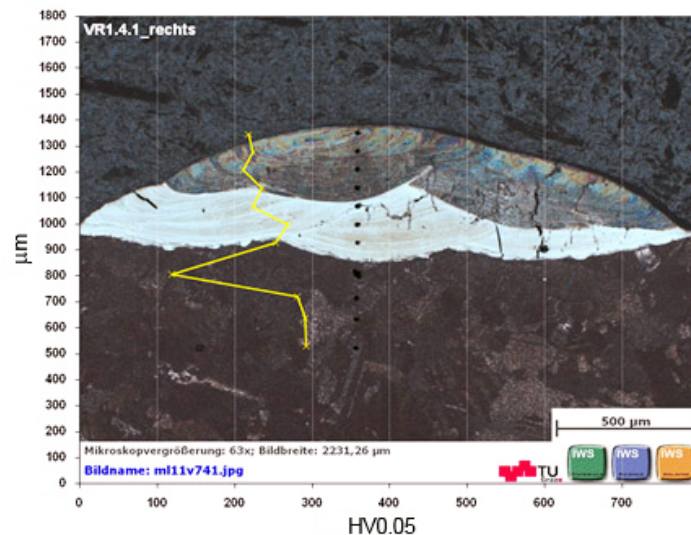


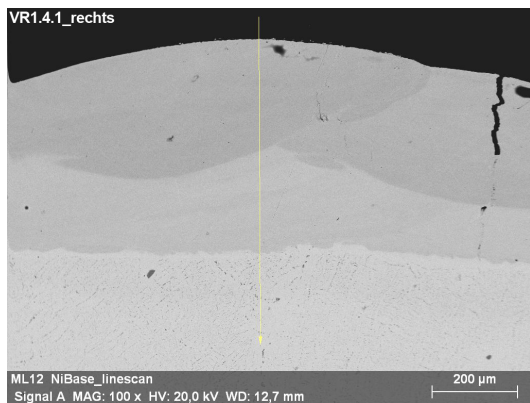
Figure 50: VR1.4.3 1: Hardness line on optimized Ni-base buffer layer cladding.

²All these values are outside of the HRC scale.[56]

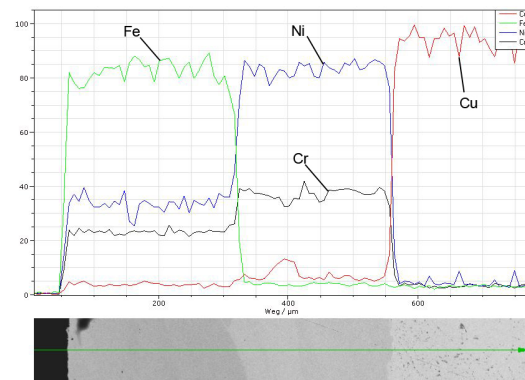
Linescan

A linescan of VR1.4.1 is presented in fig. 51. It can be observed that the Ni-content is constantly high inside the steel layer. The Ni-content of the JOKE[®] is approximately 72%.

The line-scan reveals that inside the second layer the Ni-content is approximately a third of the first layer's Ni-content. Hence the Ni-content inside the second layer can be estimated to be about 24%. Ni is a gamma forming element. Therefore it can inhibit the martensitic transformation and is therefore believed to cause the relatively soft weld metal of the second layer.



(a) Location linescan Ni-base buffer layer cladding.



(b) Linescan Ni-base buffer layer cladding: .

Figure 51: Linescan on Ni-base buffer layer cladding.

4.4.3 Shear strength

This section presents the results from tensile shear testing of at optimized parameters performed welds. Three samples of each of the two material concepts were measured and are presented.

Additionally three samples of a deposition weld of the same 0.4mm laser Mold[®] 50 wire to a S355 steel plate are presented as reference values.

Table 24 presents the fracture shear strengths for both material concepts and the reference weldments.

The results show that the direct steel cladding's maximum fracture shear strength (282 MPa) is almost twice as high as the maximum fracture strength of Ni-base buffer-layer weldments (154 MPa).

The maximum shear strength of the steel-to-steel reference weldment is still significantly higher (609 MPa). The strength of the direct steel deposition weld reaches almost half the strength of the reference weldment whereas the Ni-base buffer layer weldment is only 25% of it. By comparing the the two optimized concepts none of the weldments of the Ni-base buffer layers could pass the smallest maximum shear stress of the direct steel claddings.

τ_{IFmax}	minimum	median	maximum
Ni-base buffer	108 MPa	148 MPa	154 MPa
direct steel cladding	156 MPa	221 MPa	282 MPa
steel-to-steel cladding	586 MPa	599 MPa	609 MPa

Table 24: Fracture shear strength of interface of optimized weldments.

The scatter of fracture shear strengths for both the dissimilar material combinations is more significant than for the steel-to-steel reference weldment.

- Ni-base buffer layer cladding: $\Delta\tau_{IF} = 48MPa$, an increase of 44% from min. to max. τ_{IFmax} .
- direct steel cladding: $\Delta\tau_{IF} = 126MPa$, an increase of 80% from min. to max. τ_{IFmax} .
- steel-to-steel cladding: $\Delta\tau_{IF} = 23MPa$, an increase of 4% from min. to max. τ_{IFmax} .

This fact depicts again the sensitiveness of this process when dissimilar welding.

The results from the shear test are depicted in fig. 52. The shear stresses at the interface τ_{IF} are displayed over the stroke of the tensile testing machine.

The curves for both concepts climb at similar gradients in the first section of the curve. Right before the maximum stress is reached the gradient softly decreases forming a smooth peak before the almost vertical drop of stress of the curve appears, indicating the shear off of the weld bead.

The same characteristic can be observed for the steel-to-steel weldments. However, the stress-deformation curves have lower gradients in the first third of stroke. After that the gradient increases to approximately the same value as it can be observed for the dissimilar welds. A smooth peak just as for the other curves appears right before shear-off.

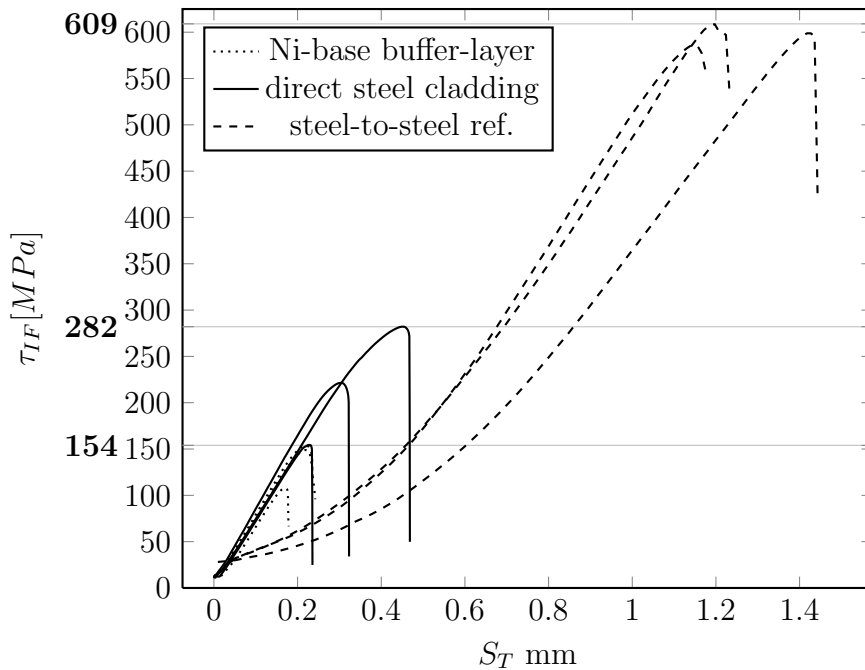


Figure 52: Shear strength diagram. S_T stroke of the cross beam, τ_{IF} tensile shear stress in the interface.

Summing up, the direct steel cladding shows better fracture shear strength results than the Ni-base buffer layer which is in accordance with hardness.

The maximum shear strength of the direct steel cladding is almost half of the strength of the reference steel-to-steel cladding. This strength of the joint is therefore believed

4 Results and discussion

to be sufficiently high in order to form a good protective layer. A clear statement can however not be given, as an exact required strength is not available.

4.4.4 Characterization of failure behavior of direct steel claddings

This section presents results from investigations on the failure behavior of the direct steel cladding shear strength samples. The intention is to explain the significant scatter which was observed in the measured fracture shear strengths.

The shear samples' cross sections of the three direct steel claddings are presented together with the corresponding dilution and fracture shear strengths in tab. 25.

It can be observed that, although all have been welded at constant optimized parameters, only one of the samples shows a proper dilution, VR1.5.6. The shear strength for this is significantly higher than the other two measured samples.

The dilution is equally low for probes VR1.5.4 and VR1.5.6. However the difference in shear strength is 65 MPa.

These facts indicate that the one weldment with in terms of defects identified proper dilution also shows higher fracture shear strength. For low dilutions the shear strength is significantly lower. Hence, the dilution influences the shear strength of the interface. Sufficiently high dilution results in higher shear strength.

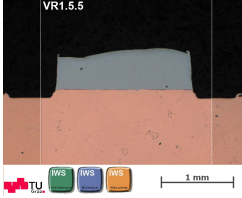
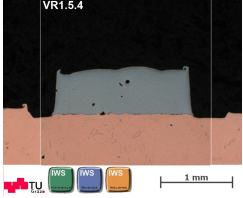
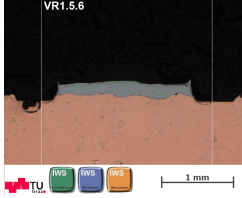
exp. no.	VR1.5.5 = rel. min.	VR1.5.4 = rel. med.	VR1.5.6 = rel. max.
cross section			
τ_{IF}	156 MPa	221 MPa	282 MPa
dilution	2%	2%	13%

Table 25: Shear strength and corresponding dilution of direct steel claddings: weld bead comparison.

EDX of crack surface

Table 26 depicts EDX-maps of the crack surfaces of VR1.5.5 and VR1.5.6, which corresponds to the minimum and the maximum fracture shear strength for the direct steel claddings.

The crack surface on the substrate and of the sheared off weld is presented. The meaning of the indicated widths of the weld are described in the figures' label.

The welding direction and the loading direction are depicted as well.

It can be observed from the element mappings that very little of the deposited material still adheres to the surface of the substrate after shearing off the welds for both samples. However, by comparing the crack surface of the sheared off welds it can be derived that the amount of red Cu-rich areas is a lot higher in VR1.5.6. The Fe-rich areas run parallel to weld direction. These appearances indicate the following failure mechanism in dependence of the dilution:

- For proper dilution the joint between substrate and cladding is well established. The substrate is sheared off. The failure happens along the heat affected, soft zone that could be identified by the hardness line measurements. The connection strength is limited by the strength of this weak zone: Fig. 53(a).
- For too low dilution the joint is not well established. The substrate is sheared only partially. The weakest zone inside is the interface. The failure happens along the interface: Fig. 53(c).

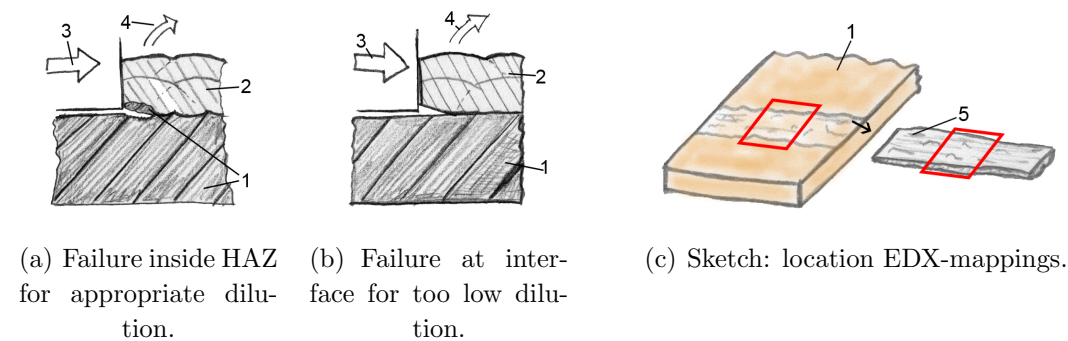


Figure 53: Failure mechanisms. **1** substrate, **2** cladding, **3** loading, **4** shearing off, **5** sheared off weld bead.

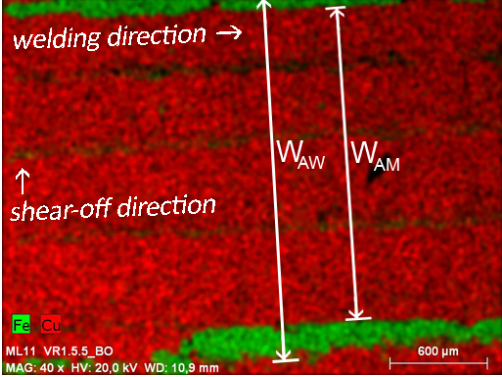
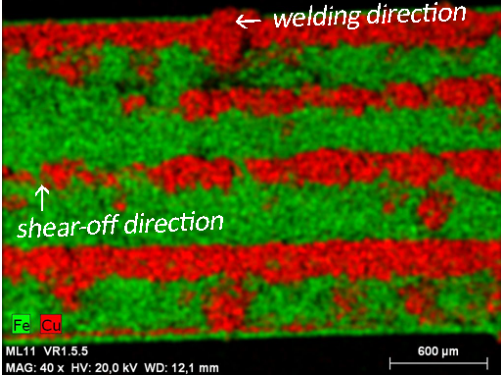
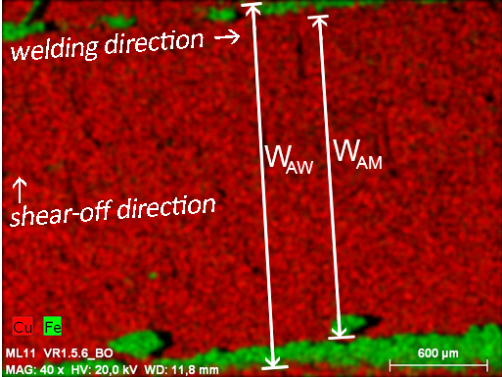
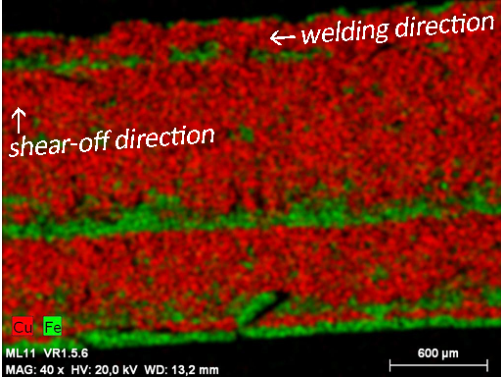
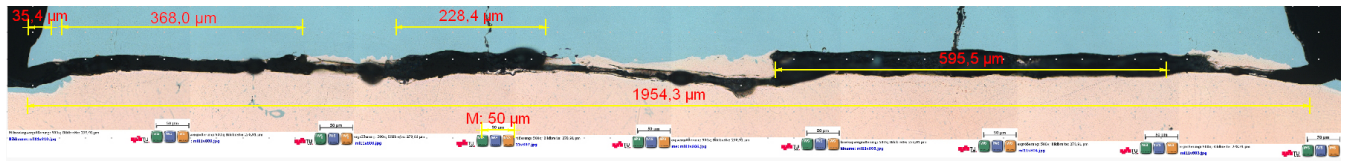
exp. no	crack surface on substrate	crack surface weld bead
<p>VR1.5.5</p> <p>τ_{IF} : 156 MPa</p> <p>dilution: 2%</p>		
<p>VR1.5.6</p> <p>τ_{IF} : 282 MPa</p> <p>dilution: 13%</p>		

Table 26: EDX-maps of crack surface: Min. vs Max shear strength comparison. W_{AW} width of weld after welding, W_{AM} width of weld after machining.

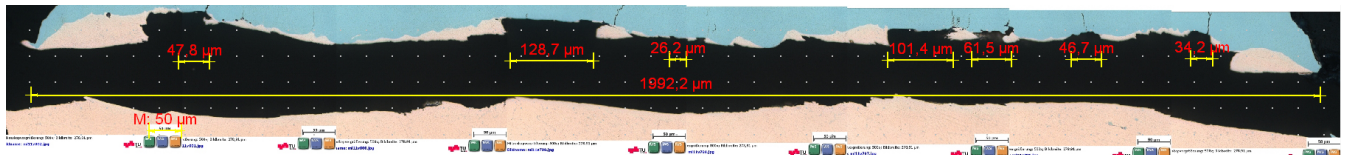
Panoramic views

Additionally panoramic light microscopy images of cross section of the two sheared off and relocated weld beads are presented in fig. 54. Areas where no substrate material adheres on the sheared off beads are indicated. In these areas the material failure has happened right at the interface. The measured lengths are compared to the total length of the interface. The resulting fraction is presented in the figures.

The relation is much higher for the probe of lower fracture shear strength (VR1.5.5). This investigation emphasizes the findings from the EDX-mappings.



(a) VR1.5.5: $\tau_{IF} = 156$ MPa, $L_{SifRel} = 61,7\%$



(b) VR1.5.6: $\tau_{IF} = 282$ MPa, $L_{SifRel} = 22,4\%$

Figure 54: Panoramic views of sheared off and relocated welds. τ_{IF} shear strength, L_{SifRel} ... fraction of length along total failure line where separation of materials happens inside the interface.

Shear strength at too high HI

Based on the insights on the scattering shear strengths additional three direct steel clad samples shear strength testing were produced. The optimized HI parameter were neglected for these weldments. The HI was intendedly set to too high values. The resulting increased crack formation was neglected. The purpose of this additional investigation was to approve the findings and to find out whether the shear strength can be further increase by an increased degree of dilution.

The second layer is still welded at reduced heat input as appropriately indicated by the optimization. Hence it can be more in detail determined if the closing of appearing cracks is also influenced by the deeper weld penetration of the first layer.

The measured tensile shear strengths and the corresponding dilutions are depicted in tab. 27.

The images depict cross sections of the partially sheared off and on the crack surface relocated welds.

The maximum fracture shear strength τ_{IFmax} is significantly higher compared to all three direct steel cladding shear test samples, welded at optimized parameters. The investigation confirms the insights from the first measurement series. The maximum τ_{IFmax} rose from 282 MPa to 365 MPa, VR1.6.4. Compared to the steel-to-steel welding this is significantly more than 50% of the reference strengths.

However, scatter in shear strengths can still be observed. Its appearance can be explained by the observed failure behavior.

It can be observed from the cross section of VR1.6.2 that the weld bead is still on the substrate. The separation behavior partially changed compared to the samples of low dilution. During testing of VR1.6.2 and VR1.6.4 there was no sudden fracture of the entire weld bead as it was experienced by all the samples of the initial shear tests. The material failure, which again could be identified during testing by a significant drop of the measured stress, happened inside the weld metal. The weld beads were only partially separated from the substrate.

Furthermore, VR1.6.2's cross section indicates that the failure initiation can be drawn back to one of cracks in the weld metal.

The different behavior can not be observed in the cross section of 1.6.4. The material failure for this sample did not happen where the actual cross section is taken out.

Still for this sample not the entire weld was sheared off at once. However, the material failure did not happen perpendicular to load direction but parallel.

Probe VR1.6.6 shows the same behavior as the sample from first measurements series where the entire weld metal pops off in one sudden moment. Shear strength and dilution

4 Results and discussion

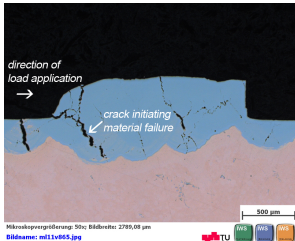
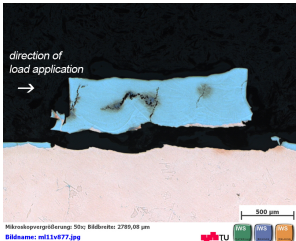
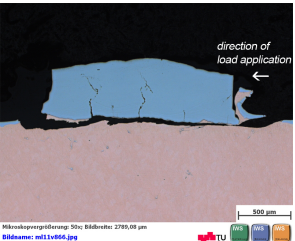
exp. no.	VR1.6.2	VR1.6.4	VR1.6.6
τ_{IF} dilution	 <p>344 MPa 47%</p>	 <p>365 MPa 16%</p>	 <p>320 MPa 12%</p>

Table 27: Shear strengths of three direct steel claddings, welded at intendedly too HI.

is comparable to the maximum shear strength of the initial testing.

For what regards weld quality, it can be seen that all probes show cracks inside the weld metal. However cracks that reach to the surface of the weld bead only appear at probe VR1.6.2 . For the two probes of proper dilution the cracks stop inside the weld metal.

It turns out that the maximum fracture shear strength is not given at the maximum dilution. At too high dilution the significant crack formation acts as a weakening point of the weld metal. Hence, the augmentation of shear strength by an increased degree of dilution is limited. The maximum τ_{IFmax} was measured for a weld that still is inside a optimum dilution in terms of weld quality, refer to page 105.

SEM topography of crack surface

In this section SEM topographies of the crack surface on the substrate of the shear test samples VR1.5.6 and VR1.5.5 are presented. The purpose of this investigation was to find a possible link to the differing shear strength of the two weldments. The overview images in fig. 55(a) and 56(a) correspond to the substrate surface EDX-maps in table 26. The welding direction and direction of loading are therefore the same.

From the overview images it can be observed that the crack surfaces of the maximum shear strength, VR1.5.6, and the minimum shear strength, VR1.5.5, have significantly different topographies.

Fig. 55(a) shows extensively grooves in loading direction. These grooves have very plane sheared surfaces. A detailed view of such a groove is depicted in fig. 55(b).

On the load application side the grooves have rounded cutting edges. It is believed that these topographies are a result from a cutting of the cladding by the shear-off-edges of the testing jig.

On the opposite side the grooves sections end in terraces, running perpendicular to loading direction. Next to these terraces the structures appear more fine. The detailed appearance of this topography is presented in fig. 55(c). Dimple structure can be observed, indicating ductile material separation. Hence the joint is well established during welding in this areas and the attainable strength is exploited.

The topography of VR1.5.5, fig. 56(a), shows less extensive cutting grooves. Only at the lateral areas of the weld the cutting grooves can be observed.

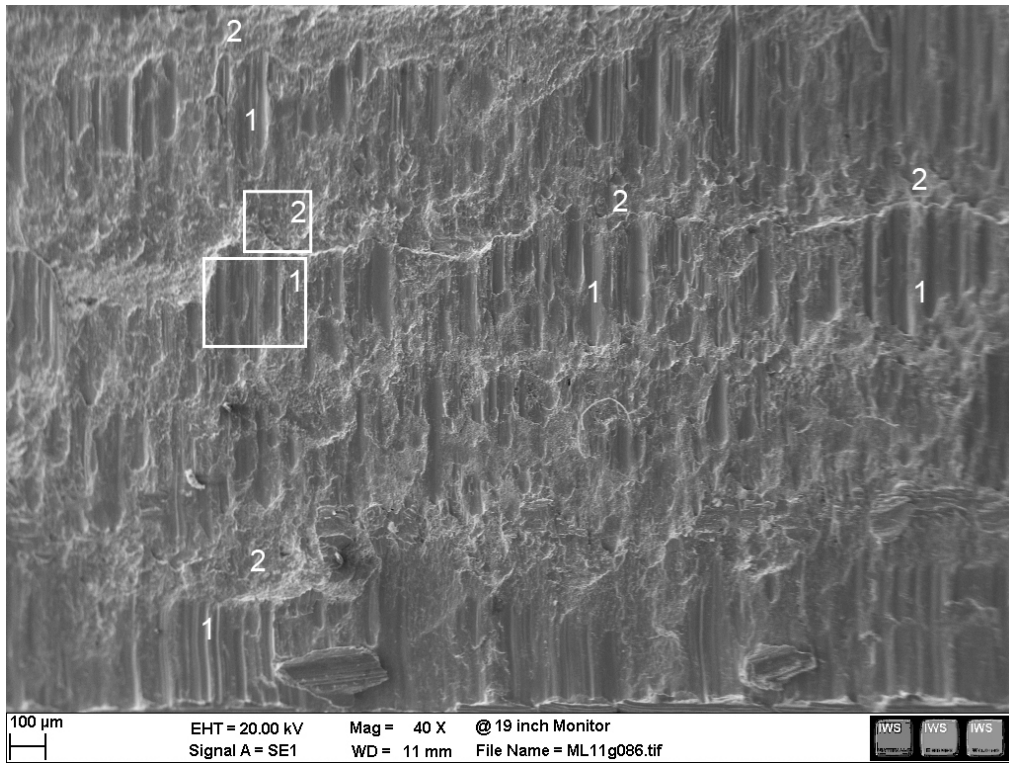
The topography of this crack surface shows a finer structure. Two surface types in terms of brightness can be distinguished. It can be drawn back to a difference topographies.

Lighter areas show a flat and scratchy surface. These surface appear extensively in the middle of the surface. The main part of the surface shows this topography.

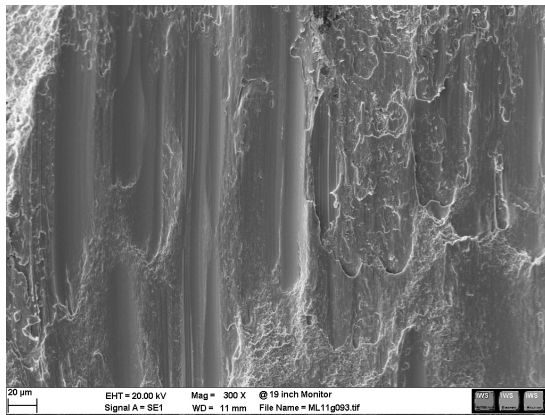
The darker horizontal bands show a dimple structure that is similar to the one found next to terraces in VR1.5.6.

Summing up, both crack surfaces show cutting grooves from the shear test jig. Ductile crack surfaces can be observed on both samples. However, their appearance is more significant on the sample of higher shear strength.

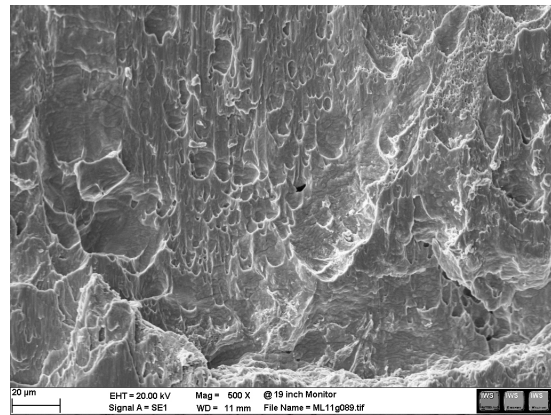
The scratchy crack surface of sample VR1.5.5 indicates that the weld was rather scratched off than teared off. The joint was not well established, which resulted in a lower shear strength.



(a) VR1.5.6: Overview of crack surface of direct steel cladding rel. maximum shear strength.

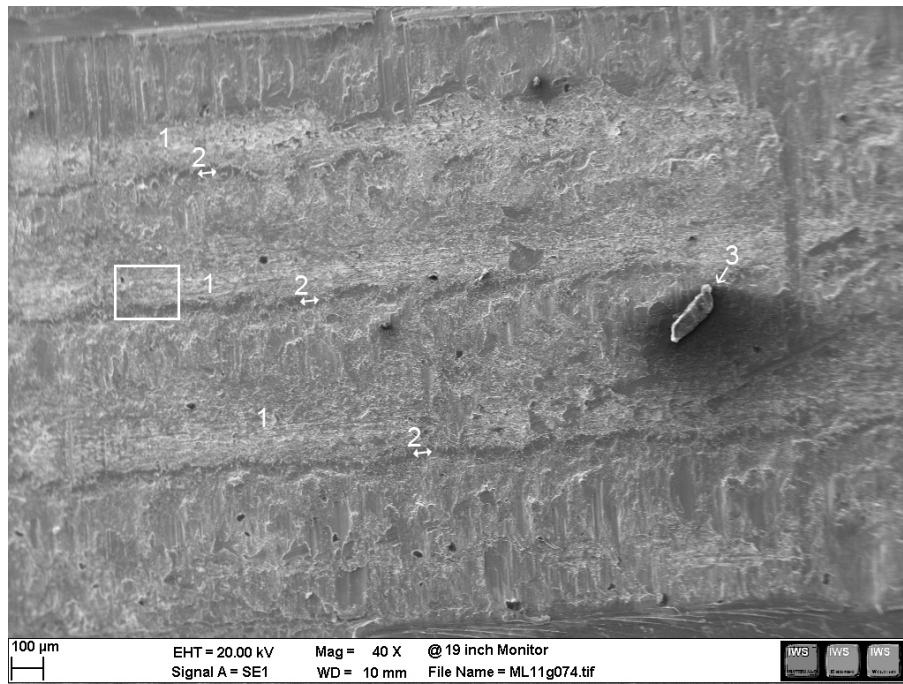


(b) VR1.5.6: Shear groove.

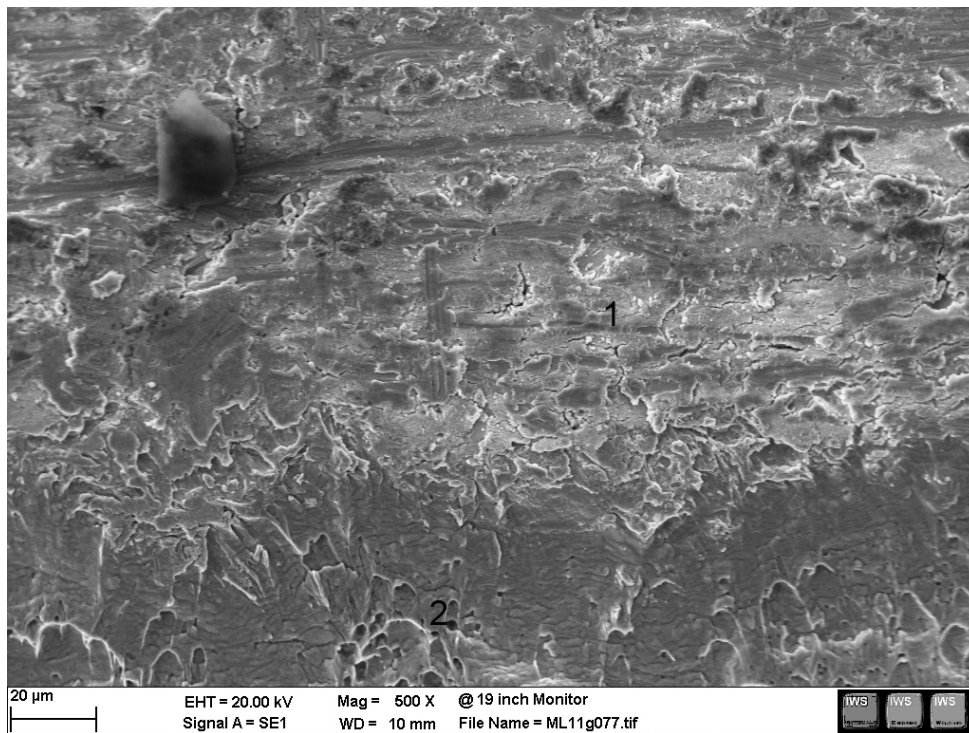


(c) VR1.5.6: Detail of ductile crack surface of direct steel cladding of rel. maximum shear strength.

Figure 55: VR1.5.6: SEM topographies of crack surface of direct steel cladding of rel. maximum shear strength. **1** shear grooves, **2** terraces with ductile dimple fracture surface.



(a) VR1.5.5: Overview of crack surface of direct steel cladding rel. minimum shear strength.



(b) VR1.5.5: Detail of partially and scratched and partially ductile crack surface of direct steel cladding of rel. minimum shear strength.

Figure 56: VR1.5.5: SEM topographies of crack surface of direct steel cladding of rel. minimum shear strength. **1** scratched off surface, **2** ductile dimple surface, **3** pollution particle.

4.5 VR1: Conclusion

The results from VR1 experimental series can be concluded as follows:

- The parameter optimization could reduce the defects inside the weld metal to constantly low amounts.
- By means of reduced HI for the second layer of direct steel claddings cracks no longer reach to the surface of the weld bead.
- The Ni-base buffer layer could not help to completely avoid defect formation. Moreover, the applied reduction of HI in second layer could not avoid appearing cracks to reach the surface of the weld bead.
- The hardness of the weld metal of the direct steel cladding is constantly above 55 HRC.
- The hardness of the steel layer of Ni-base buffer layer cladding is by far below 55 HRC and even less than for the unattended substrate material.
- A narrow but significant soft zone can be observed inside the HAZ.
- The direct steel cladding has for appropriate dilution good shear strength. The Ni-base buffer claddings shear strength is less.
- Appropriate dilution given the shear strength of the direct steel cladding is limited by the identified weak HAZ. The maximum attained value is 365 MPa.

The Ni-Base buffer layer concept clearly fails. The direct steel cladding could prove to fulfill weldability in all three aspects of the standard better.

However, although all identified process influencing factors were taken care of more consciously, scatter in welding results could still be observed for weldments of same laser parameters.

4.6 Simulation

This section presents the results from the FEM simulation.

Fig. 57(a) shows the temperature over time curve for point A for a blank AMPCOLOY[®] 88 core insert and for a steel layer thickness of 0.3mm and 1.0mm.

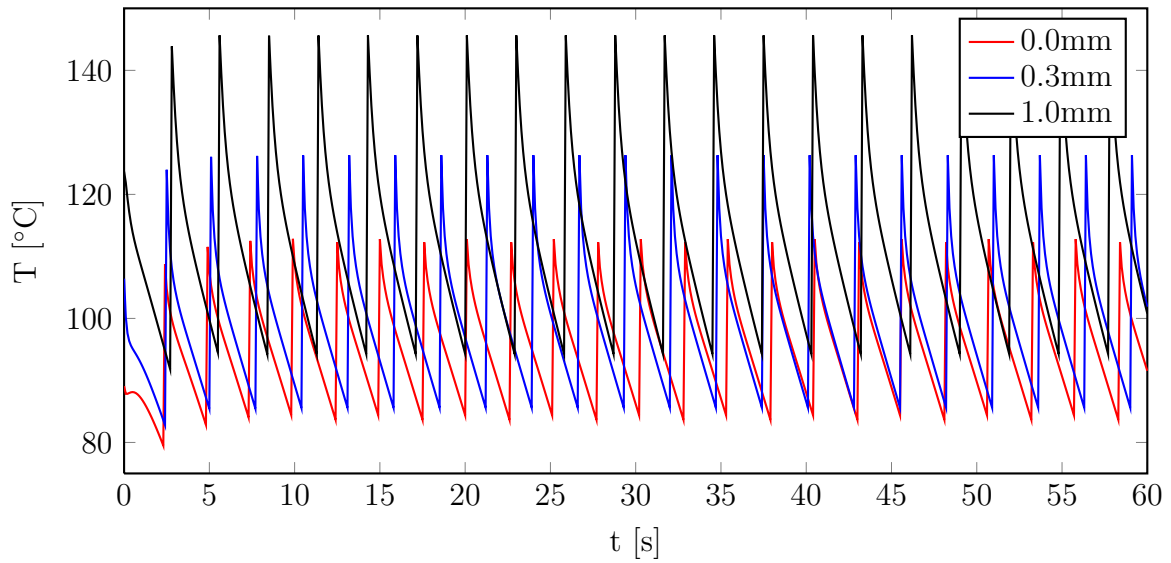
The injection cycles can be derived. Furthermore it can be seen that the process becomes constant in terms of cycle time and minimum and maximum temperatures.

The core insert's maximum temperature increases with increasing layer thickness. For the constant process it is 112°C for the blank AMPCOLOY[®] 88 core insert. However for a layer thickness of 0.3mm it is 126°C and 146°C for a 1.0mm steel layer.

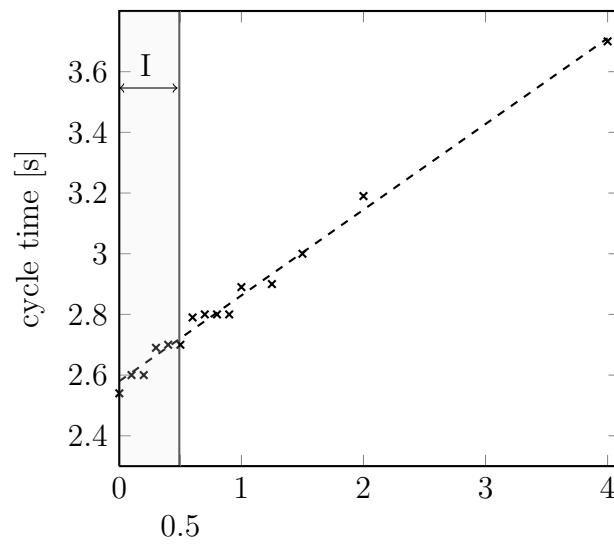
Fig. 57(b) shows the average cycle times for constant injection cycles as a function of the steel layer thickness. It can be derived that the cycle time increases linearly with increasing layer thickness.

The for this work's weldment relevant thickness domain (I) is indicated. A two layer weldment produces a cladding of approximately 0.3-0.5mm of height at max. Within this area the cycle time increases from 2.54s to 2.7s, which is 6%.

The results from the simulation show that the the increase of thermal load of the core insert's surface is relatively low. Moreover the increase of cycle time is relatively low for realistic layer thicknesses of the applied welding process. The absolute calculated values of the cycle times can not be directly transferred to a realistic core insert, for too many simplifications are inherent to this model. Still, this comparative study allows to estimate the deterioration of thermal conductivity of a clad core insert is not high.



(a) $T(t)$ in point A.



1.2343 steel layer thickness [mm]

(b) Cooling cycle time vs. steel layer thickness.

Figure 57: Results of FEM simulation.

5 Summary

Within this chapter a summary of the thesis is given.

The purpose of the presented work was to characterize the weldability of a manual laser deposition weld of high-alloyed hot work steel on an age hardened and highly thermal conductive CuBe-alloy. The investigations on weldability were based on three constituent aspects defined in the DIN 8528-1.

The assessment of weldability is based on experiments that have been carried out throughout two experimental series: VR0 and VR1.

The experimental proceedings were divided into three phases.

1. VR0: Initial process characterization.
2. VR0: Additional process studies to identify influencing factors.
3. VR1: Optimization of HI via U_L (laser pumping voltage) for two material combinations.

The finding of all three phases are summarized in corresponding sequence.

5.1 VR0: Initial process characterization

For all weldments of this thesis AMPCOLOY[®] 88 plates were used as substrate material. On these plates weldments were manually welded at different laser parameters. The laser parameters were systematically varied and the resulting quality was analyzed with help of cross sections.

For the protective top layer of the first two phases a 2 layer direct steel cladding with a 0.5mm Laser Mold[®] 10 wire was applied.

The findings from VR0's initial process capabilities assessment phase can be summarized as follows:

- Weldability is conditionally given. Good quality welds can not be produced constantly.
- The quality of the welds depends on the heat input per unit of length (HI). It can therefore be assigned to a corresponding dilution. Weldments performed at too low HI show lacks of fusion as main defect type. Weldments at too high HI mainly have cracks inside the weld metal. The domain of HI in-between, which

corresponds to a dilution in-between roughly 6% and 20%, shows the best weld quality.

- For relatively high dilution ($> 20\%$) typical crack formation could be observed. These cracks were identified to be hot cracks.
- The welding machine's capabilities are suitable in terms of available power level as well as the possibility of very accurate controllable HI.
- A proper metallurgic bond at the interface can be established, appropriate dilution given. No intermetallic phases at the interface could be found in any of the investigated weld beads.
- The intended hardness of 55 HRC can not be reached by the Laser Mold[®] 10 wire in as welded condition. For the identified optimum dilution 55 HRC could not be reached in as welded condition. Furthermore the hardness decreases for increasing dilution.
- Significant scatter in weld quality could be observed for the same laser parameter settings. The results of the weldments very sensitively react on additional process factors, meaning factors that are not directly controllable. Hence a simple laser parameter adaption is not a sufficient measure to produce constant good quality welds.

5.2 VR0: Additional influencing factors

The second phase consisted of process studies to reveal additional influencing factors. This study focuses on aspects that are defined by the operator. The provided list is only patchy and interdependencies are not considered.

- The laser pumping lamp's voltage is the dominating parameter of the varied ones, including the welding speed, to adjust the HI.
- The laser spot diameter (D_{WS}) is an important parameter as well to adjust the solidification mode of the weld beads. The applied rule of thumb, that sets D_{WS} to the double of the filler wire diameter, was proven to be appropriate.
- In order to appropriately doze the HI of a complete weldment it is necessary to adjust the laser parameters for every single weld bead. This necessity can be drawn back to different absorptivity of Cu and steel of Nd:YAG lasers and a change of the absorptivity characteristics of the substrate.

- The maximum difference of the average v_S between two single beads was found to be as high as a 76% increase. However a direct influence of v_S on the dilution and thus the welding result could not be identified.
- A variation of the average wire deposition rate of +31% and -26% at max. could be identified. Because v_S and wire deposition rate are controlled manually, it is believed that during welding they compensate scatter of each other. However, the results show that this appearance caused by the manual operation causes scatter of the welding results in terms of dilution and thus the weld quality.
- The surface condition of the substrate material was identified to have a great influence on the welding result. It is believed that it reacts with industrial environments and forms a coating on the surface that influences absorptivity.
- The temperature of the surface was identified to strongly influence the welding results. A more constant process could be attained when the surface starting temperature was held below 35°C.

During the additional process studies scatter in the welding results again could be observed. The identified scatter is partly greater than the total identified optimum domain of dilution. It is believed that the manual operation mode negatively influences the weldability at surface preparation and during welding as well.

A model of different absorptivity throughout a welding sequence and precautions for weld preparation to improve the welding process were introduced to base the parameter optimization on.

5.3 VR1: Parameter optimization

A bead-by-bead optimization of the HI was carried out during VR1 at improved experimental setups, based on the insights gained during VR0. Two different material combinations were applied.

The first envisaged the protective top layer to be welded again as a two layer direct-steel-to-substrate cladding. However a 0.4mm Laser Mold[®] 50 wire was used. This wire was applied to reduce hot cracking susceptibility in the first place and to possibly increase the hardness.

For the second material concept the weld bead was built up by a Ni-base buffer in the first layer. A 0.5mm JOKE[®] Fill 120 wire was used. The protective top layer was again welded with the 0.4mm Laser Mold[®] 50 wire.

The HI for every single bead was adjusted towards the identified optimum domain of

dilution. Cross sections were analyzed again to reveal the quality of the welds. Furthermore the mechanical properties of the welds were investigated.

The results from the final optimization stage are as follows:

- The weld quality in terms of defects could be improved for both concepts. The average defect fraction was decreased from $S_E = 3.7\%$ (VR0) to $S_E = 0.6\%$ (VR1 final optimization stage). However, a defect free weld could not be produced.
- The direct steel cladding concept could deliver satisfying results in an optimized stage for all evaluated aspects. The defects inside the weld metal could be reduced to an acceptable amount. Because of reduced HI cracks are smaller and don't reach to the surface of the weld bead. They stop inside the first layer. The hardness inside the cladding in as welded condition was constantly above 55 HRC. The maximum fracture shear strength of the interface is $\tau_{IFsdMax} = 282MPa$ for optimized HI (13% dilution).
- The Ni-base buffer layer concept did not show the expected improvements. Compared to the direct steel cladding the amount of defects was less. However cracks still reached to the weld surface. The hardness of the top layer for this weldments was even lower than the hardness of the substrate material. The maximum fracture shear strength of the interface, $\tau_{IFnbMax} = 154MPa$, was lower when compared to the direct steel claddings.
- For direct steel cladding samples welded with too high HI in terms of the as appropriate identified dilution domain the fracture shear strength was increased to $\tau_{IFsdEMax} = 365MPa$ (16% dilution). However, a even higher increase of the dilution (42%) resulted in a lower fracture shear strength as the increased amount of cracks in the weld metal act as a failure initiation point. The shear strength's limit is defined by the HAZ:
- The hardness measurements could reveal a soft zone inside the substrate material right beneath the interface of both optimized material concepts. This heat affected zone is the weakest part in the joint, appropriate dilution given. It will therefore determine the strength of the weld.
- Scatter in welding results could still be observed in VR1. Despite of the improvements of the experimental setups the attained dilution was not fully constant. However all direct still claddings however resulted inside the appropriate dilution domain. This was not the case for the Ni-base buffer layer claddings. The dilution varied inside one weld from 16% to $< 1\%$. This scatter is greater than the appropriate domain. Therefore weldability of the Ni-base buffer layer concept is therefore worse.

The conclusion over all weldability investigation is that the direct steel cladding welded at optimized HI and with the 0.4mm Laser Mold[®] 50 wire can deliver satisfying results. It is for envisaged purpose the best option out of the investigated ones.

5.4 Heat transfer deterioration

Additionally purpose the deterioration of heat transfer of a cladded AMPCOLOY[®] 88 core insert as a function of the deposition layer's thickness, and in relation to a blank AMPCOLOY[®] 88 part, was estimated. A simplified FEM-simulation was applied to handle this task. The results can be seen separately, but still as a part of weldability as they will also determine the functional ability.

Results from simulation reveal that the deterioration of the heat transfer is relatively low for realistic deposition layer thicknesses. A two layer deposition weld was identified to be about 0.3mm to 0.5mm high from the substrate surface. Inside this domain of deposition layer thickness the relative increase of cooling time when compared to a blank AMPCOLOY[®] 88 core insert is 6%. From a functional point of view this is believed no to have tremendous influence on the cycle time during production.

5.5 In one sentence

Although results showed some scatter the weldability of hot work steel on AMPCOLOY[®] 88 by a manual laser cladding process is given.

6 Outlook

This work assessed the weldability of the envisaged laser cladding to be conditionally given. In order to apply the technology for an industrial application further process control is necessary.

According to the presented necessity of accurately maintaining a certain dilution the most important aspect is to further reduce the scatter in welding results.

It could be shown that the substrate's surface condition in terms of absorptivity has tremendous influence on the welding results. A possible parameter optimization only makes sense if this influencing factor is fully under control.

The roughness on the one hand and possible coatings as result of reactions of the surface with the atmosphere prior and during welding on the other hand, as the two main parameters influencing absorptivity, have to be characterized and adjusted. The following aspects should be taken into consideration:

- surface preparation method
- influence of welding heat
- oxidation
- pollution

Moreover improved cleanliness will help to reduce susceptibility to the formation of low melting phases, and hence to improve the hot cracking problematic.

Based on better knowledge of the surface's absorptivity characteristics the HI can again be adapted towards the as appropriate indicated dilution domain.

It is recommended to automate the process to avoid scatter from manual operation. This would involve:

- surface preparation
- wire deposition
- laser control
- substrate temperature monitoring

In order to industrially apply the technology for production these additional aspects have to be considered:

6 Outlook

- The weldments are not ready for the application in as welded condition. The surface quality and the geometry of the weld beads are not suitable. A manufacturing technique has to be developed to create a smooth surface finish. Functionally unnecessary lateral areas have to be removed.
- Because of the sensitiveness of the process quality assuring measures have to be developed. It is not sufficient to characterize the weldment by the resulting bead's surface. The dilution can not be assessed accurately enough by that.

To comply with the problem of loss of strength in the HAZ it is recommended to develop an appropriate after weld heat treatment which is able to reestablish age-hardened condition. The aspect of the different properties and strengthening mechanisms of the two joined materials has to be taken into consideration.

References

- [1] MAHLE Internatinal GmbH. *Konzernpräsentation*. MAHLE International GmbH, 2010.
- [2] G. Schulze. *Die Metallurige des Schweißens*. Springer Verlag, 2004.
- [3] Robert D. Stout and W D’orville Doty. *Weldability of steels*. Welding Research Council, 1978.
- [4] O. Pasic H. Cerjak, N. Enzinger. *Skriptum zur Vorlesung Fügetechnik*. Institut für Werkstoffkunde und Schweißtechnik TU Graz, 2007.
- [5] E. Beyer. *Schweißen mit CO₂-Hochleistungslasern*. L. Cleemann/ VDI Verlag GmbH, 1987.
- [6] U. Dilthey. *Schweißtechnische Fertigungsverfahren 2*. Springer-Verlag, 2005.
- [7] M. Khalid Imran, S.H. Masood, Milan Brandt, Sudip Bhattacharya, and Jyotirmoy Mazumder. Direct metal deposition (DMD) of H13 tool steel on copper alloy substrate: Evaluation of mechanical properties. *Material Science and Engineering A*, 528(9):3342 – 3349, 2011.
- [8] Chengwu Yao, Binshi Xu, Xiancheng Zhang, Jian Huang, Jun Fu, and Yixiong Wu. Interface microstructure and mechanical properties of laser welding copper-steel dissimilar joint. *Optics and Lasers in Engineering*, 47(7):807 – 814, 2009.
- [9] J. Fahrenwaldt and V. Schuler. *Praxiswissen Schweißtechnik Werkstoffe, Prozesse, Fertigung*. Vieweg+Teubner Verlag/SpringerLink, 2009.
- [10] J.-Y. Chen, K. Conlon, L. Xue, and R. Rogge. Experimental study of residual stresses in laser clad AISI P20 steel on pre-hardened wrought P20 substrate. *Material Science and Engineering A*, 527(27):7265 – 7273, 2010.
- [11] E. Beyer. *Schweißen mit Laser*. Springer-Verlag, 1995.
- [12] E. Letofsky. *Skriptum zur Vorlesung Sonderschweißverfahren*. Institut für Werkstoffkunde und Schweißtechnik TU Graz, 2011.
- [13] R. Poprawe E. Beyer, L. Bakowsky. *Formation and influence of laser induced plasma during CO₂ laser welding*. Springer Verlag, 1984.
- [14] T. Iwase H. Sakamoto. Energy coupling rate in aluminum welding by CO₂ laser and Nd:YAG laser. *The review of laser engineering*, 31:146–150, 2003.
- [15] U. Dilthey. *Schweißtechnische Fertigungsverfahren 1*. Springer-Verlag, 2006.

References

- [16] R. Poprawe. *Tailored Light 2: Laser Application Technology*. Springer Berlin Heidelberg, 2011.
- [17] R. Schneider. *Dissertation: Untersuchung der Einflussgrößen beim Schweißen von Kupferwerkstoffen mit dem Nd:YAG-Laser*. Fakultät für Maschinenbau und Elektrotechnik TU Braunschweig, 1994.
- [18] B. Razny. *Laserstrahlschneiden*. Deutscher Verlag für Schweißtechnik, 1995.
- [19] H. Eichler, H.-D. Kronfeldt, and J. Sahm. *Das Neue Physikalische Grundpraktikum*. Springer Verlag, 2006.
- [20] Joachim Eichler, Jürgen Eichler. *Laser Bauformen, Strahlführung, Anwendung*. Springer, 2006.
- [21] H. Herberg. *Vorlesungsunterlagen: 9. Polarisation: Mathematische Beschreibung*. Fakultät für Feinwerk- und Mikrotechnik, Physikalische Technik, Hochschule München, downloaded from Institute's homepage on 20.09.2011.
- [22] Adolf Senner. *Fachkunde Elektrotechnik*. Verlag Willing und Co, 1964.
- [23] Georg A. Raider. *Photonik: eine Einführung in die Grundlagen*. Springer Wien, 2005.
- [24] Wikipedia. Fresnel'sche formeln. <http://de.wikipedia.org/wiki/FresnelscheFormeln>, downloaded 17.02.2012.
- [25] E. Beyer. Dissertation: Einfluss des laserinduzierten Plasmas beim Schweißen mit CO₂-Lasern. *Forschungsbericht Schweißtechnik DVS, Bd.2*, 1985.
- [26] G. Stern. *Absorptivity of cw-CO₂-, CO- and Nd:YAG -Laser Beams by different Metallic Alloys*. Institutsbericht ISL Saint Louis CO 233/90, 1990.
- [27] Zhou Biro, Weckmann. Pulsed Nd:YAG laser welding of copper using oxygenated assist gases. *Metallurgical and Materials Transactions A*, 33:2019–2030, 2002.
- [28] R. W. Messler. *Principles of welding: Processes, Physics, Chemistry and Metallurgy*. John Wiley & Sons, Inc, 1999.
- [29] G. Lange. *Systematische Beurteilung technischer Schadensfälle*. Deutsche Gesellschaft für Metallkunde e. V., 1997.
- [30] E. Folkhard. *Welding Metallurgy of Stainless Steels*. Springer Verlag, 1988.
- [31] C.E. Cross. On the origin of weld solidification cracking. In *Hot Cracking Phenomena in Welds*, pages 3–18. Springer-Verlag, 2005.

References

- [32] N.N. Prokhorov. The problem of the strength of metals while solidifying during welding. In *Svar Proiz* 6, pages 5–11. n.k., 1956.
- [33] T. Senda, F. Matsuda, and G. Takano. Studies on solidification crack susceptibility for weld metals with trans-varestraint test. In *J Japan Weld soc* 42, pages 48–56. Japan Weld Soc, 1973.
- [34] Deutsches Kupferinstitut. *Schweißen und Brennschneiden von Kupfer und Kupferlegierungen*. Deutsches Kupfer-Institut E.V., 1963.
- [35] ASM International Alloy Phase Diagram and Handbook Committees. *ASM Handbook Volume 3 Alloy Phase Diagrams*. Number 4. print. ASM Internatinal, 2007.
- [36] C. Pohle. *Schweißen von Werkstoffkombinationen: metallkundliche und fertigungstechnische Grundlagen sowie Ausführungsbeispiele*. Verlag für Schweißen und verwandte Verfahren DVS-Verlag GmbH, 1999.
- [37] DIN 6520. *Schweißen und verwandte Prozesse - Einteilung von geometrischen Unregelmäßigkeiten an Metallen*. European Committee for Standardization, 2002.
- [38] ASM International Handbook Committee. *ASM Metal Handbook Properties and selection: Nonferrous alloys and special-purpose materials.*, volume 2. ASM International, 7. printing edition, 1990.
- [39] O. Pasic. *Skriptum zur Vorlesung Schweißen von Kunststoffen und Nichteisenmetallen*. Institut für Werkstoffkunde und Schweißtechnik TU Graz, 2009.
- [40] H. Schumann. *Metallographie*. Deutscher Verlag für Grundstoffindustrie, 1991.
- [41] S. Kleber. *Vortragsfolien zur Vorlesung Werkstoffkunde Stahl*. Institut für Werkstoffkunde und Schweißtechnik TU Graz, 2012.
- [42] H. Berns and W. Theise. *Eisenwerkstoffe*. VDI-Buch. Springer Berlin Heidelberg, 2008.
- [43] ASM International Handbook Committees. *ASM Handbook Volume 1 Properties and Selection: Irons, Steels, and High-Performance Alloys*. Number 10. print. ASM Internatinal, 2008.
- [44] Lange, Kammerer, Pöhlandt, Schöck J., Schöck K., and Kammerer M. *Fließpressen*. VDI-Buch. Springer Berlin Heidelberg, 2008.
- [45] Uddeholm. Welding of tool steel. <http://www.bucorp.com/files/uddeholmweldingoftoolsteel>, downloaded 20.02.2012.

References

- [46] M. Khalid Imran, S.H. Masood, Milan Brandt, Sudip Bhattacharya, Stefan Gulizia, Mahnaz Jahedi, and Jyotirmoy Mazumder. Thermal fatigue behavior of direct metal deposited H13 tool steel coating on copper alloy substrate. *Surface and Coatings Technology*, pages 2572 – 2580, 2012.
- [47] H. Khalid Rafi, G.D. Janaki Ram, G. Phanikumar, and K. Prasad Rao. Friction surfaced tool steel (h13) coatings on low carbon steel: A study on the effects of process parameters on coating characteristics and integrity. *Surface and Coatings Technology*, pages 232 – 242, 2010.
- [48] Edelstahlwerke Buderus AG. *Werkstoff Datenblatt für Buderus Kunststoff-Formstahl 2344 ISO-BM*. Wetzlar, 2011.
- [49] D. R. Lide. *CRC Handbook of Chemistry and Physics*. CRC Taylor and Francis, 2009.
- [50] Wikipedia. Beryllium. <http://en.wikipedia.org/wiki/Beryllium>, downloaded 20.02.2012.
- [51] L Anik, S Dorn. *Schweißbeignung metallischer Werkstoff*. Deutscher Verlag für Schweißtechnik DVS-Verlag GmbH, 1995.
- [52] Ampco Metal SA. *Technische Informationen AMPCOLOY 88*. Kollmann Metal, Vienna, 2011.
- [53] JUTZ Lasertechnik GmbH. *DSI Laser Schweißzusätze*. Jutz Lasertechnik GmbH, 2011.
- [54] Alpha Laser GesmbH. *Bedienungsanleitung AL Flak 300mobil*, 2006.
- [55] Tübingen DatInf GmbH. Datainf measure demo. <http://datinf.de/produkte/measure/index>, downloaded 02.04.2011.
- [56] TTC Informatik. Härteumwerter DIN 50150:1976. <http://www.ttc-informatik.com/cms/haerteumwerter.jnlp>, downloaded 28.03.2011.
- [57] TTC Informatik. Härteumwerter DIN EN ISO 18265:2003. <http://www.ttc-informatik.com/cms/haerteumwerter18265.jnlp>, downloaded 28.03.2011.

List of Figures

1	Exemplary MAHLE products.	4
2	Injection molding and wear on core inserts at MAHLE tool making department.	6
3	Three aspects of weldability according to DIN 8528 1 st part.	9
4	Heat encapsulation when laser welding.	16
5	Degree of dilution.	19
6	Influencing factors of absorption.	21
7	Absorptivity as a function of material properties.	22
8	Laser beam vs. ordinary light.	23
9	Wave model of light propagation.	24
10	Polarization.	26
11	Absorptivity as a function of surface temperature for CO_2 -laser.	27
12	Influence of oxygen on absorption when pulsed Nd:YAG laser welding.	29
13	Welding residual stresses.	32
14	Critical ductility curve and deformation curve vs. temperature after Senda's theory.	35
15	Binary phase diagram of Fe and Cu indicating phases compositions areas of different susceptibilities to hot cracking.	36
16	Microstructure changes in HAZ of age hardened material. Initial state: aged.	41
17	CCT diagram of 1.2343 hot work steel and X45CrSi9-3 valve steel.	47
18	Schäffler-Diagramm for used deposition wires.	47
19	Binary phase diagrams of selected main alloying elements.	54
20	Sawitzki-Burcharow ellipses for Iron.	55
21	Applied experiment numeration: an example.	59
22	Schematic sketches of weld bead structures.	65
23	AL Flak 300mobil.	68
24	Handling of AL Flak mobil 300.	70
25	Experimental setups at MAHLE and metallography probe extraction.	72
26	Schematic sketch: Exposure of crack surface.	75
27	Screenshot: <i>Datainf Measure</i> manual measurements of defects in weld metal.	77
28	Tensile shear strength measuring.	79
29	Shear strength samples.	79
30	Modeling of the heat transfer simulation.	82
31	Initial welding tryouts.	86
32	Limits of appropriate HI.	90
33	VR0.3.3: main elements EDX-mappings.	92

List of Figures

34	VR0.3.3: line-scan interface.	93
35	VR0.3.3, VR0.3.7: interface zones.	94
36	VR0.3.3 and VR0.3.7: Weld metal overview.	96
37	VR0.3.3: Light microscopy of weld metal microstructure.	97
38	VR0.3.7: Light microscopy of crack appearance.	98
39	VR0.3.7: Inhomogeneous weld metal, Cu-rich inclusions.	99
40	Interface EDX at different dilution.	100
41	VRR0.3.7: SEM topography of crack surface.	101
42	Hardness is function of dilution.	102
43	Defects in weld metal as a function of dilution.	106
44	Change of welding speed.	107
45	Wire deposition rate.	110
46	Welding sequence study.	112
47	Sketch: Differing reflexion of laser beam during welding sequence	120
48	Defects in weld metal of optimized direct steel cladding.	126
49	VR1.3.21: Hardness line on direct steel cladding.	128
50	VR1.4.3 1: Hardness line on optimized Ni-base buffer layer cladding.	129
51	Linescan on Ni-base buffer layer cladding.	130
52	Shear strengths diagram.	132
53	Failure mechanisms.	135
54	Panoramic views of sheared off and relocated welds.	137
55	VR1.5.6: SEM topographies of crack surface of direct steel cladding of rel. maximum shear strength.	141
56	VR1.5.5: SEM topographies of crack surface of direct steel cladding of rel. minimum shear strength.	142
57	Results of FEM simulation.	146

List of Tables

1	Absorptivity as a function of surface roughness R_a	28
2	Physical properties of relevant elements.	51
3	VR0: process and influencing factors characterization experiments.	58
4	VR1: parameter optimization experiments.	58
5	Chemical composition of AMPCOLOY [®] 88	61
6	Mechanical and physical properties of AMPCOLOY [®] 88.	61
7	Chemical composition of laser Mold [®] 10 wire.	63
8	Chemical composition of laser Mold [®] 50 wire.	63
9	Chemical composition of JOKE [®] 120 Fill Ni-base wire.	64
10	Adjustable laser parameters for AL Flak300 mobil.	69
11	Etching methods for metallography.	74
12	Laser pumping lamp voltage U_S for each bead.	86
13	First cycle (VR0.1): weld bead comparison.	88
14	Second cycle (VR0.2): weld bead comparison.	89
15	Macro hardness measurements of VR0.1 welds.	103
16	Macro hardness measurements of VR0.3 welds.	104
17	Average welding speed in $\frac{mm}{s}$ of welding speed study.	108
18	Influence of welding speed: weld bead comparison.	109
19	Influence of substrate preparation: weld bead comparison.	114
20	Influence of initial substrate temperature on weld quality.	115
21	Influence of D_{WS} : weld bead comparison.	117
22	Optimized direct steel cladding: weld bead comparison.	124
23	Optimized Ni-base buffer cladding: weld bead comparison.	125
24	Fracture shear strength of interface of optimized weldments.	131
25	Shear strength of direct steel claddings: weld bead comparison.	134
26	EDX-maps of crack surface: Min. vs Max shear strength comparison. W_{AW} width of weld after welding, W_{AM} width of weld after machining.	136
27	Shear strengths at intendedly too HI.	139

Addendum A1

Welding experiment protocol VR0.1.1-VR0.1.6

date, time: 24.3, 13:45-14:45
location: Werkstatt Werkzeugbau, Mahle Filtersysteme Austria GmbH, St. Michael
diplomand: Leonhard Weingrill
welder: Beate Karnitschnig
welding apparatus: AL-FLAK 300 mobil
shielding gas: Argon UT1006, 10l/min
substrate/preparation: 2mm AMPCOLOY88 plates, wire cut and sand blasted, cleaned with Tunap Micro 215
Tv: room temp.
deposition wire: LM 10TM (X45CrSi9-3) 0,5mm, wire deposition manual

Exp. No.	U_L [V]	L_I [ms]	F_I [Hz]	D_WS [mm]	v_s [mm/s]	E_I [J]	F_I	TVI1 [°C]	TVI2 [°C]	TVf1 [°C]	TVf2 [°C]	evaluation of weldability by the welder/ remarks
VR0.1.1	300	5	10	1	-	-	S3	-	-	-	-	weldability good, clean bead surface/ welding sequence: 4 beads in 1 layer at little overlap, 2 layers; plate heats a little during welding, let cool down after welding to ~room temperature
VR0.1.2	300	7,5	10	1	-	-	S3	-	-	-	-	weldability good, discreet process, quality of the bead's surface good
VR0.1.3	300	5	8	1	-	-	S3	-	-	-	-	very sound bead surface, weldability gut, in second layer more material is molten; the weld pool geometry changes during welding: after 1 layer round and straight transition from weld pool to substrate, in second layer weld pool no longer round, frayed outer contour at the transition from steel to substrate, the welding drop run away from the weld pool.
VR0.1.4	300	7,5	8	1	-	-	S3	-	-	-	-	bead surface optically very sound, weldability good, same appearance of running away weld drops in second layer but not as strong as in VR0.1.3
VR0.1.5	320	5	8	1	-	-	S3	-	-	-	-	weldability goo, weld drop already run away in first layer, geometry of drops not round, the bead surface not as sound as for the prior weldments
VR0.1.6	320	5	10	1	-	-	S3	-	-	-	-	slight splashes from weld pool, optical evaluation: worse when compared to other weldments of this series

Addendum A2

Welding experiment protocol VR0.2.1-VR0.2.6

date, time: 11.4. -

location: Werkstatt Werkzeugbau, Mahle Filtersysteme Austria GmbH, St. Michael

diplomand: Leonhard Weingrill

welder: Beate Karnitschnig

welding apparatus: AL-FLAK 300 mobil

shielding gas: Argon UT1006, 10l/min

substrate/preparation: 2mm AMPCOLOY88 plates, wire cut and sand blasted, cleaned with Tunap Micro 215
room temp.

deposition wire: LM 10TM (X45CrSi9-3) 0,5mm, wire deposition manual

*expressed in average time for one bead measured manually with stop watch
**the laser is guided over the bead's surface again after welding without further filler material deposition. Same laser parameters.

Exp. No.	U_L [V]	L_I [ms]	F_I [Hz]	D_WS [mm]	v_s* [mm/s]	E_I [J]	F_I	TVI1 [°C]	TVI2 [°C]	TVf1 [°C]	TVf2 [°C]	evaluation of weldability by the welder/ remarks
VR0.2.1	300	6	10	1	23,1s	-	S3	38,9; 42	-	-	-	-
VR0.2.2	300	7,5	10	1	21,75s	-	S3	40	-	-	-	-
VR0.2.3	300	9	8	1	17,5s	-	S3	-	-	-	-	-
VR0.2.4	300	7,5	9	1	20,75s	-	S3	41; 44	-	-	-	-
VR0.2.5	300	7,5	11	1	14,7s	-	S3	35; 72	-	-	-	-
VR0.2.6**	300	6	10	1	20s	-	S3	-	-	-	-	-
VR0.2.7**	300	7,5	10	1	18,5s	-	S3	43; 60	-	-	-	-
VR0.2.8**	300	9	8	1	18s	-	S3	37	-	-	-	-
VR0.2.9**	300	7,5	9	1	18,75s	-	S3	40; 43	-	-	-	-
VR0.2.10**	300	7,5	11	1	14,5s	-	S3	65	-	-	-	-

Addendum A3

Welding experiment protocol VR0.3.1-VR0.3.5

date, time: 18.4.13:00- 13:45; VR0.3.4 and VR0.3.5 on 22.4, 9:30 bis 9:45
location: Werkstatt Werkzeugbau, Mahle Filtersysteme Austria GmbH, St. Michael
diplomand: Leonhard Weingrill
welder: Beate Karnitschnig
welding apparatus: AL-FLAK 300 mobil
shielding gas: Argon UT1006, 10l/min
substrate/preparation: 2mm AMPCOLOY88 plates, wire cut and sand blasted, cleaned with Tunap Micro 215
TV: **substrate is clamped to a to 70°C preheated steel plate
deposition wire: LM 10TM (X45CrSi9-3) 0,5mm, wire deposition manual

*expressed in average time for one bead measured manually with stop watch

Exp. No.	U_L [V]	L_I [ms]	F_I [Hz]	D_WS [mm]	v_s* [mm/s]	E_I [J]	F_I	TVI1 [°C]	TVI2 [°C]	TVf1 [°C]	TVf2 [°C]	evaluation of weldability by the welder/ remarks
VR0.3.1**	300	9	10	1	21,7s	-	S3	58	-	-	-	weldability not good/during welding strong splashes and sparks flew out of the welding spot. The bead's surface was badly frayed. The reason for this was believed to be the wrong adjustment of the shielding gaz nozzle... the nozzle was adjusted.
VR0.3.2**	300	9	10	1	21,75s	-	S3	56	-	-	-	weldability still not good/The reason for this was believed to still be the wrong adjustment of the shielding gaz nozzle... the nozzle was further adjusted.
VR0.3.3**	300	9	10	1	17,5s	-	S3	59	-	-	-	weldability very good/ no splash or sprk formation during welding any longer. Three reproduction welds had been intended. The first two were not valid-> two additional are performed.
VR0.3.4**	300	9	10	1	20,75s	-	S3	59	-	-	-	weldability good/ very little sparks from the weld pool
VR0.3.5**	300	9	10	1	14,7s	-	S3	61	-	-	-	weldability good/ surface of the weld bead more sound than at VR0.3.4

Addendum: A4**Welding experiment protocol
VR0.3.6-VR0.3.8**

date, time: 28.4.14:30- 15:15
location: Werkstatt Werkzeugbau, Mahle Filtersysteme Austria GmbH, St. Michael
diplomand: Leonhard Weingrill
welder: Beate Karnitschnig
welding apparatus: AL-FLAK 300 mobil
shielding gas: Argon UT1006, 10l/min
substrate/preparation: 2mm AMPCOLOY88 plates, wire cut and sand blasted, cleaned with Tunap Micro 215
Tv: ***substrate is clamped to controllable preheating plate and preheated to 70°C
deposition wire: LM 10TM (X45CrSi9-3) 0,5mm, wire deposition manual

*video taping weldments and measuring net-time of every single bead afterward
s for exact welding speed study.

Exp. No.	U_L [V]	L_I [ms]	F_I [Hz]	D_WS [mm]	v_s* [mm/s]	E_I [J]	F_I [J]	TVI1 [°C]	TVI2 [°C]	TVf1 [°C]	TVf2 [°C]	evaluation of weldability by the welder/ remarks
VR0.3.6***	300	9	10	1		-	S3	70	-	-	-	-
VR0.3.7***	300	9	10	1		-	S3	70	-	-	-	-
VR0.3.8***	300	9	10	1		-	S3	70	-	-	-	-

Addendum A5

Welding experiment protocol VR0.3.9.1-VR0.3.9.9

date, time: 5.5.2011, 10:50- 11:30
location: Werkstatt Werkzeugbau, Mahle Filtersysteme Austria GmbH, St. Michael
diplomand: Leonhard Weingrill
welder: Marko Onitsch
welding apparatus: AL-FLAK 300 mobil
shielding gas: Argon UT1006, 10l/min
substrate/preparation: 2mm AMPCOLOY88 plates, wire cut and sand blasted, cleaned with 70% alcohol
Tv: room temperature
deposition wire: LM 10TM (X45CrSi9-3) 0,5mm, wire deposition manual

all weldments are single bead weldments

Exp. No.	U_L [V]	L_I [ms]	F_I [Hz]	D_WS [mm]	v_s [mm/s]	E_I [J]	F_I	TVi1 [°C]	TVi2 [°C]	TVf1 [°C]	TVf2 [°C]	evaluation of weldability by the welder/ remarks
VR0.3.9.1	300	9	10	1	1,40	19,91	S3	19	20	30	21	sound bead surface, slightly bulged; used filler wire:20mm
VR0.3.9.2	300	9	10	0,8	1,40	19,91	S3	24	23	34	25	bead surface not sound, deep penetration, splashes and sparks during welding; used filler wire:24mm
VR0.3.9.3	300	9	10	1,2	1,40	19,91	S3	26	27	31	26	very sound and well bulged bead surface, shorter bead because fingers burned from welding heat; used filler wire:19mm
VR0.3.9.4	300	9	10	1	2,00	19,91	S3	26	27	31	27	sound bead surface, slightly bulged; used filler wire:20mm
VR0.3.9.5	300	9	10	1	2,50	19,91	S3	26	27	28	28	sound bead surface, slightly bulged; used filler wire:19mm
VR0.3.9.6	290	9	10	1	1,40	18,01	S3	24	27	27	29	very sound but narrow bead, distance in-between singly solidification welding drops shorter, bulging stronger; used filler wire:34mm
VR0.3.9.7	290	9	10	1	2,00	18,01	S3	26	30	37	31	sound bead surface, slightly bulged; used filler wire:17mm
VR0.3.9.8	290	9	10	1	2,50	18,01	S3	27	31	27	33	sound bead surface, slightly bulged; used filler wire:20mm
VR0.3.9.9	290	9	10	0,8	1,40	18,01	S3	27	31	27	39	strong penetration, bead surface not sound. Splashed during welding; used filler wire:24mm

Addendum A6

Welding experiment protocol VR0.3.10.1-VR0.3.10.11

date, time: 11.5.2011,14:30- 15:00
location: Werkstatt Werkzeugbau, Mahle Filtersysteme Austria GmbH, St. Michael
diplomand: Leonhard Weingrill
welder: Beate Kamitschnig
welding apparatus: AL-FLAK 300 mobil
shielding gas: Argon UT1006, 12l/min
substrate/preparation: 2mm AMPCOLOY88 plates, wire cute and sand blasted, cleaned with 70% alcohol
Tv: room temperature
deposition wire: LM 10TM (X45CrSi9-3) 0.5mm, wire deposition manual

*single bead weldment

Exp. No.	U_L [V]	L_L [ms]	F_I [Hz]	D_WS [mm]	v_s [mm/s]	E_I [J]	F_I	TVI1 [°C]	TVI2 [°C]	TVf1 [°C]	TVf2 [°C]	evaluation of weldability by the welder/ remarks
VR0.3.10.1*	300	9	10	1	1,40	19,91	S3	24	21	24	28	sound bead surface, slightly bulged; used filler wire:25mm
VR0.3.10.2*	300	9	10	1	1,40	19,91	S3	24	27	24	-	sound bead surface, bulged; used filler wire:28mm
VR0.3.10.3*	300	9	10	1	1,40	19,91	S3	24	27	24	46	weldability good; used filler wire:23mm
VR0.3.10.4	300	9	10	1	1,40	19,91	S3	28	32	34	40	weldability good, 2 beads welded at 50% overlap, used filler wire:44mm
VR0.3.10.5	300	9	10	1	1,40	19,91	S3	34	40	36	49	weldability good, slightly bulged, 2 beads welded at same parameters in 2 layer at 50% overlap, 3rd bead welded midways on top of 1st two beads, slight splashes at 2nd bead of first layer ; used filler wire:63mm
VR0.3.10.6*	300	9	10	1	1,40	19,91	S3	36	41	39,5	52	good weldability, sound bead surface, flat bead; used filler wire:19mm
VR0.3.10.7*	300	9	10	1	1,40	19,91	S3	37	41	43	47	weldability good, pushed as much wire into weld pool as possible; used filler wire:30mm
VR0.3.10.8*	300	9	10	1	1,40	19,91	S3	39	44	43	46	good weldability, bead surface flat, filler wire guided flatly on substrate surface... and not inclined; used filler wire:25mm
VR0.3.10.9*	300	9	10	1	1,40	19,91	S3	31	34	36	41	weldability good, bead surface not as sound as before; used filler wire:24mm
VR0.3.10.10*	300	9	10	1	1,40	19,91	S3	35	39	36	53	weldability good, bead surface similar to VR0.3.10.9 slightly bulged; used filler wire:26mm
VR0.3.10.11*	310	9	10	1	1,40	21,9	S3	35	40	40	51	weldability good, bead surface more sound than at VR0.3.10.9 and VR0.3.10.10, slightly bulged; used filler wire:25mm

Addendum : A7

Welding experiment protocol VR0.4.1-VR0.4.3

date, time: 22.4.2011, 09:45- 10:00
location: Werkstatt Werkzeugbau, Mahle Filtersysteme Austria GmbH, St. Michael
diplomand: Leonhard Weingrill
welder: Beate Karnitschnig
welding apparatus: AL-FLAK 300 mobil
shielding gas: Argon UT1006, 10l/min
substrate/preparation: 2mm AMPCOLOY88 plates, wire cut and sand blasted, cleaned with acetone
TV: *expressed in average time for one bead measured manually with stop watch
deposition wire: LM 10TM (X45CrSi9-3) 0,5mm, wire deposition manual

Exp. No.	U_L [V]	L_I [ms]	F_I [Hz]	D_WS [mm]	v_s* [mm/s]	E_I [J]	F_I	TVI1 [°C]	TVI2 [°C]	TVf1 [°C]	TVf2 [°C]	evaluation of weldability by the welder/ remarks
VR0.4.1	300	9	10	1	19,5s	-	S3	55	-	-	-	weldability very bad, strong flickering of the weld bead and noise, trayed bead transition,
VR0.4.2	300	7,5	10	1	18s	-	S3	52	-	-	-	weldability very bad, experiment was canceled after second bead of first layer
VR0.4.3	280	7,5	10	1	20s	-	S3	52	-	-	-	weldability much better, the beads surface is much more sound compared to the two first weldments of this series

Addendum A8

Welding experiment protocol VR1.1.1-VR1.1.11

date, time: 18.05.2011, 13:00-13:30
location: Werkstatt Werkzeugbau, Mahle Filtersysteme Austria GmbH, St. Michael
diplomand: Leonhard Weingrill
welder: Beate Karnitschnig
welding apparatus: AL-FLAK 300 mobil
shielding gas: Argon UT1006, 10l/min
substrate/preparation: 2mm AMPCOLOY88 plates, wire cut and sand blasted, cleaned with 70% alcohol
Tv: room temperature
deposition wire: Joke Fill 120-Laser 0,5mm for buffer layer, LM50TM 0,4mm for top layer, wire deposition manual

Exp. No.	U_L [V]	L_I [ms]	F_I [Hz]	D_WS [mm]	v_s [mm/s]	E_I [J]	F_I	TVI1 [°C]	TVI2 [°C]	TVf1 [°C]	TVf2 [°C]	evaluation of weldability by the welder/ remarks
VR1.1.1	300	9	10	1	manu.	19,91	S3	23	21	27	32	weld bead surface not sound, did not change to automatic feed motion
VR1.1.2	300	9	10	1	1,40	19,91	S3	26	29	27	31	weldability good
VR1.1.3	270	9	10	1	1,40	14,37	S3	28	28	28	30	weld bead surface very sound, strong bulged bead
VR1.1.4	250	9	10	1	1,40	10,90	S3	29	29	31	30	wire does not melt entirely
VR1.1.5	330	9	10	1	1,40	26,60	S3	30	30	32	33	strong penetration, splashes
VR1.1.6	280	9	10	1	1,40	16,10	S3	31	31	32	30	weldability good
VR1.1.7	280; 280	9	10	1	1,40	16,10	S3	32; -	29; -	35; 35	28; 30	2 beads at 50% overlap, weldability good for all beads
VR1.1.8	280; 280; 280	9	10	1	1,40	16,10	S3	35; -; -	30; -; -	36; 39; 40	30; 31; 32	weldability good for all beads; HI reduced for 1st bead in second layer
VR1.1.9	300; 300	9	10	1	1,40	19,91	S3	34; -	29; -	38; 43	29; 30	2 beads at 50% overlap, weldability good for all beads
VR1.1.10	300; 280	9	10	1	1,40	19,91	S3	34	29	41; 40	28; 29	2 beads welded at 50% overlap, weldability good for all beads, HI reduced for second beads
VR1.1.11	300	9	10	1	1,40	19,91	S3	35	29	40	29	weldability not good, strong splashing, welding cancelled

Addendum A8

Welding experiment protocol VR1.2.1-VR1.2.5

date, time: 26.5.2011, 14:00-14.30
location: Werkstatt Werkzeugbau, Mahle Filtersysteme Austria GmbH, St. Michael
diplomand: Leonhard Weingrill
welder: Beate Karnitschnig
welding apparatus: AL-FLAK 300 mobil
shielding gas: Argon UT1006, 10l/min
substrate/preparation: 2mm AMPCOLOY88 plates. wire cute and sand blasted, cleaned with 70% alcohol
Tv: room temperature
deposition wire: Joke Fill 120-Laser 0,5mm for buffer layer, LM50TM 0,4mm for top layer, wire deposition manual

*setting of D_W was not checked prior to welding.(forgot). Made sure after experiments.

Exp. No.	U_L [V]	L_I [ms]	F_I [Hz]	D_WS [mm]	v_s [mm/s]	E_I [J]	F_I	TVI1 [°C]	TVI2 [°C]	TVf1 [°C]	TVf2 [°C]	evaluation of weldability by the welder/ remarks
VR1.2.1	280; 280	9	10	1*	1,40	S3	16,1; 16,1	28; 34	31;31	42; 46	31; 32	2 beads welded in first layer at 50% overlap, weldability for all beads good
VR1.2.2	280; 270	9	10	1*	1,40	S3	16,1; 14,3	35; 35	33; 34	-	-	2 beads welded in first layer at 50% overlap, weldability for all beads good, reduced HI for second bead
VR1.2.3	280; 280; 270	9	10	1*	1,40	S3	16,1; 16,1; 14,3	34; 35; 35	35; 36; 36	-	-	3 beads welded in first layer at 50% overlap, weldability for all beads good, reduced HI for third bead of first layer
VR1.2.4	280; 270 270	9	10	1*	1,40	S3	16,1; 14,3; 16,1	35; 35; 36	36; 36; 37	-	-	1st bead welded at 280V-> good weldability, 2nd bead welded at 50% overlap at 270V-> good weldability, 3rd bead welded at 270 V-> weldability good but operating error... wire slides out of laser fokus-> weldment interrupted
VR1.2.5	280; 270; 270	9	10	1*	1,40	S3	16,1; 14,3; 14,3	34; 36; 35	37; 39; 38;	-	-	VR1.2.4 repeated... now good weldability for alls beads without errors

Addendum A8

Welding experiment protocol VR1.3.1-VR.1.3.7

date, time: 31.5.2011; 14:35-15:00
location: Werkstatt Werkzeugbau, Mahle Filtersysteme Austria GmbH, St. Michael
diplomand: Leonhard Weingrill
welder: Beate Karnitschnig
welding apparatus: AL-FLAK 300 mobil
shielding gas: Argon UT1006, 10l/min
substrate/preparation: 2mm AMPCOLOY88 plates, wire cute and sand blasted, cleaned with 70% alcohol
Tv: room temperature
deposition wire: Joke Fill 120-Laser 0,5mm for buffer layer, LM50TM 0,4mm for top layer, wire deposition manual

Exp. No.	U_L [V]	L_J [ms]	F_J [Hz]	D_WS [mm]	v_s [mm/s]	E_J [J]	F_J	TVi1 [°C]	TVi2 [°C]	TVf1 [°C]	TVf2 [°C]	evaluation of weldability by the welder/ remarks
VR1.3.1	286; 286	9	10	1	1,40	17,25; 17,25	S3	27; 28	30; 24	28; 29	39; 41	2 beads welded at 50% overlap, all bead of good weldability
VR1.3.2	286; 282	9	10	1	1,40	17,25; 16,48	S3	30; 31	36; 36	30; 31	36; 49	2 beads welded at 50% overlap, all bead of good weldability, welding mistake in middle of 2nd bead, welding finished... simply welded above; HI reduced for second bead
VR1.3.3	282; 282	9	10	1	1,40	16,48; 16,48	S3	32; 32	36; 36	32; 32	41; 41	weldability good for all beads, welding mistake for second bead... welding still finished
VR1.3.4	286; 286; 282	9	10	1	1,40	17,25; 17,25; 16,48	S3	32; 33; 33	37; 37; 39	32; 33; -	46; 46; -	weldability of all beads good, 3rd bead was mistakenly started in second layer... not the purpose, 3rd bead finally placed at 50% overlap as usual in first layer, HI reduced for third bead
VR1.3.5	286; 282; 282	9	10	1	1,40	17,25; 16,48; 16,48	S3	34; 35; 36	40; 40; 40	34; 35; 36	45; 45; 45	all beads welded in first layer at 50% overlap and good weldability, HI reduced for second and third bead
VR1.3.6	282	9	10	1	1,40	16,48; 16,48; 16,48	S3	36; -; -	40; -; -	-	-	false attempt
VR1.3.7	282; 282; 282	9	10	1	1,40	16,48; 16,48 16,48	S3	36; 37; 38	40; 40; 40	37; 38; 39	42; 42; 42	3 beads welded at 50% overlap and good weldability

Addendum A8

Welding experiment protocol VR1.4.1- VR1.4.6

date, time: 10.6.2011, 10.30-11:15
location: Werkstatt Werkzeugbau, Mahle Filtersysteme Austria GmbH, St. Michael
diplomand: Leonhard Weingrill
welder: Beate Karnitschnig
welding apparatus: AL-FLAK 300 mobil
shielding gas: Argon UT1006, 10l/min
substrate/preparation: 2mm AMPCOLOY88 plates, wire cuted and sand blasted, cleaned with 70% alcohol
Tv: room temperature
deposition wire: Joke Fill 120-Laser 0,5mm for buffer layer, LM50TM 0,4mm for top layer, wire deposition manual

Exp. No.	U_L [V]	L_I [ms]	F_I [Hz]	D_WS [mm]	v_s [mm/s]	E_I [J]	F_I	TVI1 [°C]	TVI2 [°C]	TVf1 [°C]	TVf2 [°C]	evaluation of weldability by the welder/ remarks
VR1.4.1	292;	9	10	1,0; 0,8	1,40	18,39;	S3	21;	-	37;	-	3 beads in 1st layer welded at 50% overlap with Joke Fill 120 wire, HI reduced for 3rd bead
	292;					36;		45;		2 beads welded in 2nd layer at 50% overlap with LM50TM wire		
	290;					34;		39;		weldability of all beads good		
	250;					33;		37;				
	250					34		41				
VR1.4.2	292;	9	10	1,0; 0,8	1,40	18,39;	S3	26;	-	51;	-	First bead welded at 292V;
	292;					36;		48;		second bead with 50% overlap welded at 292V ,interruption in the last third because of welding mistake; 3rd bead with 50% overlap in first layer at 290V, unintended weldin		
	290;					35;		37;		stop at very last spot weld;		
	236;					34;		37;		2 beads in second layer welded with LM50TM wire, just enough HI to melt off wire,		
	236					36		37		and after welding switched substrate plate; weldability of all beads good		
VR1.4.3	296;	9	10	1,0; 0,8	1,40	19,15;	S3	29;	-	40;	-	3 beads in first layer welded at good weldability;
	296;					35;		45;		2 beads in second layer welded with LM50TM wire at increased HI, after welding		
	294;					36;		45;		switched substrate plate, weldability better in 2nd layer		
	250;					37;		42;				
	250					36		41				
VR1.4.4	296;	9	10	1,0; 0,8	1,40	19,15;	S3	30;	-	47;	-	1st bead welded at 296V righth at the beginning a little mistake, was simply welded
	296;					36;		47;		above and carried on, 2. bead welded with 50% Überlappung at 296V ; 3rd bead		
	294;					36;		53;		welded with 50% overlap at 294V; 2. layer welded 2 beads at 236V;weldability of all		
	236;					38;		50;		beads good; exchanged plate after welding		
	236					37						
VR1.4.5	256;	9	10	0,8	1,40	10,55	S3	-	-	-	-	trial shear strength testin probe, welded at optimized parameters, LM50TM on auf
	254;									Hovadur K285, 8 beads in first layser, weldability good		
	248											
VR1.4.6	248	9	10	0,8	1,40	10,55	S3	-	-	-	trial shear strength testing probe, welded at standard parameters for steel to steel weldments, LM50TM on S355, 8 beads in first layser, weldability good	

Addendum A9

Welding experiment protocol

VR1.1.21-VR1.1.28

date, time: 18.05.2011,13:30- 13:45
location: Werkstatt Werkzeugbau, Mahle Filtersysteme Austria GmbH, St. Michael
diplomand: Leonhard Weingrill
welder: Beate Karnitschnig
welding apparatus: AL-FLAK 300 mobil
shielding gas: Argon UT1006, 10l/min
substrate/preparation: 2mm AMPCOLOY88 plates, wire cutte and sand blasted, cleaned with 70% alcohol
Tv: room temperature
deposition wire: LM50TM (X45CrSi9-3) 0,4mm, wire deposition manual

Exp. No.	U_L [V]	L_J [ms]	F_J [Hz]	D_WS [mm]	v_s [mm/s]	E_J [J]	F_J	TVf1 [°C]	TVf2 [°C]	TVf1 [°C]	TVf2 [°C]	evaluation of weldability by the welder/ remarks
VR1.1.21	260	9	10	0,8	1,40	12,63	S3	30	26	31	29	weldability goo
VR1.1.22	280	9	10	0,8	1,40	16,10	S3	30	28	34	30	splashes
VR1.1.23	260	9	10	0,8	1,40	12,63	S3	32; 34	30; 31	35; 36	31; 32	1 st bead good, for second bead at the end splashes, 2 beads welded at 50% overlap at 260V
VR1.1.24	260; 250	9	10	0,8	1,40	12,63	S3	32; 32	30; 32	32; -	33; -	weldability good, easier to weld than previous beads, 2 beads welded at 50% overlap, whereas the 1 was welded at 260V and the 2nd was welded at 250V
VR1.1.25	230	9	10	0,8	1,40	7,82	S3	33	32	-	-	filler material does not melt properly
VR1.1.26	210	9	10	0,8	1,40	5,53	S3	33	31	-	-	filler material does not melt at all
VR1.1.27	260; 250; 250	9	10	0,8	1,40	12,63	S3	33; 34	36; 32;	34; 34; 35	31; 32; 33	weldability good, two bead welded at 50% overlap in first layer, on bead welded midways in second layer
VR1.1.28	260; 250; 240	9	10	0,8	1,40	12,63	S3	35; 35; 35	32; 31; 31	36; 36; 35	32; 32; 31	weldability good, two bead welded at 50% overlap in first layer, on bead welded midways in second layer

Addendum A9

Welding experiment protocol

VR1.2.21-VR.1.2.32

date, time: 26.5.2011, 16.15-14:00
location: Werkstatt Werkzeugbau, Mahle Filtersysteme Austria GmbH, St. Michael
diplomand: Leonhard Weingrill
welder: Beate Karnitschnig
welding apparatus: AL-FLAK 300 mobil
shielding gas: Argon UT1006, 10l/min
substrate/preparation: 2mm AMPCOLOY88 plates, wire cut and sand blasted, cleaned with 70% alcohol
Tv: room temperature
deposition wire: LM50TM (X45CrSi9-3) 0,4mm, wire deposition manual

Exp. No.	U _L [V]	L _J [ms]	F _J [Hz]	D _{WS} [mm]	v _s [mm/s]	E _J [J]	F _J	TV11 [°C]	TV12 [°C]	TVf1 [°C]	TVf2 [°C]	evaluation of weldability by the welder/ remarks
VR1.2.21	250	9	10	0,8	1,40	10,90	S3	23	25	-	-	HI too low, wire melts irregularly
VR1.2.22	256	9	10	0,8	1,40	11,90	S3	28	27	33	28	weldability good at 256V
VR1.2.23	256	9	10	0,8	1,40	11,90	S3	30	28	-	-	cancellation of bead because operating mistake, wire glided out of weld spot
VR1.2.24	256; 256	9	10	0,8	1,40	11,90; 11,90	S3	31; 39	31; 31	39; 38	30; 32	weldability good
VR1.2.25	256; 250	9	10	0,8	1,40	11,90; 10,90	S3	34; 34	34; 32	37; -	32; -	weldability good, wire got stuck at 2nd bead
VR1.2.26	256; 250	9	10	0,8	1,40	11,90; 10,90	S3	34; -	34; -	37; -	35; -	weldability good, after welding new substrate plate in use
VR1.2.27	250	9	10	0,8	1,40	10,90	S3	27	27	41	-	weldability good for all beads
VR1.2.28	250; 250	9	10	0,8	1,40	10,90; 10,90	S3	32; 35	31; 32	44; 39	31; 33	weldability good for all beads
VR1.2.29	250; 244	9	10	0,8	1,40	10,90; 9,89	S3	35; 35	33; 35	44; 39	34; 35	wire does not melt on ampco-side for second layer. HI too low.
VR1.2.30	250; 250; 250	9	10	0,8	1,40	10,90; 10,90; 10,90	S3	33; 35; 35	35; 36; 35	40; 39; -	35; 36; -	weldability good for all beads
VR1.2.31	256; 250; 250	9	10	0,8	1,40	11,90; 10,90; 10,90	S3	33; 34; 34	35; 36; 36	38;-; -	35; -; -	weldability good for all beads, wire did not properly melt at the right ending of bead number two
VR1.2.32	256; 256; 250	9	10	0,8	1,40	11,90; 11,90; 10,90	S3	33; 35; 35	36; 38; 36	35;38,- -	36; 40; -	weldability good for all beads

Addendum A9

Welding experiment protocol VR1.3.21-VR.1.3.23

date, time: 31.5.2011, 14.15-14:35
location: Werkstatt Werkzeugbau, Mahle Filtersysteme Austria GmbH, St. Michael
diplomand: Leonhard Weingrill
welder: Beate Karnitschnig
welding apparatus: AL-FLAK 300 mobil
shielding gas: Argon UT1006, 10l/min
substrate/preparation: 2mm AMPCOLOY88 plates, wire cut and sand blasted, cleaned with 70% alcohol
Tv: room temperature
deposition wire: LM50TM (X45CrSi9-3) 0,4mm, wire deposition manual

Exp. No.	U_L [V]	L_I [ms]	F_I [Hz]	D_WS [mm]	v_s [mm/s]	E_I [J]	F_I	TVI1 [°C]	TVI2 [°C]	TVf1 [°C]	TVf2 [°C]	evaluation of weldability by the welder/ remarks
VR1.3.21	256; 256; 254; 250; 250	9	10	0,8	1,40	11,59; 10,9	S3	21; 23; 24; 25; 26	23; 30; 33; 30; 35	21; 23; 25; 25; 26;	40; 41; 36; 42; 45	1. bead well welded at 256V; 2. bead at 50% overlap at 256V well welded; 3. bead at 50% overlap at 254V welded; 4. bead(1. bead in 2. layer)mitways well welded at 250 V; 5. bead (2nd bead in 2. layer) midways well welded at 250V
VR1.3.22	256; 256; 254; 236; 236	9	10	0,8	1,40	...; 8,62;	S3	27; 28; 29; 29; 29	34; 35; 34; 35; 35	27; 28; 29; 29; 29	40; 47; 48; 40; 40	1. bead well welded at 256V; 2. bead at 50% overlap at 256V well welded; 3. bead at 50% overlap at 254V welded; 4. bead(1. bead in 2. layer)mitways well welded at 236 V; 5. bead (2nd bead in 2. layer) midways well welded at 236V
VR1.3.23	256; 256; 254; 220; 220	9	10	0,8	1,40	...; 6,47	S3	29; 30; 30; 31; 31	35; 35; 30; 36; 36	29; 30; 30; 30; 31	46; 45; 40; -; 41	1. bead well welded at 256V; 2. bead at 50% overlap at 256V well welded; 3. bead at 50% overlap at 254V welded; 4. bead(1. bead in 2. layer)mitways well welded at 220 V; 5. bead (2nd bead in 2. layer) midways well welded at 220V

Addendum A10

Welding experiment protocol VR1.5.1-VR1.5.6

date, time: 20.6.2011; 13:00-14:15
location: Werkstatt Werkzeugbau, Mahle Filtersysteme Austria GmbH, St. Michael
diplomand: Leonhard Weingrill
welder: Beate Karnitschnig
welding apparatus: AL-FLAK 300 mobil
shielding gas: Argon UT1006, 13l/min
substrate/preparation: 2mm AMPCOLOY88 plates, wire cut and sand blasted, cleaned with 70% alcohol
TV: room temperature
deposition wire: Joke Fill 120-Laser 0,5mm for buffer layer and LM50TM 0,4mm, wire deposition manual

Exp. No.	U_L [V]	L_I [ms]	F_I [Hz]	D_WS [mm]	v_s [mm/s]	E_I [J]	F_I	TV1 [°C]	TV2 [°C]	TVf1 [°C]	TVf2 [°C]	evaluation of weldability by the welder/ remarks
VR1.5.1	286; 284; 236	9	10	1,0; 0,8	1,40	17,25; 8,62	S3	21; 35	-	-	-	Ni-base buffer layer shear testing probe, 1st bead was not welded in parallel to the marking, the gap was filled once all other beads were successfully finished. Plate was exchanged after first layer was finished
VR1.5.2	286; 284; 236	9	10	1,0; 0,8	1,40	17,25; 8,62	S3	30; 57; 57; 46; 60; 53; 55	-	-	-	Ni-base buffer layer shear testing probe, at 1st bead weldment was interrupted in the middle because wire glided out of the welding spot, weldin gwas simply carried on. at 3rd bead at little piece of wire did not melt entirely because again the wire got out of the welding spot, the wire part could be melted be passing the laser again over the spot, Plate was exchanged after first layer was finished
VR1.5.3	286; 286; 284; 236	9	10	1,0; 0,8	1,40	17,25; 8,62	S3	36; 46; 50; 55;38; 43; 45; 49;50; 51	-	-	-	Ni-base buffer layer shear testing probe, 2nd bead was welded mistakenly at 286 V and not at 284V as instructed, 6th the wire moved out of the welding spot and there interruption, bead finished at good weldability, Plate was exchanged after first layer was finished
VR1.5.4	258; 256;	9	10	0,8	1,40	11,94; 10,35	S3	38; 47; 54; 56; 39; 46; 50; 52; 54; 55; 55	-	-	-	direct-steel-to-substrate shear testing probe, at 1 st bead in first layer little interruption in the last third of the bead, at 10th bead of first layer little interruption in first layer
VR1.5.5	258; 256	9	10	0,8	1,40	11,94; 10,35	S3	39; 43; 49; 51; 53; 55; 55; 56; 40; 43; 45; 49; 51; 52	-	-	-	alle beads well welded at instructed His
VR1.5.6	258; 256	9	10	0,8	1,40	11,94; 10,35	S3	39; 44; 47; 50; 54; 54; 57; 38; 44; 52; 52; 52; 40; 47; 49; 50; 52; 54	-	-	-	alle beads well welded at instructed His

Addendum A11

Welding experiment protocol VR1.6.1-VR1.6.6

date, time: 1.7.2011; 9:15-9:45
 location: Werkstatt Werkzeugbau, Mahle Filtersysteme Austria GmbH, St. Michael
 diplomand: Leonhard Weingrill
 welder: Beate Karnitschnig
 welding apparatus: AL-FLAK 300 mobil
 shielding gas: Argon UT1006, 13l/min
 substrate/preparation: 2mm AMPCOLOY88 plates, wire cut and sand blasted, cleaned with 70% alcohol
 TV: room temperature
 deposition wire: Joke Fill 120-Laser 0,5mm for buffer layer and LM50TM 0,4mm, wire deposition manual

Exp. No.	U_L [V]	L_I [ms]	F_I [Hz]	D_WS [mm]	v_s [mm/s]	E_I [J]	F_I	TVI1 [°C]	TVI2 [°C]	TVf1 [°C]	TVf2 [°C]	evaluation of weldability by the welder/ remarks
VR1.6.1	248	9; 5,5	10	0,8	1,40	10,55; 6,76	S3	<60°C		-	-	1 bead welded at 9ms L_I, weldability not good, IL shortened to 5.5ms for subsequent beads, 1st and 2nd layer welded at same settings, 50% overlap, 6mm S355 Blech, LM50 (X35CrMoMn7-2) top layer
VR1.6.2	268; 264; 252; 250	9	10	0,8	1,40	14,2; 13,3; 11,52; 10,9	S3	<60°C		-	-	cracks appear are visible under microscope of laser-> due to too high HI, -> HI lowered for subsequent beads, 2mm AMPCOLOY88 plates; X35CrMoMn7-2 for top layer, shear testing probe at intently too high HI,
VR1.6.3	248	5,5	10	0,8	1,40	6,76	S3	<60°C		-	-	1 st and 2nd layer welded at same settings, 50% overlap, 6mm S355 Blech, LM50 (X35CrMoMn7-2) top layer
VR1.6.4	254; 252; 250; 244	9	10	0,8	1,4	11,59; 11,52; 10,9; 9,86	S3	<60°C		-	-	based on appearances from above the 2. was welded at reduced HI... 244V, 2mm AMPCOLOY88 plate; X35CrMoMn7-2, shear testing probe at intently too high HI,
VR1.6.5	248	5,5	10	0,8	1,40	6,76	S3	<60°C		-	-	1 st and 2nd layer welded at same settings, 50% overlap, 6mm S355 Blech, LM50 (X35CrMoMn7-2) top layer, shear testing reference probe,
VR1.6.6	254; 252; 250; 244	9	10	0,8	1,40	11,59; 11,52; 10,9; 9,86	S3	<60°C		-	-	all beads well welded at reduced HI, 2mm AMPCOLOY88 plates; X35CrMoMn7-2 for top layer, shear testing probe at intently too high HI,